7-2024

Heat Stress Changes the Bovine Methylome and Transcriptome and Investigation of Two Novel Genetic Defects in Cattle

Rachel Renae Reith
University of Nebraska-Lincoln, rreith2@huskers.unl.edu

HEAT STRESS CHANGES THE BOVINE METHYLOME AND TRANSCRIPTOME AND INVESTIGATION OF TWO NOVEL GENETIC DEFECTS IN CATTLE

by

Rachel R. Reith

A DISSERTATION

Presented to the Faculty of

The Graduate College at the University of Nebraska

In Partial Fulfillment of Requirements

For the Degree of Doctor of Philosophy

Major: Animal Science

Under the Supervision of Professor Jessica Petersen

Lincoln, Nebraska

July, 2024

HEAT STRESS CHANGES THE BOVINE METHYLOME AND TRANSCRIPTOME AND INVESTIGATION OF TWO NOVEL GENETIC DEFECTS IN CATTLE

Rachel Renae Reith, Ph.D.

University of Nebraska, 2024

Advisor Jessica L. Petersen

Heat stress is a major concern for livestock producers due to its negative impact on animal health and productivity. Heat stress does so by altering expression of genes through different regulatory mechanisms such as DNA methylation. Understanding how heat stress alters gene expression will help elucidate the genetic basis of physiological changes as well as identify targets for possible heat stress mitigation. The purpose of the first study was to understand how heat stress alters the adipose and skeletal muscle transcriptomes in zilpaterol-fed Brahman, as zilpaterol improves muscle growth and may mitigate the effects of heat stress. Differential expression and pathway analyses indicated that Brahman were overall resistant to effects of heat stress but may have experienced mitochondrial dysfunction and stress due to interaction of zilpaterol and heat stress. This contrasts prior results that indicated zilpaterol mitigated some effects of heat stress in *Bos taurus* cattle. The second study investigated the effects of heat stress on DNA methylation in Red Angus skeletal muscle. Heat stress altered methylation of genes and promoters involved in oxidative stress and inflammation, which was also predicted by RNA analysis. However, the methylated genes did not overlap with previously identified differentially expressed genes, suggesting DNA methylation was not the sole mechanism through which heat stress altered gene expression. The third study compares DNA methylation of Red Angus skeletal muscle at 48 hours of heat stress to the same animals

five days post-heat stress. There were methylation changes in growth and inflammation genes, indicating possible anti-inflammatory mechanism and activation of growth pathways during recovery. Overall, these findings indicate heat stress alters expression of genes involved in inflammation and oxidative stress. However, results suggest altering DNA methylation is not the main mechanism for this.

The last two chapters investigate genetic defects in two cattle breeds: blindness in Herefords and bovine familial convulsions and ataxia in Angus. Whole-genome sequencing of affected and unaffected cattle revealed novel variants with predicted high impact on gene function. Pathohistological results and similarities to human genetic diseases support that the identified variants are likely causative in these cattle.

ACKNOWLEDGMENTS

Thank you to my committee members, Dr. Petersen, Dr. Yates, Dr. Ciobanu, and Dr. Brown-Brandl, for their patience and guidance during my program. Your expertise has helped me develop academically as well as professionally. I especially thank my advisor Dr. Petersen, for cultivating my passion for genetics and learning, as well as making the UNL lab feel like family. Thank you, Anna, for being the best lab manager, teaching me so much and talking about life when I needed a break. Thanks to Mackenzie, Lauren, and all current and former lab members for not only helping me with my own projects, but for being great friends and lab mates. I want to thank the many graduate students, past and present, for their help and friendship over the last several years. Many thanks to the Animal Science building staff for coordinating all the communications, travel plans, and meetings these past years.

Thank you to my friends outside of work for reminding me how to have fun and relax when I was stressed. Thank you to my parents, grandmother, and brothers for supporting me the whole way, motivating me to do my best.

Lastly, thank you to Riley, my love. You have been with me through everything, always supporting me and my goals. You and our sweet kitty, Ike, were my greatest comforts at my lowest times. I love you so much.

TABLE OF CONTENTS

LIST OF FIGURES

LIST OF TABLES

SECTION I: HEAT STRESS CHANGES THE BOVINE METHYLOME AND TRANSCRIPTOME

Section I Abstract

As global temperatures have reached new extremes, heat stress is an increasing concern for livestock producers. Heat stress has a negative impact on animal health, causing inflammation and oxidative stress. Animal productivity is also impacted by heat stress through the impairment of muscle growth and decreasing adipose accumulation, leading to decreased carcass quality and quantity. Heat stress causes these changes, in part, by altering expression of genes through different regulatory mechanisms. Understanding through what gene regulatory mechanisms heat stress functions to alter gene expression will help elucidate the genetic basis of physiological changes as well as identify genes and biological pathways of interest for possible heat stress mitigation. The purpose of the first study was to understand how heat stress alters adipose and skeletal muscle transcriptomes in zilpaterol-fed Brahman, as zilpaterol improves muscle growth and may mitigate the effects of heat stress. Differential expression and pathway analyses indicated that Brahman were overall resistant to effects of heat stress but may have experienced mitochondrial dysfunction and stress due to interaction of zilpaterol and heat stress. This contrasts prior results that indicated zilpaterol mitigated some effects of heat stress in *Bos taurus* cattle. The second study investigated the effects of heat stress on DNA methylation in Red Angus skeletal muscle. Heat stress altered methylation of genes and promoters involved in oxidative stress and inflammation, which was also predicted by RNA analysis. However, the methylated genes were not associated with previously identified differentially expressed genes. This suggests DNA methylation was not the

main mechanism through which heat stress altered gene expression. The third study compares DNA methylation of Red Angus skeletal muscle at 48 hours of heat stress to the same animals five days post-heat stress. There were methylation changes in growth and inflammation genes, indicating possible anti-inflammatory mechanism and activation of growth pathways during recovery. Overall, these findings indicate heat stress alters expression of genes involved in inflammation and oxidative stress. However, results suggest altering DNA methylation is not the main mechanism for this.

CHAPTER 1: LITERATURE REVIEW

Introduction

Sustaining the health of livestock is critical not only for optimal food production but also for maintaining livestock welfare. Animals that suffer from disease, injury, or stress will not achieve their growth potential and experience a poor quality of life. Heat stress (hyperthermia) is a major concern for livestock producers due to its impact on livestock health and productivity. Effects of heat stress include increased respiration and heart rate, inflammation, oxidative stress, and impaired muscle growth and metabolism. Heat stress also induces changes in the transcriptome and methylome that can negatively impact the animal, such as increased expression of inflammatory genes, or help the animal adapt, for example, by increasing expression of heat shock proteins to acclimate to the heat. These changes can be measured through gene expression counts and methylation of DNA. Analyzing the transcriptome and methylome of heat-stressed animals will clarify how heat stress causes the observed negative effects and may lead to innovative treatment and management of heat-stressed livestock.

Heat Stress

Heat stress is predicted to cost the global beef cattle industry $11.39 billion annually by 2045 (Thornton et al., 2022). Heat stress decreases average daily gain and dry matter intake, and reduces muscle growth resulting in a lighter carcass, thus reducing profit (Mitlöhner et al., 2001; St-Pierre et al., 2003; Swanson et al., 2020). There is also a cost from the increased mortality and decreased reproduction caused by heat stress in cattle (St-Pierre et al., 2003).

Heat stress occurs when the heat production of an animal exceeds heat loss, upsetting the body's thermal homeostasis (Brown-Brandl, 2018). Heat is generated by body maintenance, digestion, physical activity, and milk production. To decrease heat production, livestock will decrease their feed intake and reduce physical activity except to seek shade (Gonzalez-Rivas et al., 2020; Kim et al., 2021). Heat production is balanced by heat loss. Behavioral changes to increase heat loss include standing in water, wind, or shade to dissipate heat. Livestock also sweat and pant which evaporates water to lose heat, but the effectiveness decreases as humidity rises. A physiological response is vasodilation of surface blood vessels, which releases heat through radiation. The effectiveness of any heat loss method depends on the temperature gradient between the animal's environment and its skin temperature (Brown-Brandl, 2018), as well as the environmental humidity and ventilation. Therefore, cattle without shade in high temperature and/or in humid conditions will struggle to dissipate enough heat to maintain thermal homeostasis and will develop heat stress. Thus, investigating molecular changes due to heat stress could innovate new treatments or practices to help cattle deal with heat stress.

When cells detect elevated body temperatures, multiple signaling pathways are activated (Figure 1.1). Heat shock factors (HSF) in the cell cytosol detect the stress and move to the nucleus. They bind to heat shock elements in the promoters of heat shock proteins (HSP) to upregulate their transcription (Abravaya et al., 1992; Gill et al., 2017). Heat shock proteins have a variety of functions including stabilizing protein folding and regulating the immune response to stress (Asea et al., 2000; Asea, 2008; Kim et al., 2023). Heat shock proteins can induce inflammation by binding to toll-like receptors,

initiating a signaling cascade that results in cytokine production (Asea, 2008; Ju et al., 2014). Heat stress also dysregulates mitochondrial function by slowing the rate of electron transport, allowing increased electron leakage from the mitochondria, and slowing oxidative phosphorylation (Qian et al., 2004; Yang et al., 2010; Emami et al., 2021). The leaked electrons interact with oxygen to generate reactive oxygen species (ROS), which are normally controlled by antioxidant enzymes (Nolfi-Donegan et al., 2020). Accumulation of ROS within the mitochondria and the cell causes oxidative stress, as excessive ROS damages proteins, lipids and DNA (Hu et al., 2019). The accumulated ROS will also stimulate signaling pathways that induce inflammation (Lo et al., 1996; Kabe et al., 2005).

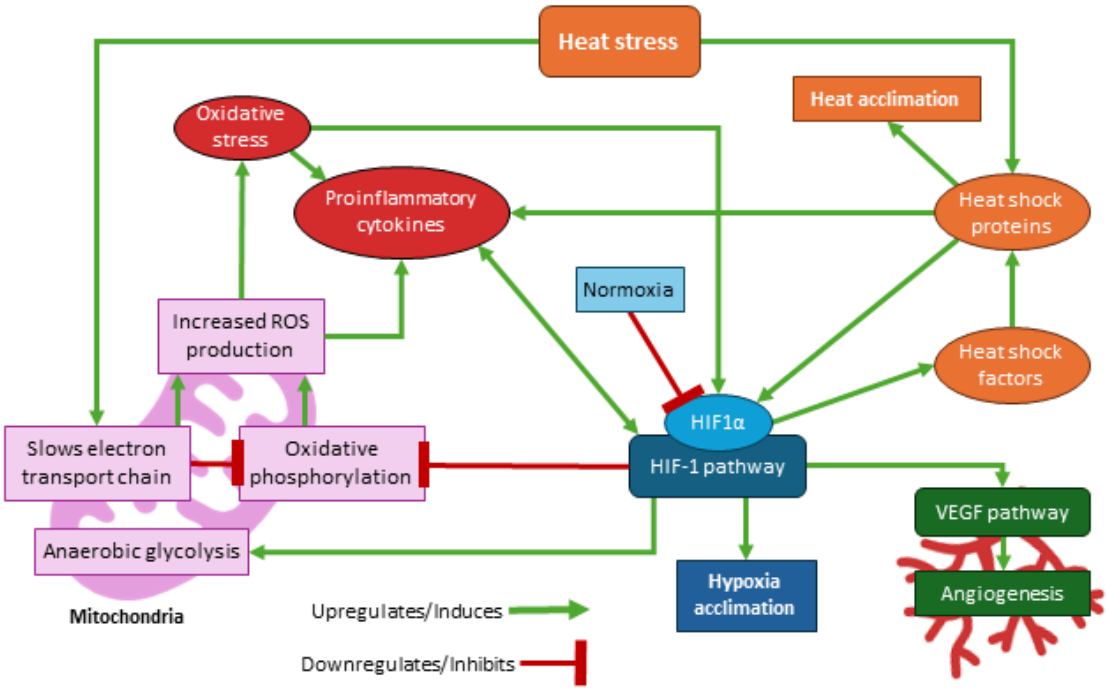

Figure 1.1 Effects of heat stress on inflammation, mitochondria, and HIF-1 pathway.

The systemic impact of heat stress is often marked by changes in hormone concentrations and inflammation. Cortisol, which regulates inflammation and induces lysis of glycogen, protein and adipose, is released in response to heat stress to maintain glucose levels and mediate the immune response (Bagath et al., 2019; Gonzalez-Rivas et al., 2020; Kim et al., 2021). However, the increased plasma cortisol concentrations due to heat stress are negated when animals are pair-fed, demonstrating it is an effect of decreased feed-intake and not heat stress directly (Swanson et al., 2020). Insulin is also affected by heat stress, observed by increased plasma insulin concentrations despite decreases in feed intake (Wheelock et al., 2010; Barnes et al., 2019). Like cortisol, differences in insulin concentrations between heat stress and control groups are eliminated in pair-feeding trials (Swanson et al., 2020). Still, heat stress decreases insulin sensitivity and activity in adipose and skeletal muscle tissue, impairing glucose and fatty acid metabolism (Ganesan et al., 2018; Barnes et al., 2019; Swanson et al., 2020). Another hormone affected by heat stress is epinephrine (adrenaline), plasma concentrations of which are elevated due to heat stress even in pair-feeding trials (Gonzalez-Rivas et al., 2020; Swanson et al., 2020). Epinephrine, released in response to stress by the adrenal medulla, increases heart rate, respiration rate, adipose lipolysis, muscle glycogenolysis, and redistributes blood flow from the gastrointestinal tract to skeletal muscles and skin (Gonzalez-Rivas et al., 2020; Swanson et al., 2020). The increased respiration rates and blood flow to skin help with heat loss during heat stress.

It is well-established that heat stress induces inflammation (Ganesan et al., 2016; Min et al., 2016; Swanson et al., 2020). Inflammation is controlled by cytokines such as interleukins (IL) that can induce, suppress, or amplify the intensity of inflammation

(Akdis et al., 2016). As previously explained, cytokine production can be upregulated by HSPs and oxidative stress. The hypoxia-inducible factor 1 alpha (HIF1α) pathway is normally induced under low-oxygen conditions but has been shown to be induced by heat stress and oxidative stress as well, despite heat stress usually causing hyperoxemia due to hyperventilation (Greer et al., 2012; H.-S. Li et al., 2019; Swanson et al., 2020; X. Zhang et al., 2023). The main function of the HIF1α pathway is to maintain oxygen homeostasis through transcriptional induction of genes involved in glycolysis, angiogenesis, and the immune system (Hu et al., 2003; Majmundar et al., 2010). HIF1α promotes anaerobic glycolysis and inhibits mitochondrial oxygen consumption to reduce total oxygen consumption (Majmundar et al., 2010). The HIF1α pathway helps to adapt to low oxygen conditions and protect against oxidative stress, therefore, the induction of the HIF1α pathway during heat stress should relieve some of its negative effects (Corcoran and O'Neill, 2016; H.-S. Li et al., 2019). There is also evidence of interaction between heat stress and hypoxia pathways that lead to acclimation to both stressors (Ely et al., 2014). The HSPs induced by heat stress stabilize *HIF1α* mRNA, which results in activation of the HIF-1 pathway (Ely et al., 2014). HIF-1α protein upregulates expression of HSFs that then induce expression of HSPs and activate heat shock pathways (Ely et al., 2014). Activation of both HIF-1 and heat shock help the animal adapt to hypoxic and heat stress environments.

Since profit from meat animals comes from the quantity and quality of the carcass, the negative impact of heat stress on muscle and adipose is a concern for production systems. The effects of heat stress in skeletal muscle include decreased protein synthesis, increased muscle catabolism, and increased oxidative stress (Baumgard

and Rhoads, 2013; Ganesan et al., 2017). Combined with decreased feed intake, the growth of muscle is greatly reduced in heat-stressed animals when compared to controls (Barnes et al., 2019). This effect persists even in pair-feeding trials that eliminate differences due to feed-intake, indicating that the non-dietary effects of heat stress still have a notable impact on muscle growth (Swanson et al., 2020). Both cortisol and epinephrine released by heat stress cause lipolysis in adipose tissue, though chronic stimulation may cause desensitization (Ferlay and Chilliard, 2018; Gonzalez-Rivas et al., 2020; Reith et al., 2020). Overall, heat stress causes inflammation, oxidative stress, and impaired growth in livestock.

Transcriptome and Methylome

The effects of heat stress in cattle are driven by changes in gene expression. These adjustments in gene expression, which may be critical to survival, can greatly impact animal production and health, for better or for worse. Therefore, investigation into what genes may be altered by heat stress is critical for understanding the mechanisms by which livestock adjust to heat stress. One way to measure gene expression is through RNA-sequencing (RNA-Seq), which captures counts of mRNA in a sample, providing a glimpse into the transcriptome of an animal at the time of sampling.

Gene expression occurs when RNA polymerase transcribes a gene's DNA sequence into RNA. The transcriptome describes the expression profile of a cell or tissue. While all cells in an organism share the same genome, their transcriptomes can widely vary, due to different genes being expressed at different amounts based on the function and current state of each cell (Söllner et al., 2017; Booth et al., 2022; Nan et al., 2023).

Transcription is regulated by multiple genomic features and mechanisms including promoters, enhancers, transcription factors (TFs), chromatin structure, and DNA methylation (Table 1.1; Cramer, 2019). Promoters and enhancers are DNA sequences that TFs bind to promote or repress transcription (Zabidi and Stark, 2016; Haberle and Stark, 2018). Transcription factors cannot bind to promoters and enhancers when DNA is wrapped around histones (nucleosome); access to promoters and enhancers is blocked until chromatin remodelers open the region for transcription (Fuda et al., 2009; Hu and Tee, 2017). Methylation of cytosines in promoters silences transcription, but cytosines can be demethylated to allow gene expression (Moore et al., 2013; Li et al., 2018). Together, these factors determine how much a gene is transcribed, from completely silenced to constitutively expressed.

Table 1.1 Mechanisms of transcription regulation.

Mechanism	Molecule type	Location relative to target	Function	*Cis*- or *trans*-acting*
Promoter	DNA sequence (100-1000 bp)	Within ~2000 bp upstream of target gene	Initiate transcription by TFs and RNA polymerase binding to it	*Cis*-acting
Enhancer	DNA sequence (50-1000 bp)	Up to a million base pairs away from target promoter; can be physically moved closer with chromatin folding	Binding site for TFs to recruit other TFs and RNA polymerase to the target promoter	*Cis*-acting
Transcription factors (TF)	Proteins	In membrane or cytoplasm of cell	Bind to enhancers, promoters, RNA polymerase, or other TFs to initiate OR repress transcription	*Trans*- acting
Chromatin remodeling	DNA wrapped around histones	Same DNA strand as target	Represses transcription when condensed, allows transcription of target when "open" (no histones)	*Cis*-acting
DNA methylation	Methyl group added by DNA methyltransferases	CGs in DNA sequence of target	Inhibits binding of TFs to promoters	*Cis*-acting

**Cis*-acting mechanisms only affect the target on the same allele as itself; *trans*-acting mechanisms affect targets on both alleles.

The transcriptome changes when the previously described mechanisms are altered. Signals that invoke change in transcription can come from cell itself, such as during cell differentiation, or from the environment like during heat stress through signal transduction pathways (Nan et al., 2023; Su et al., 2024). For example, as explained earlier, when HSFs detect stressful stimuli or high temperatures, they transport to the nucleus and bind to HSP promoters to initiate transcription. A critical transcription factor,

nuclear factor-κB (NF-κB), is activated by infection, inflammation, and stress (Oeckinghaus and Ghosh, 2009; Liu et al., 2017). NF-κB induces transcription of inflammatory cytokines, acute phase proteins, and genes associated with cell survival (Brasier, 2006; Doyle and O'Neill, 2006). When the signals that activate NF-κB cease, it stops upregulating transcription of its target genes; the transcriptome is actively changing. Thus, it is important to note that RNA-Seq is a snapshot of the transcriptome at the time the cells or tissue was sampled; the context of when and where RNA was collected is critical to the results and interpretation.

Investigating the effect of heat stress in various tissue types reveal systemic and tissue-specific transcriptome changes. Due to its ease of accessibility, whole-blood and peripheral blood mononuclear cells (PBMCs) are often used for RNA-seq to examine systemic and immune system changes of leukocytes due to heat stress (Garner et al., 2020; Luna-Ramirez et al., 2023). Because of both the sample and environmental effect, genes involved in cytokine production, inflammation, and metabolism are often reported as affected by heat stress in RNA studies of blood (Garner et al., 2020; Luna-Ramirez et al., 2023). Liver is also a common tissue of interest because of its high metabolism and responsiveness to stress (Y. Li et al., 2019; Lu et al., 2019). Inflammatory response and metabolic pathways such as lipid and carbon metabolism are predicted to be altered in the liver due to genes affected by heat stress (Y. Li et al., 2019; Lu et al., 2019).

For meat animals, the impact of heat stress on adipose and skeletal muscle transcriptomes is of interest and concern (Kubik et al., 2018; Reith et al., 2020; Wang et al., 2021; Reith et al., 2022). Transcriptome studies have indicated that heat stress induced inflammation pathways in skeletal muscle and adipose tissue (Reith et al., 2022),

like that of the blood transcriptome (Garner et al., 2020; Luna-Ramirez et al., 2023). The transcriptomes of reproductive organs have also been studied since heat stress reduces fertility (Liu et al., 2022; Song et al., 2022). Heat stress alters genes and pathways involved in cell cycle and meiosis in testis, and apoptosis and mitochondrial function in oocytes (Diaz et al., 2021; Song et al., 2022); this helps explain the lower quality of sperm and oocytes collected in these studies. The tissue-specific results of RNA-Seq help clarify the pathology of heat stress on organs, possibly leading to treatments that act on the genes and pathways affected by heat stress.

Analysis of DNA methylation gives insight into changes in gene regulation. The methylome refers to the methylation pattern of a genome, which tends to follow certain trends. DNA methylation in mammals occurs almost exclusively on a cytosine followed by a guanine ("CpG" sites), though CHG and CHH (H = A/T/C) methylation can occur (Del Corvo et al., 2021; J. Zhang et al., 2023). CpG islands (CGI) are ~1 kb regions with a high frequency of CpG sites, often in gene promoters and transcription start sites (Li et al., 2018; Del Corvo et al., 2021; J. Zhang et al., 2023). About 70% of promoters are associated with CGIs and are typically not methylated, with transcription often regulated by chromatin state or other non-methylation mechanisms (Saxonov et al., 2006; Deaton and Bird, 2011; Anastasiadi et al., 2018). When CGIs in promoters are methylated, transcription is silenced, either by the methyl group physically blocking TFs or through the recruitment of other proteins that bind to the site and prevent transcription (Moore et al., 2013; Li et al., 2018). Similarly, methylation of the first exon of a gene is negatively correlated with gene expression, thus methylation of both the promoter and first exon

effectively silences gene expression (Moore et al., 2013; Anastasiadi et al., 2018; Li et al., 2018).

While methylation of the other exons seems to be independent of the expression of the gene overall, exon methylation density is positively associated with exon expression levels and exon inclusion, suggesting that methylation of exons affects alternate splicing (Anastasiadi et al., 2018; Li et al., 2018). Introns tend to be highly methylated, though first introns are more likely to be unmethylated which is associated with increased gene expression (Anastasiadi et al., 2018). About 21% of human autosomal CpG sites have dynamic regulation of methylation under normal conditions, meaning only a fraction of all CpG sites change methylation status (Ziller et al., 2013). Thus, methylation changes due to outside factors like stress could alter methylation of genes that are normally static.

The methylome of a mammal is established after two rounds of programming: once during germ cell development of the sperm and egg that eventually creates the animal, and then again during embryo development. Primordial germ cells, the cells that become sperm or eggs, undergo a global cytosine demethylation that includes nearly all genes and promoters (Guibert et al., 2012; Barlow and Bartolomei, 2014). Sperm cells are remethylated at an earlier stage than oocytes, and almost 90% of CpGs are methylated in sperm compared to 40% in oocytes (Kobayashi et al., 2012; Zeng and Chen, 2019). Parental imprinting occurs during this remethylation; maternally imprinted genes are methylated in oocytes and paternally imprinted genes are methylated in sperm (Kobayashi et al., 2012; Zeng and Chen, 2019). As a result, imprinted genes are those where specifically the maternal or paternal copy is silenced with methylation, which is

vital for the function of certain genes and maintenance of gene interactions (Tucci et al., 2019). When a zygote is formed by a sperm and egg, both genomes undergo demethylation again, except for the imprinted genes (Zeng and Chen, 2019). Soon after implantation, *de novo* methylation occurs in the blastocyst genome to create the previously described patterns of methylation (Auclair et al., 2014). After this, only a small portion of CpGs will change their methylation state due to normal cell functions or may be changed due to external factors such as stress.

Like transcriptomes, methylomes are tissue specific. The methylation of CpG sites and proportion of hypermethylated and hypomethylated CpG sites can vary among tissue types (Lokk et al., 2014; Li et al., 2018; Zhou et al., 2020). Sperm cells tend to be highly methylated while oocytes and placental tissues are the least methylated tissues (Kobayashi et al., 2012; Zhou et al., 2020). Differently methylated genes among tissue types often reflect the functions of the tissues. For example, genes involved in vasculature development are hypomethylated in heart tissue but hypermethylated in adipose tissue (Lokk et al., 2014; Zhou et al., 2020). Thus, some genes are hypermethylated because they do not contribute to the tissue-specific function.

Detecting DNA methylation status can be done using several methods, depending on if whole-genome or site-specific methylation is of interest. For instance, whole-genome bisulfite sequencing (WGBS) covers the entire genome while reduced representation bisulfite sequencing (RRBS) targets CpG sites specifically (~13% of genome) (Chatterjee et al., 2017). This means RRBS will have high coverage of promoters and other CGIs but may miss enhancers and other regulatory elements that WGBS would cover. The price of sequencing is also an important factor as the cost of

performing WGBS on one sample is approximately the same as RRBS for eight samples (Chatterjee et al., 2017). So, WGBS could be conducted on a few samples to examine genome-wide methylation, or many more samples could be studied by RRBS to examine CGI methylation. Both techniques identify single CpG sites, including the number of reads per site and the number of methylated bases for each site that can be used for differential analysis. Other methylation analysis techniques such as methylation immunoprecipitation (MeDIP-seq) or methyl-CpG binding domain protein-enriched genome sequencing (MBD-seq) obtain relative methylation levels and are not as accurate as WGBS or RRBS (Chatterjee et al., 2017; J. Zhang et al., 2023). Thus, the use of RRBS to investigate methylation changes due to heat stress would provide accurate and informative data about the methylation of promoters and genes.

Conclusion

As temperatures reach record highs across the globe, the issue of heat stress in livestock is a concern for producers. Connecting the physiological changes to changes in gene expression will improve the understanding of how heat stress alters molecular mechanisms in livestock. Additionally, investigating how heat stress alters livestock methylomes may explain changes in gene expression from RNA data. By elucidating the effect of heat stress on transcriptomes and methylomes, we can better understand how livestock are affected by or adapt to heat stress.

The purpose of the studies in Chapters 2 to 4 was to understand how heat stress alters gene expression in cattle. Chapter 2 utilizes RNA-seq to identify differentially expressed genes due to heat stress and supplementation of beta agonists in adipose and

skeletal muscle of Brahman cattle. Chapter 3 investigates DNA methylation changes due to heat stress in Red Angus cattle muscle using RRBS. Chapter 4 also uses RRBS to compare methylation differences between 48 hours of heat stress and five days post-heat stress in Red Angus muscle.

CHAPTER 2: PREDICTED EFFECTS OF HEAT STRESS AND ZILPATEROL SUPPLEMENTATION ON THE SKELETAL MUSCLE AND ADIPOSE TISSUE TRANSCRIPTOME OF BRAHMAN CATTLE

Introduction

Heat stress (HS) is predicted to cost the global cattle industry $14.65 billion annually by 2045 (Thornton et al., 2022). Heat-stressed animals have decreased average daily gain, dry matter intake, and reduced muscle growth (Mitlöhner et al., 2001; Swanson et al., 2020). Effects of HS in skeletal muscle include decreased protein synthesis, increased muscle catabolism, and increased oxidative stress (Baumgard and Rhoads, 2013; Ganesan et al., 2017). In acute HS, cortisol is released causing lipolysis in adipose tissue (Gonzalez-Rivas et al., 2020). However, increased plasma cortisol concentrations attributed to heat stress are negated when animals are pair-fed, suggesting it is an effect of decreased feed-intake and not HS directly (Swanson et al., 2020). Despite pair-feeding, HS induces systemic inflammation and elevated plasma epinephrine (Swanson et al., 2020). Inflammation is controlled, in part, by activity of cytokines such as interleukins (IL) that can have pro- or anti-inflammatory effects to control the severity of inflammation (Akdis et al., 2016). The elevated epinephrine increases respiratory rate and vasodilation to dissipate heat (Gonzalez-Rivas et al., 2020), and induces lipolysis in adipose tissue to utilize fatty acids for energy (Ferlay and Chilliard, 2018). However chronic HS reduces the adipocytes' response to epinephrine, likely due to desensitization of the receptors (Ferlay and Chilliard, 2018; Reith et al., 2020). Altogether, HS causes a decrease in livestock productivity and negatively impacts their health due to both decreased feed intake and the upregulation of inflammation.

Beta-adrenergic agonists (β-AA), such as zilpaterol hydrochloride (ZH), improve growth performance traits such as average daily gain, hot carcass weight, and longissimus muscle area when supplemented to livestock; β-AA are usually supplemented in the last 21 days of feeding before harvest (Elam et al., 2009; Lean et al., 2014). However, ZH supplementation also reduces marbling scores and fat deposition (Elam et al., 2009). The alteration in growth and carcass traits are attributed to ZH binding to β-adrenergic receptors (β-AR) on skeletal muscle and adipose tissue. In muscle, this activates pathways that increase protein synthesis and inhibit protein turnover, leading to muscle hypertrophy (Johnson et al., 2014; Barnes et al., 2019). In adipose tissue, β-AR activation induces lipolysis and inhibits lipogenesis, reducing the amount of adipose tissue in the carcass (Arp et al., 2014; Hwang et al., 2021). Epinephrine is the endogenous agonist for β-ARs, which induces the previously described effects in skeletal muscle and adipose but is normally released by the adrenal medulla and has a very short half-life (Johnson et al., 2014; Motiejunaite et al., 2021).

A prior transcriptome study of Red Angus steers indicated that HS induced inflammatory pathways in both skeletal muscle and subcutaneous adipose but the additional supplementation of ZH was predicted to moderate some adverse effects of HS (Reith et al., 2022). Skeletal muscle was also predicted to have an increase in oxidative stress due to HS that may have been moderated due to interaction with ZH. Brahman, cattle of indicine origin, have greater heat tolerance than taurine cattle such as Red Angus as exemplified by lower respiration rates and rectal temperatures when in HS environments (Hammond et al., 1991; Mateescu et al., 2023). However, when Brahman are raised and finished the same as *Bos taurus* cattle, Brahman have a smaller ribeye area,

less marbling, and less tender meat despite having similar carcass weights as *Bos taurus* (Gruber et al., 2007; Elzo et al., 2012; Wright et al., 2018). Thus, integrating Brahman genetics into *Bos taurus* cattle may have a negative effect on meat quality and growth efficiency, but their heat tolerance may prevent the negative impact HS has on muscle and adipose (Gruber et al., 2007; Elzo et al., 2012; Wright et al., 2018; Mateescu et al., 2020). Investigation into how HS and ZH affect the Brahman transcriptome may clarify some of the molecular basis of differences in heat tolerance and carcass traits between Brahman and Red Angus.

The purpose of this study is to elucidate the effects of HS, ZH, and their interaction on the muscle and adipose transcriptomes of Brahman steers at three timepoints over a 21-day trial. Due to their heat tolerance, we hypothesized that HS alone will not upregulate many inflammatory or stress pathways in the Brahman tissues, and interaction with ZH will negate or downregulate stress pathways induced by HS.

Materials and Methods

Experimental Design

This study was approved by the Institutional Animal Care and Use Committee at the University of Arizona (Protocol 12-396). Twenty-one Brahman steers (338 ± 39 kg) were acclimated to individual tie stalls or pens for 6 day prior to initiation of the 21-day trial. Steers were randomly allocated within a 2x2 factorial design: no supplementation (NS) or ZH supplementation (ZH), and either a thermoneutral (TN) or heat stress (HS) environment. Steers within the ZH treatment group (n=12) were supplemented ZH at rate of 8.38 mg/kg DM/day mixed in soybean meal. Steers within the NS treatment group

(n=10) received only the soybean meal. Heat-stressed steers were fed an 88% concentrate diet consisting of cracked corn, chopped alfalfa hay, mineral mix, molasses, soybean meal, and urea *ad libitum.* Thermoneutral steers were pair-fed based on the previous day's average feed intake (percentage of body weight) of HS steers. Steers were housed in either TN (THI=68; n=10) or HS (THI=73-85; n=11) temperature-controlled rooms. The temperature humidity index (THI) of the HS environments cycled daily reaching a maximum of 85 (39°C, 30% humidity) at midday and then decreasing to 73 (26°C, 56% humidity) overnight to simulate a natural day-night cycle and to allow the cattle to recover. The TN room stayed at a THI of 68 (21°C,70% humidity). The THI was calculated using the following formula:

$$THI = 0.8 \times T + RH(T - 14.4) + 46.4$$

where T is the air temperature (°C) and RH is relative humidity (as a proportion) (Jubb and Perkins, 2022).

Subcutaneous adipose and *Longissimus dorsi* samples were collected via biopsy on day 3, 10 and 21. At the time of biopsy, 2-3 mL of local anesthetic (2% lidocaine HCl) was injected prior to collection of samples through a 5 cm incision approximately 20 cm cranial of the pelvic bone. The samples were flash-frozen in liquid nitrogen and stored at -80°C. The second biopsy (day 10) was collected from the contralateral loin and the third biopsy (day 21) was collected from the same loin as the first biopsy.

RNA Isolation & Sequencing

RNA from subcutaneous adipose (n=56) was extracted using TRIzol reagent (Sigma-Aldrich, St. Louis, MO, USA), following the protocol from an Rneasy® Plus Mini Kit. RNA was washed and eluted on columns with DNase I treatment (Direct-zol™

RNA MiniPrep Plus, Zymo, Irvine, CA) according to the manufacturer's instructions. RNA from the *Longissimus dorsi* muscle (n=56) was isolated with the RNeasy Fibrous Tissue Mini Kit (Qiagen, Germantown, MD) following the manufacturer protocol. RNA integrity number (RIN; range 1-10, with 1 as completely degraded and 10 as intact) and concentration was determined using the Nano chip on the Agilent Bioanalyzer 2100 (Santa Clara, CA, USA).

Longissimus dorsi samples with a RIN ≥ 7.5 (n=54) and subcutaneous adipose sample with a RIN ≥ 6 (n=49) were sequenced using 100 bp single-end, 3' Tag-Seq reads at Admera Health (South Plainfield, NJ) to a targeted minimum depth of 8 million reads/sample. Reads were trimmed using TrimGalore (Babraham Bioinformatics - Trim Galore!) and HTStream (HTStream); minimum read quality was set to 20, the adapter removed, and minimum output read length set to 35 bp. Transcripts were quantified with STAR (Dobin et al., 2013) as annotated in GCF_002263795.1_ARS-UCD1.3.

Data Analysis

Statistical analysis of transcript counts was performed with DESeq2 (Love et al., 2014). Genes with fewer than 20 counts observed across all samples per day (N=14-19) were excluded from analysis to remove genes with zero or very few counts. Each sample collection time point was individually analyzed with a model that included supplement, environment, and their interaction.

$$design = \sim Temp + Supp + Temp{:}Supp$$

To identify outlier samples, a variance-stabilizing transformation was conducted on the normalized count matrix, and then a heatmap was utilized to visualize the correlation of gene expression for each pairwise combination among samples from within

the time point (Kolde, 2019). An average correlation of 0.75 or lower was considered the outlier cutoff. To further identify outliers, the normalized count matrix was rlog transformed and input into the rrcov R package PcaGrid (Todorov and Filzmoser, 2009). Outliers were detected using a robust principal component analysis as previously described (Chen et al., 2020). Samples with an orthogonal distance or score distance outside of the cutoff values determined by default parameters were considered outliers and removed. DESeq2 uses the Wald test to calculate individual raw *P*-values and calculates an adjusted *P*-value with the Benjamini-Hochberg method using a false discovery rate 0.1. Individual genes with an adjusted *P*-value < 0.05 were considered differentially expressed (DE). Based on the stringent false discovery rate cutoff there were few genes that were individually DE. Therefore, all genes with a non-adjusted *P*<0.05 were used to predict molecular pathway changes using Ingenuity Pathway Analysis (Qiagen, Germantown, MD). The log fold change and *P*-value of each DEG were used to predict the direction of change and significance threshold ($P < 0.05$) of each pathway.

Results

Muscle

The average RIN score was 9.3 ± 0.08 (standard error) for the muscle RNA. The average number of reads for the muscle samples was 11.7 million with 93.7%, on average, uniquely mapping. Two samples were identified as outliers and removed (day 3 HS/NS, day 21 HS/NS) leaving a total of 50 samples for analysis (Table 2.1).

Table 2.1. Count of LD muscle samples analyzed per treatment group and timepoint after outlier removal.

Day	Treatment Groups			
	TN/NS	TN/ZH	HS/NS	HS/ZH
3	5	3	4	6
10	5	3	3	3
21	5	3	4	6

While all effects and timepoints had DEGs with $P < 0.05$, only the effect of environment on day 10 had more than one DEG with an adjusted *P*-value (P_{adj}) < 0.05 (Table 2.2). The full list of DEGs for the LD muscle tissue is found in Supplementary Table 2.1. The single DEG with a $P_{adj} < 0.05$ on day 3 due to supplement was SH3 Domain Containing GRB2 Like 1 (*SH3GL1*), which was downregulated. Genes involved in skeletal muscle contraction and organization affected by HS on day 10 included *TNNI2*, *MYH1*, and *MYH4*, which were downregulated, and *NEURL2* and *RYR3* which were upregulated. Heat stress on day 10 downregulated thyroid hormone receptor beta (*THRB*), and DNA Damage Inducible Transcript 4 (*DDIT4*). *GSTM1-like* and *GSTM3* were downregulated due to HS on day 10; both are glutathione S-transferases which detoxify compounds including environmental toxins and products of oxidative stress. *MDM2*, a proto-oncogene, was the single DEG with a $P_{adj} < 0.05$ on day 10 due to interaction of the main effects; *MDM2* was upregulated compared to the expression of the single treatment groups (TN/ZH and HS/NS), with similar expression to the untreated group (TN/NS; Figure 2.1).

Table 2.2. Number of DEGs in LD muscle tissue across days and effects.

	Environment		Supplement		Interaction	
Day	P<0.05	P_{adj} <0.05	P<0.05	P_{adj} <0.05	P<0.05	P_{adj} <0.05
3	371	0	970	1	793	0
10	540	37	689	0	719	1
21	649	0	341	0	494	0

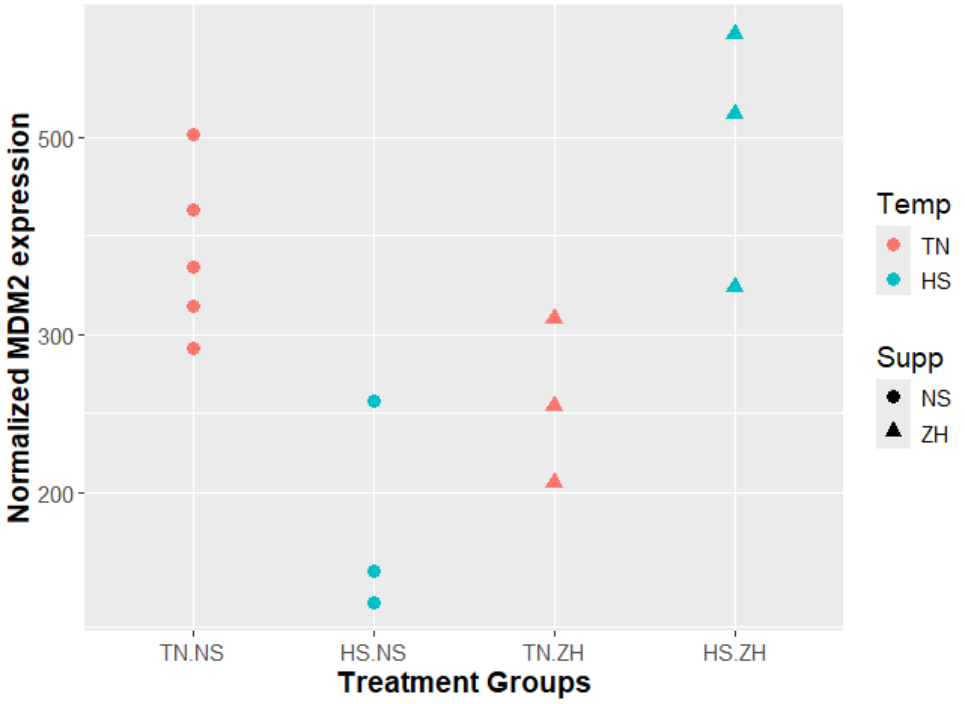

Figure 2.1 Normalized expression of *MDM2* in skeletal muscle on day 10 across treatment combinations.

For skeletal muscle, 286 pathways were predicted to be altered by HS, 239 by ZH, and 359 due to the interaction of HS and ZH (Table 2.3, Supplementary Table 2.2). On day 3, HS was predicted to downregulate immune response pathways such as inflammasome, IL-6, natural killer cell signaling and NF-kB pathways in skeletal muscle. Heat stress was predicted to upregulate signaling of chemokines, GNRH, GPCR, growth

hormone, and Gαq pathways. Pathways predicted to be altered by HS with no clear direction of change include glycolysis, cholesterol biosynthesis, cardiac β-adrenergic signaling, TNFR1, IL-17A, IL-17F, and IL-2. Zilpaterol on day 3 was predicted to downregulate IGF-1, VEGF and VEGF receptor signaling. The HIF1α pathway was also predicted to be downregulated due to ZH on day 3. Immune response pathways predicted to be downregulated by ZH on day 3 include signaling of neutrophil, CXCR4, cytokine storm, IL-8, IL-3, IL-17A pathways and IL-15 production. The Gαq, cardiac β-adrenergic, adrenergic receptor signaling pathways were predicted to be downregulated on day 3 due to supplementation, while α-adrenergic signaling was predicted to be upregulated. The interaction of HS and ZH on day 3 was predicted to upregulate immune pathways including signaling of CXCR4, chemokine, IL-33, IL-8, NF-kB pathways and production of nitric oxide and reactive oxygen species in macrophages. Interaction on day 3 also was predicted to upregulate Gαq, VEGF, and VEGF receptor signaling. Downregulated pathways due to interaction on day 3 were signaling of α-adrenergic, insulin receptor, and apoptosis pathways.

Heat stress on day 10 in skeletal muscle was predicted to downregulate metabolic pathways including gluconeogenesis, glycolysis, growth hormone and insulin receptor signaling. Predicted downregulated pathways also included cardiac β-adrenergic, GPCR, and HIF1α signaling. Pathways predicted to be upregulated due to HS on day 10 included mitochondrial dysfunction, sirtuin signaling and natural killer cell signaling. Zilpaterol was predicted to downregulate oxidative phosphorylation, Gαq, and IL-8 pathways, but upregulate IL-1 signaling, mitochondrial dysfunction, and NRF2-mediated oxidative stress response. The interaction between treatments on day 10 was predicted to

upregulate immune system functions including acute phase response, production of nitric oxide and reactive oxygen species in macrophages, signaling of chemokine, IL-10, IL-2, IL-6, IL-8, and TGF-β pathways. The interaction of main effects on day 10 was also predicted to upregulate mitochondrial dysfunction, NRF2-mediated oxidative stress response, and signaling of sirtuin, GPCR, growth hormone, Gαq, and HIF1α pathways. The interaction was predicted to downregulate antioxidant action of Vitamin C, insulin receptor signaling, fatty acid beta-oxidation, and oxidative phosphorylation.

In skeletal muscle on day 21, HS was predicted to upregulate signaling of cardiac β-adrenergic, Gαs, and IL-8 pathways. Predicted downregulated pathways due to HS on day 21 include glycolysis and signaling of adrenergic receptors, GPCR, Gαq, HIF1α, and α-adrenergic pathways. Supplementation of ZH on day 21 was predicted to upregulate Gαq signaling, two Sertoli cell pathways, and downregulate 3-phosphoinositide degradation and the superpathway of inositol phosphate compounds. Of the 32 pathways predicted to be altered by ZH on day 21, 27 had no predicted direction of change. Interaction on day 21 was predicted to upregulate signaling of GPCR, HIF1α, and IL-8, and downregulate Gαs signaling.

Table 2.3. Number of pathways predicted to be altered (P<0.05) by DEGs in skeletal muscle across days and effects.

Day	Environment	Supplement	Interaction
3	95	141	118
10	109	66	169
21	82	32	72

Adipose

The average RIN score for subcutaneous adipose tissue was 7.1 ± 0.09. The average number of reads was 8.8 million/sample with an average of 91.9% uniquely mapped reads. No samples were identified as outliers.

Table 2.4. Count of subcutaneous adipose tissue samples per treatment group.

Day	TN/NS	TN/ZH	HS/NS	HS/ZH
3	5	4	4	5
10	4	3	2	3
21	5	3	5	6

In adipose tissue, HS had 42 DEGs total and ZH had 98; there were no DEGs due to the interaction of HS and ZH (Table 2.5; Supplementary Table 2.3).

Supplementation of ZH on day 3 downregulated Solute Carrier Family 27 Member 6 (*SLC27A6*), which is involved in the uptake of long-chain fatty acids (Gimeno et al., 2003).

On day 10, the only upregulated gene due to HS was Gastrin Releasing Peptide (*GRP*). Heat stress downregulated heat shock protein family B member 7 (*HSPB7*) and genes involved in mitochondrial function including *CACNA1S, CACNG1,* and *COX6A2*. Supplementation of ZH downregulated *COX5A, COX6A1, COX7A1,* and *COX8B*, all of which encode components of cytochrome c oxidase, a part of oxidative phosphorylation. Zilpaterol on day 10 downregulated other genes involved in mitochondrial function including, *SLC25A4, ATP5IF1, ATP5MG, NDUFA3, NDUFA4, VDAC3,* and *UQCRFS1*. All DEGs (Padj < 0.05) due to ZH on day 21 were upregulated, including fat storage

inducing transmembrane protein 1 (*FITM1*) and RAR Related Orphan Receptor C (*RORC*).

Table 2.5. Number of DEGs in subcutaneous adipose tissue across days and effects.

	Environment		Supplement		Interaction	
Day	$P<0.05$	$P_{adj}<0.05$	$P<0.05$	$P_{adj}<0.05$	$P<0.05$	$P_{adj}<0.05$
3	578	0	1268	26	531	0
10	965	42	1473	52	615	0
21	569	0	1300	20	1062	0

For adipose tissue, a total of 268, 419, and 243 pathways were predicted to be altered by HS, ZH, and the interaction thereof, respectively (Table 2.6, Supplementary Table 2.4). In adipose tissue on day 3, HS was predicted to downregulate the complement system and IL-8 signaling, but upregulate acute phase response, IL-7 signaling, and macrophage activation. Heat stress was predicted to affect signaling of Gαs, Gαq, α-adrenergic, IL-1, and IL-23, but the direction of change was unclear due to mixed expression of the genes involved. Zilpaterol supplementation was predicted to upregulate the role of IL-17A in psoriasis, mitochondrial dysfunction, glycolysis, signaling of IL-8, sirtuin, and GPCR. Predicted downregulated pathways due to ZH include oxidative phosphorylation and triacylglycerol biosynthesis. The interaction of HS and ZH of zilpaterol was predicted to downregulate the Th1 and Th2 pathways and signaling of IL-6 and IL-23. VEGF signaling was predicted to be upregulated due to interaction.

On day 10, metabolic pathways (glycolysis, gluconeogenesis, insulin secretion, white adipose tissue browning pathway, apelin adipocyte signaling, GNRH signaling) were predicted to be downregulated due to heat stress in adipose tissue. Heat stress was also predicted to downregulate oxidative phosphorylation, HIF1α, signaling of GPCR,

adrenergic receptor and α-adrenergic pathways, but upregulate mitochondrial dysfunction and sirtuin signaling pathway. IL-1 and IL-8 signaling were predicted to be upregulated due to HS on day 10 while TGF-β was predicted to be downregulated. Zilpaterol supplementation was predicted to downregulate metabolism pathways including glycolysis, gluconeogenesis, fatty acid β-oxidation, and GNRH signaling. Zilpaterol supplementation was predicted to downregulate oxygen related pathways including oxidative phosphorylation, TCA cycle II, and superoxide radicals degradation. Other predicted downregulated pathways due to ZH were the inflammasome pathway, and signaling of Toll-like receptor, Gαs, and VEGF pathways. Pathways predicted to be upregulated due to ZH on day 10 were sirtuin signaling, mitochondrial dysfunction, white adipose tissue browning, and signaling of cardiac β-adrenergic, Gαq, HIF1α, IL-10, and IL-2 pathways. The interaction of HS and ZH on day 10 was predicted to upregulate oxidative phosphorylation, TCA cycle II, IL-12 signaling and production in macrophages, and IL-8 signaling. The interaction of HS and ZH was predicted to downregulate immune pathways including signaling of IL-2, IL-3, IL-6, IL-13, and VEGF receptors. Other pathways predicted to be downregulated by interaction were mitochondrial dysfunction, and signaling of sirtuin, cardiac β-adrenergic, and IGF-1 pathways.

On day 21, HS was predicted to upregulate the adipogenesis pathway, and signaling of Gαs, GPCR and IL-6 pathways. Adrenergic receptor signaling was predicted to be downregulated on day 21 due to HS. Supplementation of ZH on day 21 was predicted to downregulate mitochondrial dysfunction, apoptosis, production of nitric oxide and reactive oxygen species in macrophages, and signaling of HIF1α, α-adrenergic,

IGF-1, IL-7, IL-8, TGF-β, VEGF and VEGF receptor pathways. Pathways predicted to be upregulated by ZH on day 21 include glycolysis, white adipose tissue browning, and adrenergic receptor signaling. The interaction of the main effects was predicted to downregulate production of nitric oxide and reactive oxygen species in macrophages, NRF2-mediated Oxidative Stress Response, Gαq Signaling; the interaction was also predicted to upregulate the acute phase response.

Table 2.6. Number of pathways predicted to be altered by DEGs in subcutaneous adipose tissue across days and effects $P<0.05$.

Day	Environment	Supplement	Interaction
3	56	78	55
10	140	174	118
21	72	167	70

The HIF1α, mitochondrial dysfunction, and oxidative phosphorylation pathways were predicted to be altered in both Brahman tissues across most treatments and days (Table 2.7 and Table 2.8).

Table 2.7. Predicted direction of change (z-score) of the HIF1α pathway due to main treatments and interaction in Brahman tissues across days.

	Day	Heat stress	Zilpaterol	Heat stress x Zilpaterol
Brahman Muscle	3		-2.84	
	10	-1.155		0.832
	21	-1.667		1.414
Brahman Adipose	3			
	10	-1.387	0.243	
	21		-0.229	

Table 2.8. Predicted direction of change (z-score) of oxidative phosphorylation (Ox.Phos.) and mitochondrial dysfunction (Mit.Dys.) due to main treatments and interaction in Brahman tissues across days.

	Day	Pathway	Heat stress	Zilpaterol	Heat stress x Zilpaterol
Brahman Muscle	10	Ox.Phos.		-2.714	-4.146
		Mit.Dys.	0.784	2.041	2.967
Brahman Adipose	3	Ox.Phos.		-2.84	
		Mit.Dys.		2.777	
	10	Ox.Phos.	-4.69	-7.937	3.873
		Mit.Dys.	3.781	7.209	-4.811
	21	Ox.Phos.			
		Mit.Dys.		-0.2	

Discussion

In this study, RNA analysis of Brahman skeletal muscle and adipose predicted that HS alone was largely tolerated while the addition of ZH supplementation to HS was predicted to induce inflammation and oxidative stress in muscle but mitigate inflammation and improve mitochondrial function in adipose. The few upregulated and multiple downregulated inflammatory genes and pathways across both tissues support heat tolerance in Brahman. Predicted downregulation of HIF1α due to HS also supports thatvBrahman are resistant to the effects of HS. In adipose, the interaction of HS and ZH was predicted to downregulate inflammatory pathways and mitochondrial dysfunction while upregulating oxidative phosphorylation, supporting our hypothesis. However, interaction of HS and ZH in muscle was predicted to upregulate inflammatory pathways and genes, as well as mitochondrial dysfunction, contrary to our hypothesis. These results

explain in part the heat tolerance of Brahman but are also new evidence that the interaction of HS and ZH may negatively impact the health and welfare these cattle.

The predicted downregulation of the HIF1α pathway due to HS in both tissues support the heat tolerance of Brahman cattle. The main function of the HIF1α pathway is to maintain oxygen homeostasis through transcriptional induction of genes involved in glycolysis, angiogenesis, and the immune system (Hu et al., 2003; Majmundar et al., 2010). The HIF1α pathway is normally induced under low-oxygen conditions but has also been shown to be induced by both HS and oxidative stress despite normoxia or hyperventilation (Greer et al., 2012; Li et al., 2019; Zhang et al., 2023). The predicted changes to the HIF1α pathway in these cattle attributed to HS suggest it as a possible heat tolerance mechanism. There is a link between HS and hypoxia, as heat-induced HIF-1 protects cells from hypoxia and contributes to heat acclimation (Treinin et al., 2003; Maloyan et al., 2005; Sugimoto et al., 2014). Heat stress in livestock usually causes hyperoxemia due to hyperventilation (Barnes et al., 2019; Swanson et al., 2020). As expected, heat stress increased respiration rates, which presumably increased blood O2 in turn (Rios et al., 2023). This is a likely mechanism for the heat stress-induced reduction in HIF1α signaling observed in both muscle and adipose. This is further supported by results from the prior study of Red Angus, which are less heat tolerant than Brahman (Mateescu et al., 2020). The HIF1α pathway was predicted to be upregulated due to HS in Red Angus adipose, while the *HIF1α* gene was upregulated due to HS in Red Angus skeletal muscle (Reith et al., 2022). While both HS groups in the Red Angus and Brahman trials had higher respiration rates than their TN counterparts, the RNA results imply that the Red Angus cattle experienced stress conditions due to HS that induced

HIF1α that was not evident in the data from the Brahmans. These results provide some explanation as to how *Bos indicus* are heat tolerant through regulation of the HIF1α pathway.

Though Brahman muscle and adipose seemed tolerant of HS alone, there was evidence that the interaction of HS and ZH seemed to induce stress in muscle, but not adipose. In Brahman adipose on day 10, HIF1α was predicted to be downregulated by HS and upregulated by ZH with no significant effect due to their interaction, likely in part due to their heat tolerance. It is possible that upregulation of HIF1α due to ZH alone was negated when interacting with HS, thus not significantly altering the HIF1α pathway. However, in the Brahman skeletal muscle, the interaction of HS and ZH on day 10 was predicted to upregulate the HIF1α pathway, despite predicted downregulation by HS and no predicted effect due to ZH alone. It is possible that in muscle, the combination of HS and ZH triggered a stress response. The effects of HS and ZH on adipose metabolism are similar (catabolic) while HS and ZH have contrasting effects on muscle metabolism (catabolic vs. anabolic) (Johnson et al., 2014; Ganesan et al., 2018; Gonzalez-Rivas et al., 2020). These contrasting signals may have created stress in skeletal muscle that induced the HIF1α pathway. The upregulation of several other stress-related pathways such as acute phase response and multiple interleukins due to the interaction of HS and ZH in skeletal muscle, but much fewer in adipose, supports this.

Evidence indicates skeletal muscle was experiencing oxidative stress on day 10 due to the interaction of ZH and HS; this would negatively impact the health of the cattle by damaging tissues and triggering inflammation. Oxidative stress occurs when there is an imbalance of reactive oxygen species (ROS) production and antioxidants to clear the

ROS (Belhadj Slimen et al., 2014). Oxidative phosphorylation is regulated so that the amount of ROS produced as a by-product is controllable by antioxidant mechanisms (Murphy, 2009). Reducing oxidative phosphorylation too much, which can occur due to HS (Qian et al., 2004; Belhadj Slimen et al., 2014), causes oxidative stress as unused oxygen molecules become ROS (Murphy, 2009). Increased oxidative phosphorylation can produce more ROS than the antioxidant measures can handle (Uslu et al., 2024). In this study, mitochondrial dysfunction was predicted to be upregulated on day 10 due to ZH and the interaction of HS and ZH, as well as HS but to a lesser degree. The mitochondrial dysfunction pathway includes the oxidative phosphorylation pathway within it, as well as factors that may alter mitochondrial function and disturb the balance of ROS production and antioxidant measures. Thus, upregulated mitochondrial dysfunction in muscle on day 10 due to the interaction of HS and ZH is hypothesized to be driven by the predicted downregulation of oxidative phosphorylation. While interaction of HS and ZH may have caused oxidative stress, the predicted upregulation of the NRF2-mediated oxidative stress response pathway due to the interaction implies there was an increase in antioxidant response as well. Predicted upregulation of the HIF1α pathway due to the interaction of HS and ZH also supports this, as HIF1α can be induced by oxidative stress, and in turn inhibits mitochondrial oxygen consumption and reduces ROS production (Majmundar et al., 2010). So, while interaction of HS and ZH in muscle may have caused oxidative stress, which would negatively impact animal health, antioxidant measures may have also been activated to counter the oxidative stress.

Along with oxidative stress, the interaction of HS and ZH may have induced inflammation in skeletal muscle, contrasting previous results and our hypothesis. Heat

stress causes systemic inflammation, which can cause damage to tissues if unregulated (Chen et al., 2017). On both day 3 and day 10, HS and ZH individually were predicted either to downregulate or impact with unclear direction multiple immune system pathways. However, the interaction of HS and ZH on those days was predicted to upregulate several of the same immune system pathways, as well as pathways that were only significant due to interaction such as TGF-β, acute phase response, and proinflammatory interleukins 2, 6, and 33 (Akdis et al., 2016). While the interaction of HS and ZH on day 10 was predicted to upregulate pathways for proinflammatory cytokines such as IL-2, IL-8, and IL-33 (Akdis et al., 2016), there were also anti-inflammatory pathways such IL-10 and IL-6 identified (Brandt and Pedersen, 2010; Akdis et al., 2016). This indicates a possible mediation of inflammation. Overall, evidence suggests the interaction of HS and ZH, at least on day 3 and 10, induced a majorly pro-inflammatory immune response in skeletal muscle tissue. This is likely related to the predicted upregulation in the HIF1α pathway on day 10 in skeletal muscle tissue since the HIF1α pathway can be induced by inflammation and in turn, signal the production of pro-inflammatory cytokines (Greer et al., 2012). In fact, the predicted oxidative stress and inflammation in skeletal muscle can each induce and be induced by the other conditions.

Zilpaterol alone may have improved mitochondrial function in Brahman skeletal muscle, without causing elevated oxidative stress or inflammation. Zilpaterol has been reported to improve mitochondrial efficiency in bovine muscle cells, increasing oxidative phosphorylation during stress and increased energy demands (Sieck et al., 2022). However, ZH alone on day 10 was predicted to downregulate oxidative phosphorylation

in Brahman skeletal muscle. One possible explanation is that ZH improved the efficiency of the mitochondria, such that gene expression of mitochondrial components was decreased since the current components were sufficient. The relatively greater activity of oxidative phosphorylation likely led to increased ROS production, suggested by predicted upregulation of the NRF2-mediated oxidative stress response on day 10. Unlike the interaction of ZH and HS, ZH alone was not predicted to alter the HIF1α pathway on day 10, which may further indicate controllable ROS production due to ZH alone. The only inflammatory pathway predicted to be upregulated by ZH alone on day 10 was IL-1, which had a low z-score, indicating low activation due to ZH. Altogether, ZH alone likely improved muscle mitochondria function with little evidence of negative impact on muscle health.

In contrast to the Brahman skeletal muscle, on day 10 there was little to no evidence of oxidative stress or inflammation due to the interaction of HS and ZH in adipose. Both tissues had a predicted increase in mitochondrial dysfunction due to HS and ZH individually on day 10. However, the interaction of HS and ZH was predicted to downregulate mitochondrial dysfunction in adipose, while muscle has predicted upregulation. This is also reflected in the oxidative phosphorylation pathway; both tissues have predicted downregulation due to ZH, but muscle also had predicted downregulation due to interaction while adipose has predicted upregulation. It is possible that ZH mitigated the negative effects of HS on mitochondria by causing an increase in gene expression of mitochondrial components, counteracting the HS-suppressed oxidative phosphorylation. Neither the HIF1α pathway nor the NRF2-mediated oxidative stress response was predicted to be altered in adipose on day 10 due to the interaction of HS

and ZH, which may indicate no oxidative stress in adipose. Similarly, the interaction of ZH and HS was predicted to downregulate multiple inflammatory pathways in adipose. There are also fewer inflammatory pathways predicted to be upregulated in adipose due to the interaction than muscle, suggesting adipose was more resistant to HS than muscle and benefitted from the interaction of HS and ZH.

The results of this study indicate interaction of ZH with HS in Brahman skeletal muscle negatively impacted tissue health, while ZH mitigated inflammation and oxidative stress in adipose tissue. This contrasts with results from the Angus study, where interaction of ZH and HS had no seemingly negative impact on cattle welfare. While Brahman have notable heat tolerance, their transcriptomic response to ZH and its interaction with HS is unfavorable for muscle growth and animal welfare.

Acknowledgments

This project is based on the research that was partially supported by the Nebraska Agricultural Experiment Station with funding from the Hatch Multistate Research capacity funding program (Accession Numbers 1011055, 7000952, 1024717) from USDA National Institute of Food and Agriculture. Portions of this work were completed utilizing the Holland Computing Center of the University of Nebraska, which receives support from the Nebraska Research Initiative.

Supplementary Files

Supplementary Table 2.1. List of differentially expressed genes in Brahman skeletal muscle across days and effects (XLSX, 266 KB).

Supplementary Table 2.2. List of pathways predicted to be altered by skeletal muscle DEGs across days and effects (XLSX, 74.3 KB).

Supplementary Table 2.3. List of differentially expressed genes in Brahman adipose tissue across days and effects (XLSX, 341 KB).

Supplementary Table 2.4. List of pathways predicted to be altered by adipose tissue DEGs across days and effects (XLSX, 83 KB).

CHAPTER 3: HEAT STRESS ALTERS METHYLATION OF STRESS AND CELL GROWTH GENES IN CATTLE

Introduction

As global temperatures reach record highs, livestock producers are concerned with the impacts of heat stress on livestock productivity, health, and genetics. Heat stress (HS) causes systemic inflammation and increases plasma epinephrine concentrations (Barnes et al., 2019; Swanson et al., 2020). Heat stress also decreases average daily gain and dry matter intake and impairs muscle growth in meat animals (Mitlöhner et al., 2001; Swanson et al., 2020).

These physiological changes can be attributed to changes in gene regulation and subsequent expression induced by HS. Previous transcriptome studies of adipose and skeletal muscle in beef cattle found HS affected expression of genes and pathways involved in inflammation, metabolism, and oxidative stress (Reith et al., 2022). One means by which heat stress can regulate gene expression is through altering DNA methylation (Del Corvo et al., 2021; Livernois et al., 2021). In general, methylation of promoters and the first exon of a gene are negatively correlated with gene expression while methylation density of internal exons is positively correlated with exon expression and retention (Anastasiadi et al., 2018; Li et al., 2018). Methylome studies of cattle blood found that HS altered methylation of promoters and genes involved in the immune system and stress response (Del Corvo et al., 2021; Livernois et al., 2021), supporting transcriptome work (Lu et al., 2019; Reith et al., 2022; Luna-Ramirez et al., 2023). As HS negatively impacts muscle growth, investigating how HS alters the muscle methylome may elucidate the mechanisms through which this occurs and has the

potential to contribute to new interventive strategies. Thus, the purpose of this study was to investigate the effects of heat stress on the DNA methylome in beef cattle skeletal muscle at three timepoints during a 21-day trial in a controlled HS study using reduced-representation bisulfite sequencing (RRBS). Given prior studies of gene expression, we hypothesize that genes involved in inflammation and oxidative stress will have hypomethylated promoters and differentially methylated regions due to HS.

Materials and Methods

This study was approved by the Institutional Animal Care and Use Committee at the University of Arizona (Protocol 12-396). The samples used for RRBS were from the study described in Reith et al., 2022. In summary, 11 Red Angus based steers (Red Angus sire x Red Angus crossbred dams; 260 ± 25 kg) were randomly allocated for a 21-day trial in either a thermoneutral (TN, n=5) or heat stress (HS, n=6) environment. The HS steers were fed a diet consisting of cracked corn, chopped alfalfa hay, mineral mix, molasses, soybean meal, and urea ad libitum. Thermoneutral steers were pair-fed based on the previous day's average feed intake (percentage of body weight) of HS steers. The temperature humidity index (THI) for the heat stress group would reach 85 (39°C, 30% humidity) at midday, then decrease to 73 (26°C, 56% humidity) overnight. The temperature humidity index (THI) was calculated using the following formula:

$$THI = 0.8 \times T + RH(T - 14.4) + 46.4$$

where T is the air temperature (°C) and RH is relative humidity (as a proportion) (Jubb and Perkins, 2022). A THI of 85 is considered severely stressful for cattle while 73 is mildly stressful (Jubb and Perkins, 2022). The pair-fed TN cattle were housed at a

consistent THI of 68 (21°C, 70% humidity). *Longissimus dorsi* samples were collected via biopsy on day 3, 10, and at harvest (day 21). At the time of biopsy, 2-3 mL of local anesthetic (2% lidocaine HCl) was injected prior to collection of samples through a 5 cm incision approximately 20 cm cranial of the pelvic bone. The samples were flash-frozen in liquid nitrogen and stored at -80°C. The second biopsy (d 10) was collected from the contralateral loin. The cattle were harvested on d 21 at the University of Arizona Food Products and Safety Laboratory. A third sample of skeletal muscle was collected from the same regions of the carcass as biopsies were taken and flash frozen following evisceration and skinning.

DNA was isolated using the Qiagen Gentra Puregene kit (Qiagen, Germantown, MD) following the manufacturer protocol for 30 mg of tissue, with an RNase A digestion step. RRBS library prep and sequencing were performed at the DNA Technologies & Expression Analysis Core at the University of California – Davis. The samples (N=33) were sequenced on Illumina NovaSeq using 150 bp paired-end reads to a targeted depth of 14 million reads/sample. The quality of the sequence reads was checked using FastQC v0.11.7. TrimGalore v0.6 was used with rrbs, non_directional, and paired options to trim the sequence adapters (Krueger et al., 2023). Bismark v0.24 (Krueger and Andrews, 2011) was used to bisulfite-convert the bovine reference genome (ARS-UCD1.2) then align trimmed reads to the converted genome (options: score_min L,0,-0.4 and non_directional). Methylated calls were extracted with Bismark methylation extractor (options: paired-end, merge_non_CpG, bedGraph, counts, no_overlap, ignore_3prime 1 options).

Analysis of differentially methylated regions (DMR) was performed using R package Methylkit (Akalin et al., 2012). The analysis compared methylation of the HS group to the TN group of the same day. A minimum read coverage of 5 reads at each base position were required for analysis. Regions were generated using a sliding-window of 1 kb with a 500 bp step size, then filtered for regions with a minimum of 10 bases. DMRs had the thresholds of 15% methylation difference and a q-value < 0.05. For all analyses, hypomethylated refers to the HS group having less methylation than the TN groups, while hypermethylated means the HS group had more methylation than the TN group. Differentially methylated promoter regions (DMPs) were defined as DMRs 2 kb upstream of a gene. DMRs that overlapped with genes were input into DAVID to explore KEGG pathways (Huang et al., 2009; Sherman et al., 2022).

The lists of genes with DMPs and DMRs for each day were compared to the differentially expressed genes due to HS from the same day in muscle from the RNA study (Reith et al., 2022) to find genes common in both analyses.

Results

The average number of reads per sample was 13.4 million with an average total mapping rate of 89.13% and an average unique mapping rate of 36.5%. One TN sample from day 21 was removed due to having only 4.2 million reads. Using the correlation clustering and PCA plot functions in methylkit, one sample from day 3 TN was determined to be an outlier and was removed from the analyses, leaving at least 4 samples per treatment group/day (Table 3.1).

Table 3.1. Number of samples used for RRBS analysis by day and treatment.

	Environment	
Day	Thermoneutral	Heat Stress
3	5	6
10	5	5
21	4	6

DMPs

There was a total of 747 DMPs across the three sampling days (Table 3.2, Supplementary Table 3.1).

Table 3.2. Number of DMPs due to HS across sampling times.

Day	DMPs	Hypomethylated	Hypermethylated
3	203	35.5%	64.5%
10	271	45.0%	55.0%
21	273	62.6%	37.4%

On day 3, there were 8 hypomethylated and 9 hypermethylated DMPs in microRNAs. Hypomethylated DMPs included helicase like transcription factor (*HLTF*), histone acetyltransferase 1 (*HAT1*), insulin-like growth factor-binding protein complex acid labile subunit (*IGFALS*), and TNF superfamily member 8 (*TNFSF8*). Day 3 hypermethylated DMPs included single Ig and TIR domain containing (*SIGIRR*), troponin I2 (*TNNI2*) and troponin I3 (*TNNI3*).

On day 10, there were 15 hypomethylated and 19 hypermethylated DMPs in microRNAs. Hypomethylated DMPs included *HLTF, SIGIRR,* and protein inhibitor of activated STAT 4 (*PIAS4*). Hypermethylated DMPs included TNF receptor superfamily member 1A (*TNFRSF1A*) and *TNFSF8*.

On day 21, there were 12 hypomethylated and 4 hypermethylated DMPs in microRNAs. Hypomethylated DMPs included *IGFALS,* insulin-like growth factor 2 (*IGF2*), and *TNNI2*. Hypermethylated DMPs included heat shock transcription factor 4 (*HSF4*), and TNF superfamily member 13b (*TNFSF13B*).

DMRs in genes

There was a total of 8,527 DMRs that overlapped with genes across the three sampling days (Table 3.3, Supplementary Table 3.2).

Table 3.3. Number of DMRs in genes due to HS across sampling times.

Day	DMRs in genes	Hypomethylated	Hypermethylated
3	2703	42.1%	57.9%
10	2943	49.3%	50.7%
21	2881	61.7%	38.3%

On day 3, hypomethylated DMRs included genes such as *IGF2,* Insulin Like Growth Factor 2 MRNA Binding Protein 1 (*IGF2BP1*), and vascular endothelial growth factor A (*VEGFA*). Hypermethylated DMRs included heat shock transcription factor 2 binding protein (*HSF2BP*), fibroblast growth factor receptor 4 (*FGFR4*), angiopoietin 4 (*ANGPT4*), interleukin 34 (*IL34*), and interleukin 16 (*IL16*). Genes that had both hypermethylated and hypomethylated regions included insulin like growth factor 1 receptor (*IGF1R*), insulin like growth factor 2 receptor (*IGF2R*), and actin alpha 4 (*ACTN4*).

On day 10, hypomethylated DMRs included myosin heavy chain 3 (*MYH3*), heat shock protein family b member 3 (*HSPB3*), and tumor necrosis factor-alpha (*TNF*). Hypermethylated DMRs included *IGF2BP1,* insulin like growth factor 2 mRNA binding

protein 2 (*IGF2BP2*), *IGF2*, inhibitor of nuclear factor kappa b kinase subunit beta (*IKBKB*), NF-Kappa-B inhibitor Beta (*NFKBIB*), fibroblast growth factor 1 (*FGF1*), fibroblast growth factor 5 (*FGF5*), nitric oxide synthase 3 (*NOS3*), NADPH oxidase 5 (*NOX5*), actinin alpha 1 (*ACTN1*), heat shock 70 kDa protein 12B (*HSPA12B*), and *VEGFA.* Genes that had both hypermethylated and hypomethylated regions included *IGF1R, IGF2R,* and *ACTN4*.

On day 21, hypomethylated DMRs included *ACTN1,* actinin alpha 1 (*ACTN3*), *IL16*, interleukin 27 (*IL27*), interleukin 4 receptor (*IL4R*), and *IGF2.* Hypermethylated DMRs included *HSF2BP*, *ACTN4*, and myosin heavy chain 11 (*MYH11*). Genes that had both hypermethylated and hypomethylated regions included *IGF1R, IGF2R, IKBKB, NOS3*, and fibroblast growth factor 18 (*FGF18*).

In total, 365 pathways were enriched by DMRs in genes (Table 3.4; Supplementary Table 3.3). 83 pathways were shared among the days including cell survival pathways such as Ras, PI3K-Akt, and MAPK signaling pathways (Figure 3.1). Pathways involved in stress response included chemical carcinogenesis receptor activation, HIF-1, chemokine signaling, and VEGF signaling. Hormone pathways shared across days included insulin, growth hormone, and parathyroid hormone signaling pathways. Day 3 and 10 shared mTOR signaling, Cushing syndrome, apoptosis, and glucagon signaling. Day 3 and 21 shared endocrine resistance and B cell receptor signaling. Day 10 and 21 shared thyroid hormone pathways. Pathways unique to day 3 included thermogenesis and cAMP signaling. TNF signaling, microRNAs in cancer, NF-kappa B signaling, and Th1 and Th2 cell differentiation were unique to day 10. Pathways

unique to day 21 included transcriptional misregulation in cancer and rheumatoid arthritis.

When the pathways were sorted in major categories by function, the top three categories across all days were signaling pathways, endocrine system, and immune system (Figure 3.2). The smallest category across all days is metabolism. The “Other” category includes pathways that did not fit with the other categories such as digestive functions and heart diseases.

Table 3.4. Number of KEGG pathways based on DMRs in genes.

Day	Number of Pathways
3	125
10	125
21	115

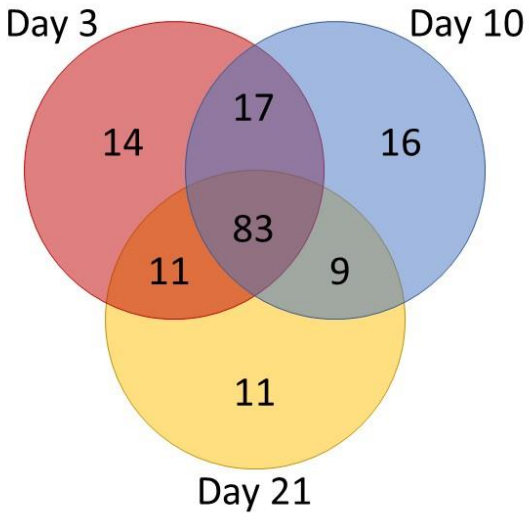

Figure 3.1. Venn diagram of KEGG pathways across days.

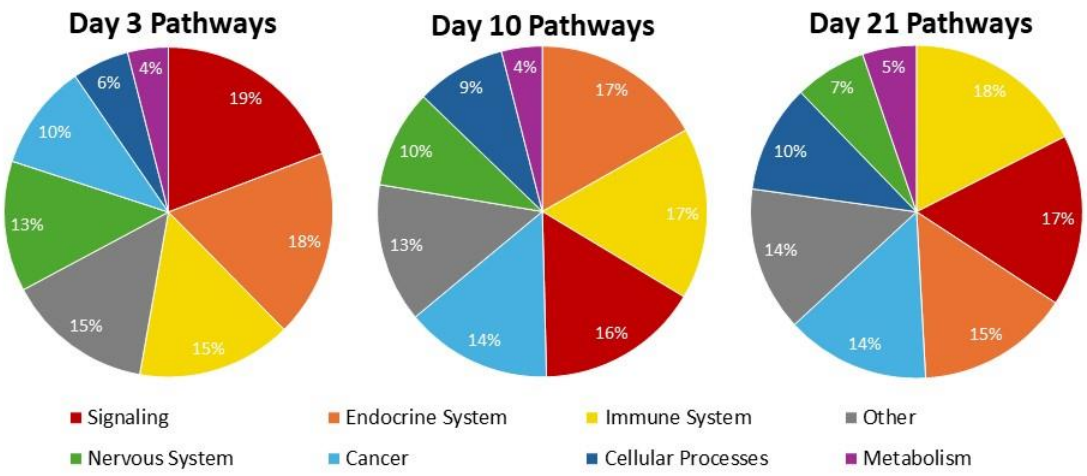

Figure 3.2. KEGG pathway categories across days.

Discussion

In this study, HS altered the methylation of genes and promoters associated with cell and muscle growth, inflammation, and stress response, which may explain the growth impairment and inflammation caused by HS. Methylation changes in growth genes and enrichment of cell proliferation pathways indicate dysregulation of said cell growth and possible tissue damage due to HS. The methylation of promoters of inflammatory and anti-inflammatory genes show a shift from acute HS on day 3 to HS adaptation on day 10. The prediction of oxidative stress due to enrichment of the HIF1A pathway agrees with the RNA analysis, also suggesting possible adaptation to the stress conditions. None of the DMPs were also differentially expressed, suggesting that DNA methylation was not the main or direct mechanism by which the genes were differentially expressed. These results demonstrate that HS alters methylation of genes involved in

growth and the immune response, which help explain physiological changes during HS, but do not fully explain changes in gene expression.

Heat stress enriched pathways involved in cell proliferation and survival, indicating methylation changes as a response and adaptation to heat stress. The PI3K-Akt and MAPK pathways can be stimulated by growth factors, inflammatory cytokines, heat shock, hypoxia, or oxidative stress (Figure 3; Bogoyevitch et al., 2010; Cuadrado and Nebreda, 2010; Cargnello and Roux, 2011; Xie et al., 2019). Both PI3K-Akt and the MAPK pathways regulate cell proliferation, survival, and apoptosis, but whether the pathways activate or inhibit these functions depends on the specific pathway and stimuli (Bogoyevitch et al., 2010; Cuadrado and Nebreda, 2010; Cargnello and Roux, 2011; Xie et al., 2019). The enrichment of these pathways across all three days suggests changes in both growth factor signaling and stress response due to HS, such as fluctuations of plasma TNFα, leukocytes, and insulin observed in prior HS studies (Swanson et al., 2020). RNA analysis of these same samples did not predict changes in cell proliferation and survival pathways due to HS (Reith et al., 2022). This implies changes in DNA methylation had little to no observable effect on expression of genes related to cell proliferation and survival. There may be indirect effects that have not yet been elucidated.

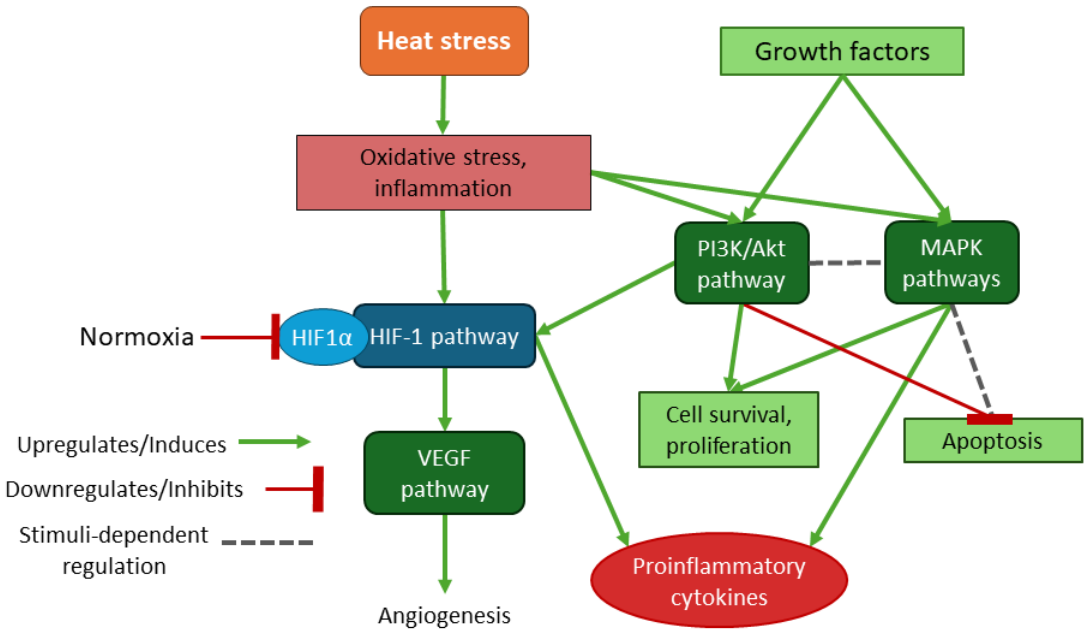

Figure 3.3 Interaction of the HIF-1 pathway with heat stress and other pathways.

Differential methylation of insulin-like growth factor (IGF) related genes and enrichment of endocrine and metabolism pathways also may explain the skeletal muscle growth deficits caused by heat stress. Skeletal muscle growth is regulated by multiple hormones including thyroid hormone (TH), glucocorticoids, growth hormone (GH), and IGF-1 (Schakman et al., 2013; Jiang and Ge, 2014; Martín et al., 2018). In broad terms, GH, TH, and IGF-1 promote skeletal muscle growth and development while glucocorticoids like cortisol breakdown muscle (Schakman et al., 2013; Jiang and Ge, 2014; Martín et al., 2018). Heat stress increases plasma cortisol concentrations while decreasing GH, TH, and IGF-1 (Rhoads et al., 2009; Baumgard and Rhoads, 2013; Kim et al., 2021; Anjali et al., 2023). However, the difference in cortisol concentration between HS and control groups is negated during pair-fed trials, suggesting other factors

are impairing growth, such elevated inflammatory cytokines (Swanson et al., 2020). GH pathways were enriched across all days, and cortisol and TH pathways were enriched on at least one day, suggesting dysregulation of muscle growth mediated by changes in methylation throughout the trial. Gene DMRs related to growth included IGFs, IGF receptors, and IGF binding proteins. The *IGFALS* promoter was hypomethylated on day 3, and both *IGFALS* and *IGF2* had hypomethylated promoters on day 21. IGFALS forms a ternary complex with an IGF and IGF binding protein to increase the half-life of IGFs in the bloodstream (Domené and Domené, 2020). While IGFs and IGFALS are mainly produced from the liver, IGFs are also produced by skeletal muscle when it is damaged and for muscle differentiation (Hill et al., 2003; Song et al., 2013; Ahmad et al., 2020). Differential methylation of IGF-related genes and promoters may be evidence of impaired growth, muscle damage, and attempts to repair damage caused by heat stress. Previous RNA analyses did not suggest changes in growth metabolism in skeletal muscle (Reith et al., 2022). While changes in DNA methylation altered the opportunity for gene expression, there may have been other regulatory factors such as mRNA stability and silencing by microRNAs that resulted in no observed difference in RNA counts. For example, microRNA-187 decreases IGF-1R protein expression (Han et al., 2017), and IGF-1 regulates IGFBP-4 mRNA stability (Huynh, 2000). Thus, post-transcriptional mechanisms may have prevented significant changes in gene expression that could not be detected in the RNA analysis.

Enrichment of the HIF-1 and vascular endothelial growth factor (VEGF) pathways across all three days may be evidence that muscle was responding to oxidative stress from HS. This could explain previously published RNA analyses from these

animals, which predicted oxidative stress in muscle due to HS (Reith et al., 2022). Both the hypoxia-inducible factor 1 pathway (HIF-1) and VEGF pathways are stimulated by hypoxia, but HIF-1 can also be induced by HS, oxidative stress, and PI3K-Akt activation (Figure 3; Majmundar et al., 2010; Xie et al., 2019; Zhang et al., 2023). The enrichment of HIF-1, VEGF, and PI3K-Akt pathways together further supports the possibility of oxidative stress in the muscle. Activation of the HIF-1 pathway under HS can help the tissue adapt to stressful conditions. Heat acclimation research suggests that the overlap of HS and hypoxia pathways can provide cross-tolerance to both stressors (Ely et al., 2014). Thus, while the muscle may have been experiencing hypoxic conditions, the HIF-1 pathway could facilitate adaptation to the stress environment.

Methylation of inflammatory genes and pathways was also affected by HS, demonstrating a possible shift from an acute heat stress response to anti-inflammatory mechanisms. On day 3 the *SIGIRR* promoter was hypermethylated while on day 10 it was hypomethylated. SIGIRR, also known as IL-1R8, is an interleukin 1 receptor that negatively regulates the activation of other interleukin and toll-like receptors, thus modulating inflammatory responses (Molgora et al., 2018). The silencing of the *SIGIRR* promoter on day 3 would inhibit *SIGIRR* expression, allowing inflammatory receptors to be activated. When combined with enrichment of immune response pathways on day 3, this may be evidence of an acute inflammatory response to heat stress. The same promoter becomes hypomethylated on day 10, indicating possible anti-inflammatory mechanisms. Further support of this is the hypermethylated promoter of *TNFRSF1A* on day 10. *TNFRSF1A* codes for TNFR1, a receptor for TNFα that is expressed in most cells (Akdis et al., 2016). When TNFα binds to TNFR1, it initiates several pathways including

MAPK and NF-kappa B, which leads to production of inflammatory cytokines (Doyle and O'Neill, 2006; Akdis et al., 2016; Wang et al., 2023). If *TNFRSF1A* expression was silenced by methylation, then the TNFα pathway would be less likely to be activated by TNFR1, decreasing or preventing production of inflammatory cytokines. The enrichment of TNF and NF-kappa B pathways on day 10 also suggests regulation of inflammatory pathway genes. Changes in expression of immune receptors and interleukins between short term HS and long-term HS have suggested cattle start adapting to HS around 10 days (Bharati et al., 2017). The methylation results support that day 10 may be a transition period from responding to acute HS to an adaptation to HS conditions.

The lack of DMPs and gene DMRs that were also differentially expressed in the RNA analysis (Reith et al., 2022) implies that HS altered gene expression mainly through other regulatory mechanisms. The samples from this study were previously used for RNA analysis. When the DMPs and gene DMRs from this study were compared to the differentially expressed genes (DEGs) due to heat stress in skeletal muscle, there was no overlap between DMP and DEGs. Only one DEG overlapped with a gene DMR from the same day: microtubule associated scaffold protein 1 (*MTUS1*), which was upregulated due to HS on day 21 and had a hypomethylated DMR in intron 1 on the same day. Transcription is regulated by multiple mechanisms including promoters, enhancers, transcription factors, chromatin structure, and DNA methylation (Cramer, 2019). Heat stress can alter histone modifications associated with chromatin remodeling, transcription activation, and gene repression (Zheng et al., 2021). There is also post-transcriptional regulation induced by HS through expression of microRNAs and N6-methyladenosine (m6A) RNA modification (Mishra, 2022; Qi et al., 2022). There were several

microRNAs that had differential methylation in putative promoter regions, implying microRNAs as a possible mechanism used to alter gene expression. The low number of animals used for the DNA methylation analyses may have also contributed to the lack of data overlap, a limitation of this study.

For the one gene significant in both studies, *MTUS1*, the changes in gene regulation may have been a response to tissue damage from HS. The hypomethylated first intron of *MTUS1* could have contributed to its upregulation as there is evidence that genes that have methylated transcription factor binding motifs in the first intron have decreased gene expression (Anastasiadi et al., 2018). *MTUS1* codes for angiotensin II (AT2) receptor-interacting proteins that have been associated with tumor suppression and DNA repair (Ranjan et al., 2021). *MTUS1* is upregulated in mice kidneys exposed to hyperoxic conditions, suggesting an association with oxidative stress (Hinkelbein et al., 2015). However, cattle in heat stress have increased respiration rates, likely causing hyperoxemia, not hypoxia, thus upregulation of *MTUS1* was likely from HS-induced oxidative stress. Overexpression of *MTSU1* in human glioblastoma cells slows cancer growth (Ranjan et al., 2021), implying *MTUS1* also controls cell growth and proliferation. By day 21, the cattle are in chronic heat stress, and likely have tissue damage from inflammation and oxidative stress. Thus, upregulation of *MTUS1* could be part of adaptation and recovery from HS.

Heat stress did not alter methylation of genes and promoters of previously differentially expressed genes, save one, implying gene expression was altered through other mechanisms. However, the differentially methylated genes and promoters were associated with cell survival, growth, and stress response, all of which are impacted by

heat stress. Thus, these data are evidentiary that DNA methylation played a small role in changes in gene expression. Further studies are needed to elucidate the mechanisms by which HS alters gene expression.

Acknowledgements

This project is based on the research that was partially supported by the Nebraska Agricultural Experiment Station with funding from the Hatch Multistate Research capacity funding program (Accession Number 1011055) from USDA National Institute of Food and Agriculture. Portions of this work were completed utilizing the Holland Computing Center of the University of Nebraska, which receives support from the Nebraska Research Initiative.

Supplementary Tables

Supplementary Table 3.1. Differentially expressed promoters due to HS across all days (XLSX, 65 KB).

Supplementary Table 3.2. Differentially expressed regions that overlap with genes due to HS across all days (XLSX, 614 KB).

Supplementary Table 3.3. Pathways enriched by DMRs across all days (XLSX, 66.4 KB).

CHAPTER 4: CHANGES IN DNA METHYLATION BETWEEN 48 HOURS OF HS AND 5 DAYS OF RECOVERY IN BEEF CATTLE SKELETAL MUSCLE

Introduction

Heat stress (HS) is a current issue for livestock producers due to its negative effect on animal health and productivity. Livestock exposed to heat stress have decreased dry matter intake and average daily gain, often resulting in a lighter carcass weight at harvest (Mitlöhner et al., 2001; Gaughan et al., 2010; Swanson et al., 2020). Heat stress also induces systemic inflammation which may interfere with growth and metabolism (Min et al., 2016; Barnes et al., 2019; Swanson et al., 2020). Heat stress causes these changes, in part, by altering gene expression and regulation. Transcriptome analyses in sheep, cattle, and chickens revealed that HS alters expression of genes associated with metabolism, inflammation, oxidative stress, and signal transduction in many tissues such as PBMCs, muscle, adipose, liver and lung (Li et al., 2019; Garner et al., 2020; Reith et al., 2022; Nan et al., 2023). Heat stress can also alter DNA methylation, often in the promoters and genes associated with immune response, metabolism, and signal transduction (Del Corvo et al., 2021; Livernois et al., 2021). DNA methylation regulates gene expression; high methylation of promoters and first exons silences gene expression (Moore et al., 2013; Anastasiadi et al., 2018; Li et al., 2018). Low methylation of the first intron and increased methylation density of internal exons have been linked to increased gene expression (Anastasiadi et al., 2018; Li et al., 2018).

Previous RNA and DNA methylation studies compared HS cattle to thermoneutral counterparts to elucidate the effects of HS on gene expression and regulation in skeletal muscle throughout a 21-day trial (Reith et al., 2022). The genes altered by HS indicated

oxidative stress, inflammation, and growth dysfunction in skeletal muscle. However, the timepoints analyzed in those studies included 10 and 21 days of HS, with no timepoints after exiting HS. Natural HS events are often more acute, such as a 2-3-day heat wave. Thus, the purpose of this study was to investigate the skeletal muscle methylome of cattle immediately after 48 hours of HS and 5-days later (recovery) using reduced representation bisulfite sequencing (RRBS). Assuming that inflammation will decrease, and growth will no longer be impaired after exiting HS, we hypothesize that inflammatory genes will be hypermethylated 5 days post-HS, but anti-inflammatory and cell growth genes will be hypomethylated.

Materials and Methods

This study was approved by the Institutional Animal Care and Use Committee at the University of Nebraska – Lincoln. A total of 14 one-year old composite (Red Angus, Simmental, Gelbvieh) steers (avg. 308.7 kg) were exposed to heat stress (HS) conditions of 35°C + 35% relative humidity (Temperature Humidity Index = 81) for 12h/day for two days (48h). The cattle were split into 4 blocks due to the size restriction of the chambers in which they were housed. Cattle were limit fed 5.9 kg/day of a diet consisting of 41% grass hay, 35% wheat straw, 20% SweetBran, and 4% mineral mix. Each round of cattle was group housed at a THI of 68 (21°C, 70% humidity) for at least six days before entering the heat chamber, and at least five days after exiting the heat chamber. Cattle were individually penned and fed while in the heat chambers with access to water 24 hours a day.

Longissimus dorsi samples were biopsied immediately after exiting the heat chamber, then again 5 days later on the contralateral side. At the time of biopsy, 2 to 3 mL of local anesthetic (2% lidocaine HCl) was injected prior to collection of samples through a 5-cm incision approximately 20 cm cranial of the pelvic bone. The samples were flash-frozen in liquid nitrogen and stored at −80 °C.

DNA was isolated using the Qiagen Gentra Puregene kit (Qiagen, Germantown, MD) following the manufacturer protocol for 30 mg of tissue, with an RNase A solution step. RRBS library prep and sequencing on an Illumina NovaSeq was performed at Admera Health (South Plainsfield, NJ) using 150 bp paired-end reads to a targeted depth of 14 million reads/sample.

The quality of the sequence reads was checked using FastQC v0.11.7 (Andrews, 2010). TrimGalore v0.6 (Krueger et al., 2023) was used with rrbs, non_directional, and paired options to trim the sequence adapters (Krueger et al., 2023). Bismark v0.24 (Krueger and Andrews, 2011) was used to bisulfite-convert the bovine reference genome (ARS-UCD1.2) then align trimmed reads to the converted genome (score_min L,0,-0.4 and non_directional options). Methylated calls were obtained with Bismark methylation extractor (options: paired-end, merge_non_CpG, bedGraph, counts, no_overlap, ignore_3prime 1 options).

The observed methylation calls were used for differentially methylated region (DMR) analysis in methylkit (Akalin et al., 2012) requiring a minimum read coverage of 5 reads per base analysis. Regions were generated using a sliding-window of 1 kb with a 500 bp step size, then filtered for regions with a minimum of 10 bases. Analysis compared samples collected 5 days post-HS to those immediately after 48 hours of HS.

DMRs had thresholds of 15% methylation difference and a q-value < 0.05. Differentially methylated promoters (DMPs) were defined as DMRs within 2 kb of the 5' of a gene. DMRs that overlapped with genes were used as an input into DAVID to explore KEGG pathways (Huang et al., 2009; Sherman et al., 2022).

Results

On average, 15.3 million reads were obtained per sample. The mapping average was 85.6% and the average of reads that mapped uniquely was 26.7%.

There were 81 DMPs when comparing samples at 5 days post-HS to samples at 48 hours of HS; 39.5% were hypomethylated and 60.5% were hypermethylated (Supplementary Table 4.1). Hypermethylated promoter regions included *HSPB9, C1QTNF3,* and *MIR187.* Hypomethylated promoter regions included *MYLK2* and *SIGIRR.*

There were 1,015 DMRs that overlapped 606 unique genes; 44.8% were hypomethylated and 55.2% were hypermethylated (Supplementary Table 4.2). Genes with hypomethylated DMRs at 5 days post-HS included *GNAS, IGF1R, IGF2, IGF2BP1, IGFBP4, IGF2R,* and *IKBKB.* Genes with hypermethylated DMRs 5 days post-HS included *FGF5, FGFR1, FGFR3, TNFAIP2* and *GNB1*.

Considering the genes with DMRs, 88 pathways ($P < 0.1$) were enriched (Supplementary Table 4.3); the pathways were categorized into general functions (Figure 4.1). Endocrine and signaling pathways were the most abundant (19% each), while metabolism was the least abundant. Of the endocrine pathways, thyroid hormone, parathyroid hormone, insulin, and growth hormone pathways were enriched. Hypoxia-

induced factor 1 (HIF-1) and vascular endothelial growth factor (VEGF) signaling pathways were also enriched. Pathways involved in cellular proliferation and survival included MAPK (contains ERK1/2, JNK, and p38 pathways), PI3K-Akt and mTOR signaling. Several of these pathways share common stimuli and interact (Figure 4.2).

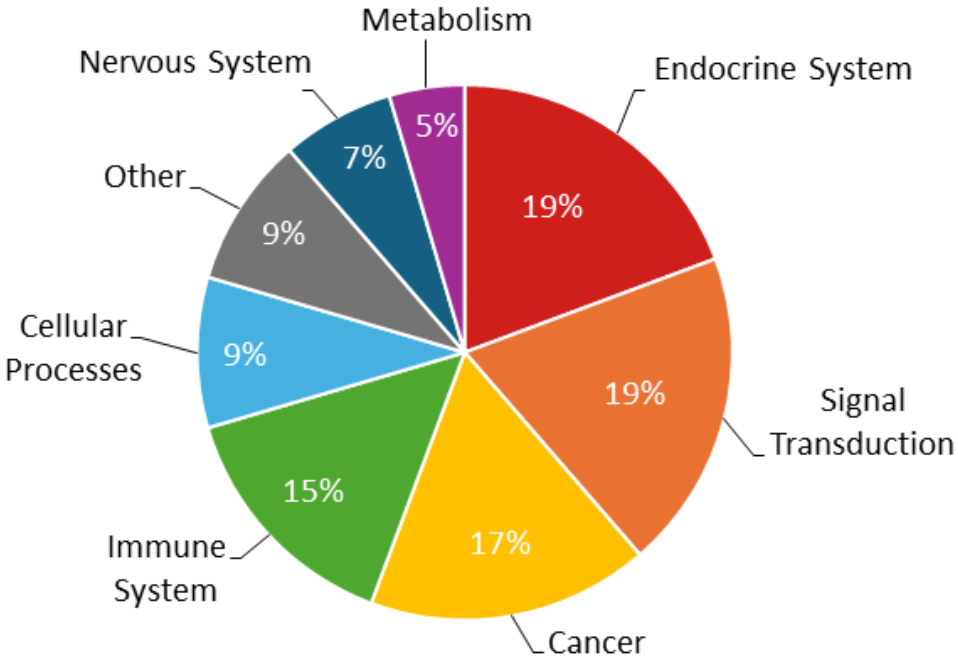

Figure 4.1. Pathway analysis of gene DMRs based upon 606 differentially methylated genes of skeletal muscle comparing samples from 5 days post-HS to 48 hours of HS.

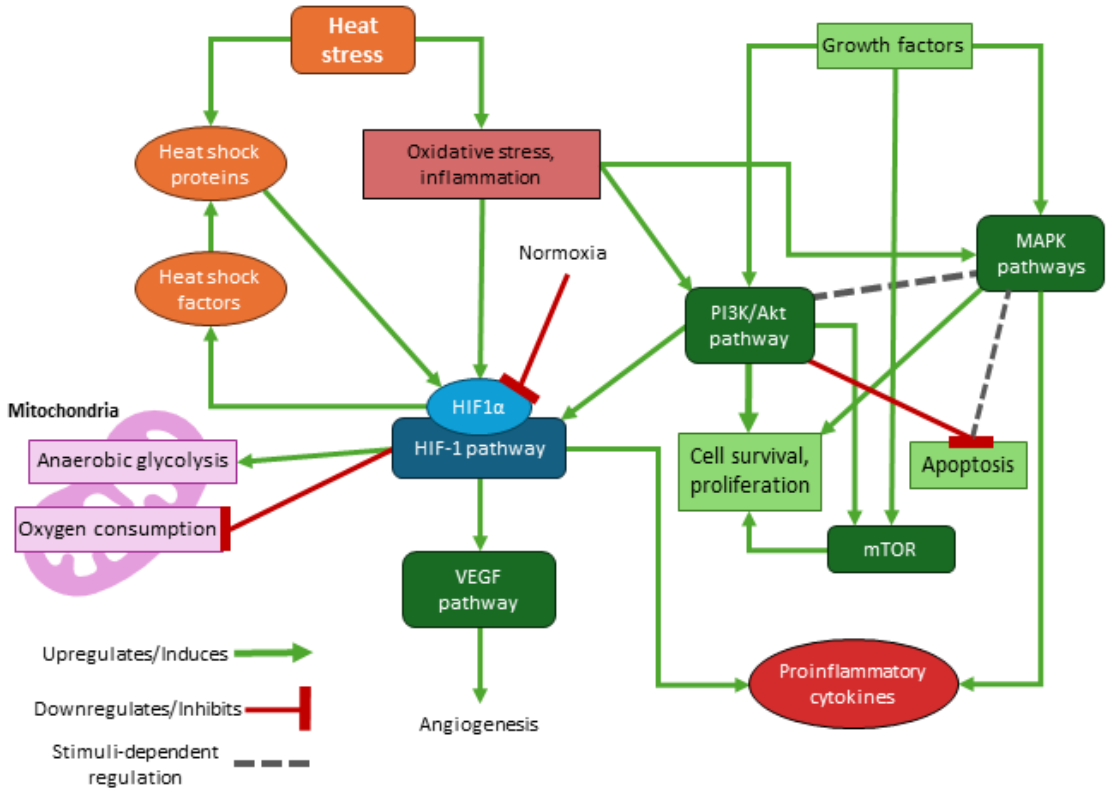

Figure 4.2. The interaction between the HIF-1 pathway, heat stress, and growth signaling.

Discussion

In this study, DNA methylation changes in muscle promoted recovery from HS by silencing inflammatory genes, demethylating anti-inflammatory and growth genes, and was predicted to enrich stress response and cell growth pathways, supporting the hypothesis. Compared to methylation status immediately after 48 hours of HS, inflammatory genes after 5 days of recovery were hypermethylated, likely preventing gene expression. This, with hypomethylated anti-inflammatory genes during recovery show suppression of HS-induced inflammation. Stress-induced pathways such as HIF-1 and VEGF were enriched, suggesting regulation of those pathways after the cattle were

removed from stress. Genes involved in cell and tissue growth were differentially methylated, indicating changes in growth regulation after HS, further supported by enrichment of PI3/Akt, MAPK, and MTOR pathways. Our results provide evidence that DNA methylation plays a role in recovery from HS in cattle, with possible HS treatments taking advantage of the differentially methylated genes found in this study to further improve recovery.

Cell and muscle growth

Evidence indicates muscle growth signaling was recovering after impairment from HS, promoting muscle growth and development. Enrichment of genes involved in cell survival pathways such as MAPK, PI3K-Akt, and mTOR indicates possible cell growth and recovery from heat stress. Cell growth and proliferation is how muscle tissues grow and develop, a critical function for meat animals (Jiang and Ge, 2014). Muscle hypertrophy is associated with activated mTOR and PI3K-Akt, thus enrichment of these pathways could also indicate muscle growth after HS-impairment (Bodine et al., 2001). There are several MAPK pathways, each named after the key mitogen-activated protein kinase (MAPK) in the pathway (Cargnello and Roux, 2011). The ERK1/2 MAPK pathway is stimulated by growth factors (Cargnello and Roux, 2011). There were genes with DMRs in the ERK1/2 MAPK pathway, including *IGF2* and *IGF1R*, which are upstream regulators, indicating possible growth factor signaling changes. In response to growth stimuli, the ERK1/2 MAPK pathway upregulates cell proliferation and inhibits apoptosis (Bogoyevitch et al., 2010; Cargnello and Roux, 2011). A change in growth signaling post-HS is also supported by enrichment of the PI3K-Akt pathway, suggested by

differential methylation of *IGF2*, *IGF1R*, *AKT1*, and hypomethylation of the *CHRM1* promoter, an upstream receptor, and 15 other genes with DMRs. This pathway also promotes cell proliferation and survival when stimulated by IGF-1, TGF, TNF-α, and insulin (Xie et al., 2019). Lastly, the mTOR pathway regulates myofibrillar protein synthesis and cell growth, and is upregulated by PI3K-Akt, insulin, and IGF-1/IGF-2 (Bodine et al., 2001; Hay and Sonenberg, 2004). Further support for changes in growth signaling post-HS is the differential methylation of growth genes and enrichment of growth hormone and thyroid hormone pathways. Growth hormone and IGF-1 promote skeletal muscle growth by upregulating cell proliferation pathways and protein synthesis, while inhibiting protein degradation (Jiang and Ge, 2014; Martín et al., 2018). Thyroid hormone induces regeneration and promotes skeletal muscle metabolism (Martín et al., 2018).

While evidence indicates growth factor stimulation for cell survival pathways, there are also a few gene DMRs in the cell survival pathways that are stimulated by stress. The p38 and JNK MAPK pathways are activated by cell stressors such as inflammation and oxidative stress (Bogoyevitch et al., 2010; Cuadrado and Nebreda, 2010). The JNK MAPK pathway regulates cell proliferation and induces apoptosis in response to stress (Bogoyevitch et al., 2010; Cargnello and Roux, 2011), while the p38 pathway produces proinflammatory cytokines, and regulates apoptosis and cell differentiation (Cuadrado and Nebreda, 2010). Post-HS there should be fewer stressors to stimulate these pathways. Therefore, methylation changes in p38 and JNK MAPK pathways may be an attempt to downregulate them.

Stress acclimation and recovery

The enrichment of the HIF-1 and vascular endothelial growth factor (VEGF) pathways may be evidence of recovery from HS. The hypoxia-inducible factor 1 (HIF-1) pathway is stimulated by HS, hypoxia, oxidative stress, and PI3K-Akt activation (Majmundar et al., 2010; Xie et al., 2019; Zhang et al., 2023). Heat acclimation research suggests that the overlap of HS and hypoxia pathways can provide cross-tolerance to both stressors, which is a possible explanation for why HIF-1 was enriched (Ely et al., 2014). Heat shock proteins induced by heat stress stabilize *HIF1α* mRNA, which results in activation of the HIF-1 pathway (Ely et al., 2014). HIF-1α protein upregulates expression of heat shock factors that induce expression of heat shock proteins (Ely et al., 2014). Thus, the HIF-1 and heat shock pathways are both activated to help the animal adapt to hypoxic or heat stress environments. The main function of the HIF-1 pathway is to maintain oxygen homeostasis through transcriptional induction of genes involved in mitochondria activity and glycolysis to reduce oxygen consumption (Hu et al., 2003; Majmundar et al., 2010). Another downstream effect of HIF-1 includes increased production of inflammatory cytokines (Majmundar et al., 2010; Corcoran and O'Neill, 2016). HIF-1 also activates the VEGF pathway, which induces angiogenesis, the formation of new blood vessels from current ones, to improve distribution of oxygen to tissues (Majmundar et al., 2010). Providing additional support to the observed differences in methylation, in prior transcriptome studies, the HIF-1 and VEGF pathways were predicted to be upregulated in adipose and the *HIF1A* gene was upregulated in muscle due to HS (Reith et al., 2022). Post-HS, these pathways may have been inactivated as the stress stimuli was removed.

It has been documented by our team as well as others that HS upregulates genes involved in stress and inflammation through both transcriptome analyses (Lu et al., 2019; Garner et al., 2020; Reith et al., 2022), and physiological observations (Min et al., 2016; Bharati et al., 2017; Zhang et al., 2023). The methylation analysis in this study suggests regulation of the stress response and inflammation post-HS. *SIGIRR*, also known as IL-1R8, is an interleukin 1 receptor that negatively regulates the activation of other interleukin and toll-like receptors, thus modulating inflammatory responses (Molgora et al., 2018). Hypomethylation of the *SIGIRR* promoter post-HS would allow increased expression of IL-1R8 which could reduce inflammation signaling. MicroRNA-187 upregulates *TNF* expression and downregulates IGF-1R post-transcription (Lynam-Lennon et al., 2016; Han et al., 2017). In these data, the promoter of *MIR-187* was hypermethylated; silencing of *MIR-187* would likely reduce expression of *TNF*, a proinflammatory mediator (Akdis et al., 2016), as well as allow IGF-1R to function as a growth regulator. The heat shock protein family B member 9 (*HSPB9*) promoter was also hypermethylated. *HSPB9*, like most heat shock proteins, is upregulated by high temperatures and regulates the stress response (Tedesco et al., 2022), though gene expression is normally low in skeletal muscle (Xun et al., 2015). Still, hypermethylation of the promoter post-HS suggests that *HSPB9* was suppressed once the animals were no longer stressed.

Complement C1q Tumor Necrosis Factor-Related Protein 3 (*C1QTNF3*) is an anti-inflammatory mediator and downstream molecule of HIF1α (Li et al., 2017; Okada et al., 2020). The *C1QTNF3* promoter was hypermethylated, which seems to contrast the other anti-inflammatory results. However, an alternate view is that the *C1QTNF3*

promoter was less methylated at 48 hours of HS compared to 5 days post-HS, implying possible increased expression during the HS trial to combat inflammation and hypoxic-like conditions. Genes such as *SIGIRR* were perhaps expressed during recovery to prevent further activation of inflammatory pathways. These results suggest that there are complex changes in the regulation of inflammation after heat exposure.

Overall, there were changes in DNA methylation of genes involved in regulation of growth, inflammation, and stress during between HS and recovery. Evidence suggests muscle growth was no longer impaired by heat stress and pro-inflammatory signaling and stress-induced pathways were inactivated. While HS induces inflammation and suppresses growth during exposure, the results of this study suggest the methylome adjusts after HS to provide for improvements in growth signaling inflammation regulation.

Supplementary Tables

Supplementary Table 4.1. Differentially methylated promoter regions at five days post-HS compared to 48 hours of HS.

Chromosome	Start of region	End of region	P-value	q-value	Methylation difference	Gene
3	26575001	26576000	<0.001	<0.001	17.80	*IGSF3*
3	31564501	31565500	<0.001	<0.001	-36.15	*INKA2*
4	12063001	12064000	<0.001	<0.001	37.88	*PEG10*
4	12063501	12064500	<0.001	<0.001	15.53	*PEG10*
4	12064001	12065000	<0.001	<0.001	32.84	*SGCE*
4	24076001	24077000	<0.001	0.007	21.02	*MEOX2*
4	68911001	68912000	<0.001	<0.001	24.41	*HOXA4*
4	71624001	71625000	<0.001	0.007	23.03	*NPY*
4	113410001	113411000	0.001	0.013	18.54	*TMEM176B*
5	104159501	104160500	<0.001	<0.001	19.05	*CD9*
5	115685001	115686000	<0.001	0.007	19.10	*UPK3A*
5	116406501	116407500	<0.001	0.004	28.10	*MIRLET7A-3*
5	116407501	116408500	<0.001	<0.001	25.32	*MIRLET7A-3*
5	116407501	116408500	<0.001	<0.001	25.32	*MIR2443*
5	116407501	116408500	<0.001	<0.001	25.32	*MIRLET7B*
5	116408001	116409000	<0.001	<0.001	18.42	*MIRLET7A-3*
5	116408001	116409000	<0.001	<0.001	18.42	*MIR2443*
5	116408001	116409000	<0.001	<0.001	18.42	*MIRLET7B*
5	119561001	119562000	<0.001	<0.001	35.79	*TRABD*
6	117382501	117383500	0.008	0.047	16.02	*MIR2449*
7	4615501	4616500	<0.001	0.002	-15.78	*KXD1*
7	52394001	52395000	<0.001	0.005	16.32	*SLC25A2*
9	42572001	42573000	<0.001	<0.001	-15.76	*SOBP*
11	98855501	98856500	<0.001	<0.001	17.90	*MIR3604-2*
11	104077001	104078000	<0.001	<0.001	26.56	*EGFL7*
11	104084501	104085500	0.002	0.018	15.76	*MIR126*
11	106206001	106207000	<0.001	0.001	19.58	*MIR12014*
11	106240501	106241500	<0.001	<0.001	22.98	*CYSRT1*
12	86498501	86499500	0.002	0.016	15.69	*F10*
13	53957001	53958000	<0.001	<0.001	16.23	*TPD52L2*
13	61354501	61355500	<0.001	<0.001	-15.60	*MYLK2*
14	81785501	81786500	<0.001	<0.001	-29.94	*MTBP*
15	13888001	13889000	<0.001	<0.001	26.17	*MAML2*
16	43656501	43657500	<0.001	0.004	-15.09	*CTNNBIP1*

16	75195501	75196500	0.002	0.018	-22.31	*MIR6121*
16	80420501	80421500	<0.001	<0.001	27.08	*PTPN7*
17	3832501	3833500	<0.001	<0.001	28.07	*SFRP2*
17	53508501	53509500	0.003	0.024	-25.52	*RHOF*
17	63426501	63427500	<0.001	0.009	19.69	*TRPV4*
17	71545001	71546000	0.002	0.02	18.69	*UPB1*
17	71653001	71654000	<0.001	0.005	-27.91	*MIR2323*
17	71653501	71654500	<0.001	0.005	-27.91	*MIR2323*
17	72789001	72790000	<0.001	<0.001	-15.91	*SEPTIN5*
18	44104001	44105000	0.002	0.02	-5.54	*CHST8*
18	55426501	55427500	<0.001	<0.001	28.99	*BCAT2*
18	56572001	56573000	<0.001	<0.001	19.50	*SPIB*
18	65545001	65546000	<0.001	<0.001	-30.70	*ZNF274*
19	37946001	37947000	<0.001	<0.001	31.39	*HOXB2*
19	42257001	42258000	<0.001	<0.001	18.74	*HSPB9*
19	42257501	42258500	<0.001	<0.001	18.74	*HSPB9*
19	49854001	49855000	<0.001	<0.001	-19.41	*ZNF750*
19	49854501	49855500	<0.001	<0.001	-22.53	*ZNF750*
19	56021001	56022000	0.002	0.015	17.46	*LLGL2*
20	5702001	5703000	<0.001	0.004	-20.78	*C20H5orf47*
20	5702501	5703500	<0.001	0.004	-20.78	*C20H5orf47*
20	39719501	39720500	<0.001	<0.001	30.91	*C1QTNF3*
20	71964001	71965000	<0.001	0.003	15.01	*LOC524810*
21	68316001	68317000	<0.001	0.007	-22.04	*XRCC3*
22	52731001	52732000	<0.001	<0.001	-18.06	*PRSS45*
22	52731501	52732500	<0.001	<0.001	-18.03	*PRSS45*
22	60447001	60448000	0.006	0.038	-15.79	*C22H3orf22*
23	27982001	27983000	0.003	0.025	-16.91	*POU5F1*
24	21218501	21219500	<0.001	0.002	20.29	*MIR187*
24	21219001	21220000	<0.001	0.002	20.29	*MIR187*
24	40126501	40127500	<0.001	<0.001	72.05	*LRRC30*
24	58202001	58203000	<0.001	0.004	-22.55	*GRP*
25	13684501	13685500	0.003	0.026	23.22	*RRN3*
25	13685001	13686000	0.003	0.026	23.22	*RRN3*
25	36086501	36087500	<0.001	<0.001	28.66	*C25H7orf61*
25	38984501	38985500	<0.001	0.003	-15.72	*SLC29A4*
26	23502001	23503000	<0.001	<0.001	20.55	*AS3MT*
27	6956001	6957000	<0.001	<0.001	26.20	*DEFB*
28	45021001	45022000	0.002	0.016	20.40	*CXCL12*
29	41233001	41234000	<0.001	<0.001	-18.80	*CHRM1*
29	44871001	44872000	<0.001	<0.001	-22.00	*LRFN4*

29	45329501	45330500	<0.001	0.005	-17.61	*PTPRCAP*
29	45935001	45936000	0.001	0.014	-22.71	*PPP6R3*
29	49637001	49638000	0.001	0.012	-25.76	*LSP1*
29	49649501	49650500	<0.001	<0.001	-17.66	*TNNI2*
29	50871001	50872000	<0.001	<0.001	-33.29	*SIGIRR*
29	50871501	50872500	<0.001	<0.001	-31.17	*SIGIRR*

Supplementary Table 4.2. Differentially methylated regions that overlap with genes at five days post-HS compared to 48 hours of HS (XLSX, 57.1 KB).

Supplementary Table 4.3 Pathways enriched by gene DMRs.

Category	Term	P-Value	Genes
Endocrine System	bta04919: Thyroid hormone signaling pathway	<0.001	PRKCB, ATP2A3, GATA4, ATP2A1, PRKCA, ACTB, SLC9A1, PLCB4, RXRA, FXYD2, AKT1, PLCG1, RAF1, PLCD1, PFKP
Signal Transduction	bta04072: Phospholipase D signaling pathway	<0.001	DGKD, PRKCA, ADCY7, DGKZ, AGPAT2, DNM1, AGPAT4, PLCB4, LPAR5, DGKQ, GNA12, GNAS, AKT1, PLCG1, RAF1, RALGDS
Signal Transduction	bta04015: Rap1 signaling pathway	<0.001	PRKCB, ITGB2, PRKCA, ADCY7, ACTB, IGF1R, FGF5, PLCB4, LPAR5, RASSF5, GNAS, RAC3, AKT1, PLCG1, RAF1, FGFR3, RALGDS, BCAR1, FGFR1
Cancer	bta05200: Pathways in cancer	<0.001	CAMK2A, ADCY7, IGF1R, FGF5, IKBKB, WNT6, RXRA, RASSF5, GNA12, ERBB2, AKT1, RAC3, PLCG1, BAK1, RALGDS, ITGA3, PRKCB, FZD7, IGF2, AXIN1, PRKCA, HEYL, PLCB4, LPAR5, COL4A1, GNB1, GNAS, BCL2, RAF1, FGFR3, PPARD, FGFR1
Cellular Processes	bta04510: Focal adhesion	<0.001	VWF, ITGA3, PRKCB, PRKCA, PARVB, ACTB, IGF1R, COMP, PARVG, COL4A1, ERBB2, BCL2, RAC3, AKT1, RAF1, BCAR1, PAK4
Cellular Processes	bta04144: Endocytosis	<0.001	IQSEC1, VPS37C, ASAP3, VPS37D, ASAP1, EPS15L1, AP2A2, IGF2R, DNM1, IGF1R, EPN2, EHD1, GRK1, CAPZB, CHMP4C, LDLRAP1, WASHC1, FGFR3, RAB7A
Cancer	bta05205: Proteoglycans in cancer	<0.001	PRKCB, FZD7, CAMK2A, IGF2, PRKCA, ACTB, SLC9A1, IGF1R, WNT6, CTTN, ERBB2, AKT1, PTPN6, PLCG1, EZR, RAF1, FGFR1
Other	bta04971: Gastric acid secretion	<0.001	PLCB4, PRKCB, KCNQ1, CAMK2A, GNAS, PRKCA, EZR, ADCY7, ACTB, SLC9A1
Cellular Processes	bta04810: Regulation of actin cytoskeleton	<0.001	ITGA3, ITGB2, BAIAP2, SSH3, ACTB, SLC9A1, FGF5, LPAR5, GNA12, RAC3, AKT1, EZR, ARHGEF7, RAF1, FGFR3, BCAR1, FGFR1, PAK4

Signal Transduction	bta04070: Phosphatidylinositol signaling system	<0.001	PLCB4, DGKD, PRKCB, DGKQ, ITPKA, ITPK1, PI4KA, PRKCA, PLCG1, DGKZ, PLCD1
Signal Transduction	bta04261: Adrenergic signaling in cardiomyocytes	<0.001	CAMK2A, ATP2A3, ATP2A1, PRKCA, ADCY7, SLC9A1, PLCB4, KCNQ1, FXYD2, GNAS, BCL2, AKT1, SCN5A, SCN4B
Signal Transduction	bta04020: Calcium signaling pathway	<0.001	RYR1, PRKCB, CAMK2A, ATP2A3, ATP2A1, PRKCA, NFATC1, ADCY7, CACNA1E, FGF5, PLCB4, GRIN3A, ERBB2, ITPKA, GNAS, PLCG1, FGFR3, PLCD1, FGFR1
Signal Transduction	bta04014: Ras signaling pathway	<0.001	PRKCB, IGF2, PRKCA, IGF1R, FGF5, IKBKB, ZAP70, SYNGAP1, RASSF5, GNB1, RAC3, AKT1, PLCG1, RAF1, FGFR3, RALGDS, FGFR1, PAK4
Immune System	bta04660: T cell receptor signaling pathway	0.001	IKBKB, ZAP70, PTPRC, GRAP2, AKT1, NFATC1, PTPN6, CD247, PLCG1, RAF1, CARD11, PAK4
Cellular Processes	bta04540: Gap junction	0.001	TUBB2B, PLCB4, MAPK7, PRKCB, GNAS, CSNK1D, PRKCA, RAF1, ADCY7, TUBA8
Cancer	bta05223: Non-small cell lung cancer	0.001	RXRA, PRKCB, RASSF5, ERBB2, AKT1, PRKCA, PLCG1, BAK1, RAF1
Signal Transduction	bta04010: MAPK signaling pathway	0.002	PRKCB, IGF2, PRKCA, NFATC1, MAPK8IP3, CACNA1E, MAPK8IP1, IGF1R, RPS6KA4, FGF5, IKBKB, MAPK7, ERBB2, GNA12, RAC3, AKT1, MAP3K9, RAF1, FGFR3, FGFR1
Cellular Processes	bta04520: Adherens junction	0.002	ERBB2, RAC3, RADIL, PTPN6, SORBS1, BAIAP2, ACTB, FGFR1, IGF1R, NECTIN1
Nervous System	bta04730: Long-term depression	0.002	RYR1, PLCB4, PRKCB, GNA12, GNAS, PRKCA, RAF1, IGF1R
Signal Transduction	bta04310: Wnt signaling pathway	0.002	TLE3, PRKCB, FZD7, CAMK2A, AXIN1, PRKCA, NFATC1, NKD1, WNT6, PLCB4, RUVBL1, RAC3, LGR5, PPARD
Immune System	bta04670: Leukocyte transendothelial migration	0.002	CLDN3, PRKCB, RASSF5, ITGB2, PECAM1, PRKCA, THY1, PLCG1, EZR, BCAR1, ACTB
Other	bta04360: Axon guidance	0.003	NRP1, UNC5B, CAMK2A, PRKCA, NTN1, SSH3, ABLIM3, PLXNA2, RAC3, PLCG1, SRGAP3, RAF1, EPHA1, PAK4
Other	bta01521: EGFR tyrosine kinase inhibitor resistance	0.003	PRKCB, ERBB2, BCL2, AKT1, PRKCA, PLCG1, RAF1, FGFR3, IGF1R
Metabolism	bta05231: Choline metabolism in cancer	0.003	DGKD, PRKCB, DGKQ, RAC3, AKT1, PRKCA, PLCG1, RAF1, DGKZ, RALGDS
Other	bta04972: Pancreatic secretion	0.003	PLCB4, PRKCB, KCNQ1, FXYD2, GNAS, ATP2A3, ATP2A1, PRKCA, ADCY7, SLC9A1
Cellular Processes	bta04148: Efferocytosis	0.003	CAMK2A, ATP2A3, ATP2A1, NFATC1, PBX1, RXRA, ADGRB1, PECAM1, PTPN6, BCAR1, RAB7A, C1QC, PPARD
Immune System	bta04662: B cell receptor signaling pathway	0.003	IKBKB, PRKCB, CD81, RAC3, AKT1, NFATC1, PTPN6, RAF1, CARD11
Endocrine System	bta04961: Endocrine and other factor-regulated calcium reabsorption	0.004	PLCB4, PRKCB, FXYD2, GNAS, PRKCA, AP2A2, DNM1

Endocrine System	bta04928: Parathyroid hormone synthesis, secretion and action	0.004	PLCB4, RXRA, PRKCB, GNA12, GNAS, BCL2, PRKCA, RAF1, ADCY7, FGFR1
Cancer	bta05214: Glioma	0.008	PRKCB, CAMK2A, AKT1, PRKCA, PLCG1, BAK1, RAF1, IGF1R
Cellular Processes	bta04550: Signaling pathways regulating pluripotency of stem cells	0.01	WNT6, MEIS1, FZD7, PCGF3, AXIN1, AKT1, RAF1, FGFR3, INHBE, FGFR1, IGF1R
Endocrine System	bta04916: Melanogenesis	0.011	WNT6, PLCB4, PRKCB, FZD7, CAMK2A, GNAS, PRKCA, RAF1, ADCY7
Endocrine System	bta04933: AGE-RAGE signaling pathway in diabetic complications	0.011	PLCB4, PRKCB, COL4A1, BCL2, AKT1, PRKCA, NFATC1, PLCG1, PLCD1
Signal Transduction	bta04012: ErbB signaling pathway	0.012	PRKCB, CAMK2A, ERBB2, AKT1, PRKCA, PLCG1, RAF1, PAK4
Endocrine System	bta04911: Insulin secretion	0.013	PLCB4, PRKCB, FXYD2, KCNMB2, CAMK2A, GNAS, PRKCA, ADCY7
Signal Transduction	bta04022: cGMP-PKG signaling pathway	0.013	PLCB4, FXYD2, KCNMB2, GNA12, ATP2A3, AKT1, GATA4, ATP2A1, GTF2IRD1, NFATC1, RAF1, ADCY7
Cancer	bta05224: Breast cancer	0.014	FGF5, WNT6, HEYL, FZD7, ERBB2, AXIN1, AKT1, BAK1, RAF1, FGFR1, IGF1R
Cancer	bta05225: Hepatocellular carcinoma	0.015	WNT6, PRKCB, FZD7, AXIN1, IGF2, AKT1, PRKCA, PLCG1, BAK1, RAF1, ACTB, IGF1R
Metabolism	bta05230: Central carbon metabolism in cancer	0.016	SLC7A5, ERBB2, AKT1, RAF1, FGFR3, PFKP, FGFR1
Endocrine System	bta04921: Oxytocin signaling pathway	0.016	RYR1, PLCB4, MAPK7, PRKCB, CAMK2A, GNAS, PRKCA, NFATC1, RAF1, ADCY7, ACTB
Signal Transduction	bta04066: HIF-1 signaling pathway	0.017	PRKCB, CAMK2A, ERBB2, BCL2, AKT1, PRKCA, PLCG1, PFKP, IGF1R
Endocrine System	bta04914: Progesterone-mediated oocyte maturation	0.018	STK10, PLK1, AKT1, CPEB3, RAF1, ADCY7, MAD1L1, IGF1R
Immune System	bta04650: Natural killer cell mediated cytotoxicity	0.019	ZAP70, PRKCB, ITGB2, SH3BP2, RAC3, PRKCA, NFATC1, PTPN6, CD247, PLCG1, RAF1
Signal Transduction	bta04150: mTOR signaling pathway	0.02	IKBKB, WNT6, SLC7A5, DEPTOR, PRKCB, FZD7, GRB10, AKT1, PRKCA, RAF1, IGF1R
Endocrine System	bta04912: GnRH signaling pathway	0.02	PLCB4, MAPK7, PRKCB, CAMK2A, GNAS, PRKCA, RAF1, ADCY7
Cancer	bta05235: PD-L1 expression and PD-1 checkpoint pathway in cancer	0.02	IKBKB, ZAP70, AKT1, NFATC1, PTPN6, CD247, PLCG1, RAF1
Nervous System	bta04724: Glutamatergic synapse	0.02	GRIN3A, PLCB4, HOMER1, PRKCB, GRIK5, GNB1, GNAS, PRKCA, ADCY7
Nervous System	bta04725: Cholinergic synapse	0.02	PLCB4, PRKCB, KCNQ1, GNB1, CAMK2A, BCL2, AKT1, PRKCA, ADCY7
Endocrine System	bta04918: Thyroid hormone synthesis	0.024	PLCB4, TG, PRKCB, FXYD2, GNAS, PRKCA, ADCY7

Endocrine System	bta04925: Aldosterone synthesis and secretion	0.024	SCARB1, PLCB4, DAGLA, PRKCB, CAMK2A, GNAS, PRKCA, ADCY7
Cellular Processes	bta04145: Phagosome	0.025	COMP, COLEC11, SCARB1, TUBB2B, ITGB2, TCIRG1, ATP6V0D2, DYNC1I1, ACTB, RAB7A, TUBA8
Cancer	bta05212: Pancreatic cancer	0.026	IKBKB, ERBB2, RAC3, AKT1, BAK1, RAF1, RALGDS
Immune System	bta04666: Fc gamma R-mediated phagocytosis	0.026	PTPRC, PRKCB, ASAP3, AKT1, PRKCA, ASAP1, PLCG1, RAF1
Endocrine System	bta04935: Growth hormone synthesis, secretion and action	0.026	PLCB4, PRKCB, GNAS, AKT1, PRKCA, PLCG1, RAF1, ADCY7, BCAR1
Signal Transduction	bta04370: VEGF signaling pathway	0.029	PRKCB, RAC3, AKT1, PRKCA, PLCG1, RAF1
Signal Transduction	bta04071: Sphingolipid signaling pathway	0.029	PLCB4, PRKCB, GNA12, BCL2, RAC3, AKT1, PRKCA, S1PR3, RAF1
Other	bta04713: Circadian entrainment	0.031	RYR1, PLCB4, PRKCB, GNB1, CAMK2A, GNAS, PRKCA, ADCY7
Immune System	bta05163: Human cytomegalovirus infection	0.033	PRKCB, PRKCA, NFATC1, ADCY7, IKBKB, PLCB4, GNA12, GNB1, GNAS, RAC3, AKT1, BAK1, RAF1, BCAR1
Signal Transduction	bta04024: cAMP signaling pathway	0.034	VIPR2, CAMK2A, ATP2A3, ATP2A1, NFATC1, ADCY7, SLC9A1, GRIN3A, FXYD2, GNAS, RAC3, AKT1, ACOX3, RAF1
Endocrine System	bta03320: PPAR signaling pathway	0.034	FADS2, RXRA, ME3, ACOX3, SORBS1, APOA5, PPARD
Cancer	bta05226: Gastric cancer	0.039	FGF5, WNT6, RXRA, FZD7, ERBB2, AXIN1, BCL2, AKT1, BAK1, RAF1
Immune System	bta05135: Yersinia infection	0.041	IKBKB, ZAP70, RAC3, AKT1, NFATC1, PLCG1, ARHGEF7, BAIAP2, BCAR1, ACTB
Cancer	bta05210: Colorectal cancer	0.05	AXIN1, BCL2, RAC3, AKT1, BAK1, RAF1, RALGDS
Immune System	bta05170: Human immunodeficiency virus 1 infection	0.05	PRKCB, PRKCA, NFATC1, IKBKB, GNB1, BCL2, RAC3, AKT1, CD247, PLCG1, BAK1, RAF1, PAK4
Metabolism	bta00561: Glycerolipid metabolism	0.052	DGKD, DGKQ, AGPAT2, DGKZ, MGLL, AGPAT4
Nervous System	bta05031: Amphetamine addiction	0.055	ARC, GRIN3A, PRKCB, CAMK2A, GNAS, PRKCA
Cancer	bta05206: MicroRNAs in cancer	0.055	PRKCB, PRKCA, FOXP1, IKBKB, MAPK7, ERBB2, IGF2BP1, BCL2, SPRY2, PLCG1, BAK1, EZR, RAF1, FGFR3, PAK4
Immune System	bta05165: Human papillomavirus infection	0.056	VWF, ITGA3, FZD7, MX1, AXIN1, TCIRG1, COMP, IKBKB, WNT6, HEYL, COL4A1, GNAS, AKT1, BAK1, RAF1, HES2, ATP6V0D2
Immune System	bta04664: Fc epsilon RI signaling pathway	0.057	ALOX5AP, RAC3, AKT1, PRKCA, PLCG1, RAF1
Immune System	bta04062: Chemokine signaling pathway	0.058	GRK1, IKBKB, PLCB4, PRKCB, GNB1, RAC3, AKT1, PLCG1, RAF1, ADCY7, BCAR1
Endocrine System	bta01522: Endocrine resistance	0.062	ERBB2, GNAS, BCL2, AKT1, RAF1, ADCY7, IGF1R

Cancer	bta05222: Small cell lung cancer	0.062	IKBKB, RXRA, COL4A1, ITGA3, BCL2, AKT1, BAK1
Metabolism	bta00562: Inositol phosphate metabolism	0.063	PLCB4, ITPKA, ITPK1, PI4KA, PLCG1, PLCD1
Cancer	bta05218: Melanoma	0.066	FGF5, AKT1, BAK1, RAF1, FGFR1, IGF1R
Signal Transduction	bta04151: PI3K-Akt signaling pathway	0.067	VWF, ITGA3, IGF2, PRKCA, IGF1R, COMP, FGF5, IKBKB, RXRA, LPAR5, COL4A1, ERBB2, GNB1, BCL2, AKT1, RAF1, FGFR3, FGFR1
Nervous System	bta05017: Spinocerebellar ataxia	0.07	RYR1, GRIN3A, PLCB4, FGF14, PRKCB, ATP2A3, AKT1, ATP2A1, PRKCA
Cancer	bta05215: Prostate cancer	0.072	IKBKB, ERBB2, BCL2, AKT1, RAF1, FGFR1, IGF1R
Other	bta04970: Salivary secretion	0.081	PLCB4, PRKCB, FXYD2, GNAS, PRKCA, ADCY7, SLC9A1
Nervous System	bta04721: Synaptic vesicle cycle	0.083	NAPA, SLC6A12, TCIRG1, AP2A2, ATP6V0D2, DNM1
Immune System	bta04613: Neutrophil extracellular trap formation	0.085	PLCB4, VWF, PRKCB, ITGB2, HDAC11, AKT1, PRKCA, PADI4, PLCG1, RAF1, ATG7, ACTB
Immune System	bta05166: Human T-cell leukemia virus 1 infection	0.087	IKBKB, NRP1, VAC14, RANBP1, RANBP3, CRTC1, ITGB2, AKT1, TSPO, NFATC1, ADCY7, MAD1L1
Other	bta03030: DNA replication	0.09	FEN1, LIG1, POLD1, MCM3
Signal Transduction	bta04390: Hippo signaling pathway	0.095	CRB1, WNT6, FZD7, ITGB2, AXIN1, CSNK1D, LIMD1, NKD1, ACTB
Endocrine System	bta04934: Cushing syndrome	0.095	WNT6, SCARB1, PLCB4, FZD7, CAMK2A, AXIN1, GNAS, ADCY7, PBX1
Endocrine System	bta04926: Relaxin signaling pathway	0.097	PLCB4, COL4A1, GNB1, GNAS, AKT1, PRKCA, RAF1, ADCY7
Other	bta04976: Bile secretion	0.097	SLC9A3, SCARB1, RXRA, FXYD2, GNAS, ADCY7, SLC9A1
Endocrine System	bta04960: Aldosterone-regulated sodium reabsorption	0.097	PRKCB, FXYD2, SCNN1A, PRKCA
Cancer	bta05213: Endometrial cancer	0.099	ERBB2, AXIN1, AKT1, BAK1, RAF1

SECTION II: INVESTIGATION OF TWO NOVEL GENETIC DEFECTS IN CATTLE

Section II Abstract

Identification of detrimental genetic variants is critical for livestock breeding programs to avoid producing affected animals. In the first case, thirteen American Hereford cattle were reported blind around one year of age and shared a common ancestor through both the maternal and paternal pedigrees, suggesting a recessive genetic origin. Ophthalmologic examinations revealed retinal degeneration while histological exams showed loss of the retinal photoreceptor layer. Whole-genome sequencing (WGS) of blind cattle and unaffected relatives revealed a 1-bp frameshift deletion in ceroid lipofuscinosis neuronal 3 (*CLN3*) for which the blind cattle were homozygous and their parents heterozygous. Genotyping of over 6,500 cattle revealed that the variant was only observed in related Hereford cattle, and only recessive in blind cattle. The identified variant is predicted to truncate the encoded protein battenin, which is involved in lysosomal function necessary for photoreceptor layer maintenance. Mutations in *CLN3* are associated with human Batten disease, which results in early-onset retinal degeneration and lesions. Thus, the *CLN3* 1-bp deletion in the cattle is likely the causative variant.

In the second case, nine Angus calves from the same herd and sire were diagnosed with Bovine familial convulsions and ataxia (BFCA) within days of birth. Necropsy revealed cerebellar and spinal cord lesions associated with the condition. The shared sire was bred to cows across two herds using artificial insemination, producing an additional 14 affected calves. WGS of the sire, six affected and seven unaffected paternal half-sibling calves and 135 unrelated controls revealed the sire and five of the six affected

calves were heterozygous for a nonsense variant in *CACNA1A*. The other affected calves were heterozygous for the variant, but it was absent in the other unaffected calves, parents of the sire, and in sequence data from over 6,500 other cattle. *CACNA1A* protein is part of a highly expressed cerebellar calcium voltage gated channel. The nonsense variant is proposed to cause haploinsufficiency, preventing proper transmission of neuronal signals through the channel and resulting in BFCA.

These cases demonstrate the importance of investigating possible genetic defects to prevent further affected cattle and to better understand the impact of variants on gene function.

CHAPTER 5: A RECESSIVE *CLN3* VARIANT IS RESPONSIBLE FOR DELAYED-ONSET RETINAL DEGENERATION IN HEREFORD CATTLE

This chapter was published in the *Journal of Veterinary Diagnostic Investigation*. Supplementary material can be found online with the article.

Reith, R. R., et al. 2024. A recessive CLN3 variant is responsible for delayed-onset retinal degeneration in Hereford cattle. J. Vet. Diagn. Invest. 36:438–446. doi:10.1177/10406387241239918.

Introduction

Blindness has a negative impact on livestock welfare (Williams, 2010). There are many potential causes of acquired vision loss in livestock, including vitamin A deficiency, lead poisoning, sulfate intoxication, (Van Donkersgoed and Clark, 1988; Hill et al., 2009; Kang et al., 2017) and eye infection (Williams, 2010; Angelos, 2022). Cataracts and neuronal ceroid lipofuscinoses (NCLs) are examples of blindness attributed to identified recessive mutations in specific cattle breeds (Houweling et al., 2006; Weber and Pearce, 2013; Braun et al., 2019; Häfliger et al., 2021). For example, a single base duplication in *CLN5* was associated with recessively inherited severe neuronal loss and retinal degeneration in Devon cattle, very similar to human CLN5 disease (Houweling et al., 2006). In Braunvieh cattle, a missense mutation in *CNGB3* was associated with recessively inherited achromatopsia and loss of cone photoreceptor function (Häfliger et al., 2021). In a study designed to identify deleterious mutations, a recessive frameshift variant in the retinitis pigmentosa-1 gene was identified as causative of vision loss in Normande cattle, akin to retinitis pigmentosa in humans and mice (Michot et al., 2016).

Three blind Hereford cows (19-, 23-, 24-mo-old) were presented to the Nebraska congenital disease investigation program (Lincoln, NE, USA). The cows had no perceived ocular issues as calves and were suspected to be blind at ~12 months of age. After the initial cases, 10 additional Hereford cattle with suspected blindness were identified.

The 3 initially reported cattle (V2, V10, V11) were born from a single sire (IV3; Figure 5.1). Two (V10, V11) were full-siblings through embryo transfer. All blind cattle shared a common ancestor (I1) through both the maternal and paternal pedigree; a recessive variant was therefore the possible cause of blindness in these cattle. In this investigation, we characterized the ophthalmo-pathological changes in the blind cattle and performed genomic analyses to identify the cause of the condition.

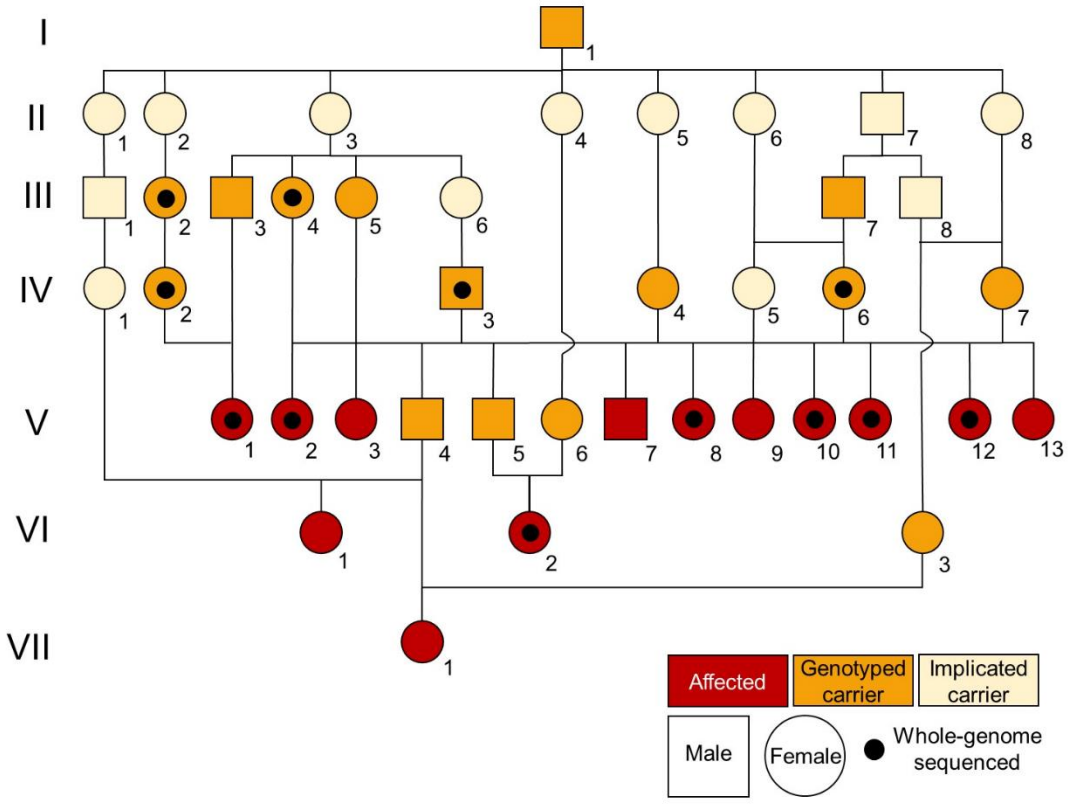

Figure 5.1. Pedigree of blind cattle and their relatives.

Materials and methods

Our study was approved by the Institutional Animal Care and Use Committee at the University of Nebraska–Lincoln (protocol 2427), which is accredited by AAALAC International.

Blind animals

The 13 blind cattle were all registered Herefords, born between 2017 and 2022, and included 3 pairs of full-siblings. Ten of the blind animals were from embryo transfer (V3, V7, V8, V9, V10, V11, V12, V13, VI1, VII1). Cows V10 and V11 had previously calved successfully and were pregnant when they were reported to the Nebraska congenital disease program.

Control cattle

Six cows at a commercial abattoir were selected for postmortem tissue collection. Five of the cattle were red with white faces and other white markings, consistent with Hereford breeding. The sixth cow was black with a white face. Tissues from 4 regions of the brain (cerebellum, cerebrum, hippocampus, brainstem), eyes, and masseter muscle were collected 20–30 min postmortem (Table 5.1).

Table 5.1. List of Hereford cattle sampled for DNA isolation, histopathology, and eye examinations.

	Phenotype	Samples collected for DNA isolation	Ophthalmologic exam (age)
Project cattle (*n* = 31)			
V1*, V8*, V12*, V13, VI2*, VII1	Blind	Blood	No
V2*	Blind	Blood	Yes (19 mo.)
V3	Blind	Blood	Yes (15 mo.)
VI1	Blind	Blood	Yes (3.4 y)
V10*, V11*	Blind	Blood	Yes (1.9, 2 y)
2 full-siblings to V10 & V11*	Normal	Blood	No
Fetuses of V10, V11	Unknown	Liver	No
Full-sister to V3	Normal	Blood	Yes (15 mo.)
IV3*	Normal	Semen	No
6 abattoir cows	Normal	Masseter muscle	No
III2*, III4*, III5, IV2*, IV6*, V5, V6, VI3	Normal	Blood	No
Other cattle sequenced (*n* = 336)			
57	Unknown	Blood	No
252	Unknown	Semen	No
12	Unknown	Hair	No
6	Unknown	Various	No
9	Unknown	Allflex TSU	No
Total: 367			

TSU = tissue sampling unit. * Animal was whole-genome sequenced.

Antemortem testing

Ophthalmologic examinations were performed on 4 blind animals and 1 phenotypically normal full-sibling of blind heifer V3. Three blind cows (V2, V10, V11) were examined by a diplomate of the American College of Veterinary Ophthalmologists (ACVO) from the Kansas State University–College of Veterinary Medicine (JM Meekins; Manhattan, KS, USA) to determine the severity of their blindness. Blood was collected from all 3 cattle for serum vitamin A evaluation. A blind heifer (V3) and her

phenotypically normal full-sister (both from embryo transfer) underwent an ophthalmic examination by an ACVO diplomate at the Veterinary Teaching Hospital–University of Georgia (KA Diehl; VTH-UGA; Athens, GA, USA). One suspected blind cow (VI1) was examined by an ACVO diplomate from the University of Wisconsin–School of Veterinary Medicine (J Seth Eaton; Madison, WI, USA).

Electroretinogram

The cattle examined at the VTH-UGA underwent electroretinogram (ERG) tests. Tropicamide 1% ophthalmic solution was instilled in both eyes for pharmacologic mydriasis. Specific dark adaptation was not performed, but all artificial barn lighting was turned off and nearby windows were covered with blackout curtains. Retinal stimulation was performed (BPM-300 electrodiagnostic system; RetinoGraphics). Standard placement of ground (~2.5 cm medial to the medial canthus) and reference (~2.5 cm lateral to the lateral canthus) needle electrodes was performed. After the instillation of proparacaine hydrochloride 0.5% ophthalmic solution for topical/corneal anesthesia, a contact lens (ERG-jet; Fabrinal) amply coated with eye lubricant plus ophthalmic lubricant (Optixcare; Aventix) was used for the recording electrode. The eyelids were manually retracted with care to not disrupt the electrodes and allow continuous visualization to ensure continued appropriate placement throughout the test. A manufacturer preprogrammed short ERG protocol was used to provide an average of 4 “yes or no” mixed rod and cone responses in response to a standard flash in a relatively scotopic environment.

Tissue collection

Blind cows V10 and V11 were ~31-mo-old when they were harvested at the USDA-inspected Loeffel Meat Laboratory at the University of Nebraska–Lincoln (Lincoln, NE, USA). After passing federal inspection, tissues from 4 regions of the brain (cerebellum, cerebrum, hippocampus, brainstem), cardiac muscle, semitendinosus muscle, liver, kidney, lung, spleen, and lymph node were collected for pathology examination as well as flash-frozen in liquid nitrogen.

Histopathology

Ocular histologic examination was performed on V10, V11, their fetuses, and the 6 normal abattoir cattle.

Scanning electron microscopy

Retinas from V10 and V11 were processed for scanning electron microscopy (SEM) at the University of Nebraska–Lincoln Microscopy Core Research Facility of the Center for Biotechnology (Lincoln, NE, USA). Eyes from V10 and V11 were bisected and fixed in 2.5% glutaraldehyde in 100 mM cacodylate buffer (pH 7.4) for 2 h at room temperature and post-fixed in 1% osmium tetroxide in distilled water for 1 h. After rinsing 3 times in deionized water, each sample was processed through a series of ethanol dehydration (30%, 50%, 70%, 2×95%, 2×100%). The eye cups were immediately processed for critical point dry (Samidri-795 system; Tousimis). The samples were mounted onto a SEM stub and coated with a thin layer of chromium (Desk V Sputter; Denton). Side-view SEM images were collected (S4700 field-emission SEM; Hitachi).

DNA isolation

DNA was isolated from the cattle (Table 5.1) using the following protocols appropriate for the type of sample collected. DNA was isolated from blood and semen (Gentra Puregene blood kit; Qiagen) following a published protocol (Sieck et al., 2020). DNA was isolated from hair roots (Gentra Puregene blood kit) following a published protocol (Petersen et al., 2020).

DNA was isolated from tissue (masseter muscle, liver; Gentra Puregene blood kit). Three hundred μL of cell lysis buffer and 7 μL of Qiagen proteinase K were added to 30 mg of tissue, and then incubated at 55°C overnight. For tissue sampling units (TSUs; Allflex), 75 μL of the liquid buffer from each sample was added to 225 μL of cell lysis buffer and 7 μL of proteinase K. All samples were then incubated overnight at 55°C, after which they were transferred to ice for 1 min. One hundred μL of protein precipitation solution was added and vortexed (20 s) before incubation on ice for >5 min and centrifugation (5 min at 15,000 × *g* at 15°C). The supernatant was poured into a new tube with 650 μL of 100% isopropanol. Tubes were inverted to mix and then centrifuged (1 min at 15,000 × g). The supernatant was discarded, and the tube placed upside down on a paper towel to drain. The pelleted DNA was washed with 300 μL of 70% ethanol and inverted several times. Samples were centrifuged (1 min at 15,000 × g), the supernatant was discarded, and the tube was placed upside down to drain for 5 min; 200 μL of DNA hydration solution was added to the DNA pellet and incubated for 5 min at 55°C before overnight hydration at room temperature. DNA concentration was determined (BioTek Epoch 2 microplate spectrophotometer; Agilent).

Whole-genome sequencing

Isolated DNA from 7 blind cattle (V1, V2, V8, V10, V11, V12, VI2) and 9 unaffected relatives (III2, III4, IV2, IV3, IV6, 1 offspring of IV3, 2 full-siblings to V10 and V11, 1 offspring of V12) was sent to Admera Health (South Plainfield, NJ, USA) for library preparation (KAPA; Roche) and 150-bp paired-end sequencing (NovaSeq; Illumina). Raw data were processed by trimming adapters and removing poor-quality bases using TrimGalore (Krueger et al., 2023). Reads were mapped to the ARS-UCD1.2 genome with BWA-MEM (Li and Durbin, 2009), and duplicates were marked with Samtools (Danecek et al., 2021). GATK was implemented to realign indels, and variants were called using GATK Haplotype Caller (Van der Auwera and O'Connor, 2020). A combined variant file was created by merging the data of the 16 related cattle sequenced for our project with 133 control cattle previously sequenced from other projects, including PRJNA513064, PRJNA663547, and PRJNA994471, PRJNA1042650, and PRJNA1042814. A case control script (SnpSift; Cingolani et al., 2012) was run with the 7 blind cattle as cases and the 142 other cattle assumed to be unaffected. Hypothesizing that blindness was attributed to a recessive genotype, the variant file was filtered to identify loci where the *p*-value assuming a recessive model was $<1 \times 10^{-6}$.

The variant call format file (VCF) was then filtered to keep loci for which all 7 blind cattle were homozygous for the alternative allele. Loci for which unaffected cattle were homozygous for the alternative allele were removed. The remaining loci were run through a variant effect predictor (VEP; McLaren et al., 2016).

Data pulled from the NCBI Sequence Read Archive database (SRA; https://www.ncbi.nlm.nih.gov/sra) were used to estimate the frequency of the candidate

variants. Cattle sequences from the SRA labeled as Hereford (*n* = 327) were aligned to the ARS-UCD1.2 genome. Variants were called using the VariantFrequency pipeline, available on GitHub (https://github.com/SichongP/VariantFrequency).

In addition, genotypes (VCF) of 95 Herefords from whole-genome sequencing were provided by the American Hereford Association (https://hereford.org/).

Sanger sequencing

Sanger sequencing was performed to determine the ceroid lipofuscinosis neuronal 3 (CLN3) candidate variant genotype in 336 additional cattle (Table 5.1). These animals included both those targeted for genotyping due to pedigree relationships with known carriers as well as samples on hand from unrelated Hereford cattle used in prior studies (Sieck et al., 2020). PCR primers (Supplementary Table 5.1) were designed using Primer3 (Untergasser et al., 2012). PCR was performed (FastStart kit; Sigma-Aldrich) in 12-μL reactions containing 4.45 μL of water, 0.25 μL of 25 mM $MgCl_2$, 1.2 μL of 20 mM 10× buffer with $MgCl_2$, 0.5 μL of dNTP (10 mM of each dNTP), 0.1 μL of Taq (5 U/μL), 0.75 μL of 20 μM forward and reverse primer, and 4 μL of 5 ng/μL DNA template. Thermal cycling conditions consisted of 94°C for 4 min, 32 cycles of 94°C for 30 s, annealing temperature (Supplementary Table 5.1) for 30 s, 72°C for 45 s, a final extension at 72°C for 10 min, then a 10°C hold. PCR product cleanup was performed (0.75 μL ExoSAP-IT; Applied Biosystems) per 4 μL of PCR product and incubation thermal cycling at 37°C for 30 min, 80°C for 15 min, and a 15°C hold.

Relative quantitative real-time PCR

RNA was isolated from the retina of 2 affected cows (V10, V11) and 2 abattoir cows (RNeasy fibrous tissue mini kit; Qiagen) following the manufacturer's protocol.

RNA was washed and eluted on columns with DNase I treatment (Direct-zol RNA MiniPrep Plus; Zymo) according to the manufacturer's instructions; 2.3 µg of RNA total for each sample was converted into cDNA (Cytiva First-Strand synthesis kit, cat. 27926101; Millipore Sigma) following the manufacturer's protocol.

The expression of *CLN3* was quantified (SYBR Green PCR master mix kit, cat. 4309155, Applied Biosystems; CFX384 real time PCR, Bio-Rad). The quantitative real-time PCR (qPCR) was performed in 10-µL reactions containing 5 µL of 2× SYBR Green master mix, 0.5 µL of 20 µM forward primer, 0.5 µL of 20 µM reverse primer, 3 µL of water, and 2 µL of cDNA template for CLN3 and 1 µL of cDNA template for the reference gene actin beta (*ACTB*). Samples were run in triplicate with negative controls. The qPCR primers (Suppl. Table 2) were designed using IDT PrimerQuest Tool (www.idtdna.com). The *CLN3* forward primer targeted the splicing region between exons 1 and 2. Thermal cycling conditions consisted of 95°C for 10 min, 40 cycles of 98°C for 15 s, 58°C for 30 s, 72°C for 30 s, then a final extension of 72°C for 60 s. Mean normalized expression (MNE) was calculated using the cycle-crossing thresholds of the replicates, incorporating qPCR efficiencies of each gene. The CLN3 MNE values for each animal were then $\log_{10}$ transformed and used to compare the phenotype groups by t-test.

Results

Animals

Of the 13 blind animals reported, samples from 11 animals were available for genetic testing. In total, DNA was obtained from 367 Herefords (Table 5.1).

Ophthalmic examinations

At the time of examination, cattle V2, V10, and V11 were unable to navigate the unfamiliar holding pen and bumped into stationary objects. Menace response was bilaterally absent, confirming functional blindness. Neuro-ophthalmic findings were consistent with retinal localization; the dazzle reflex was delayed, resting mydriasis was present, and direct and consensual pupillary light reflexes were slow and incomplete. The ocular adnexa and anterior segment were normal. Patchy, widespread tapetal hyper-reflectivity was present with moderate retinal vessel attenuation and mid-peripheral tapetal pigment clumping (Figure 5.2). The optic disc appeared dark. The 3 cattle were ophthalmoscopically diagnosed with severe retinal degeneration. Serum vitamin A concentrations (0.24, 0.25, 0.29 ppm) were just below our laboratory acceptable range of 0.3–0.7 ppm.

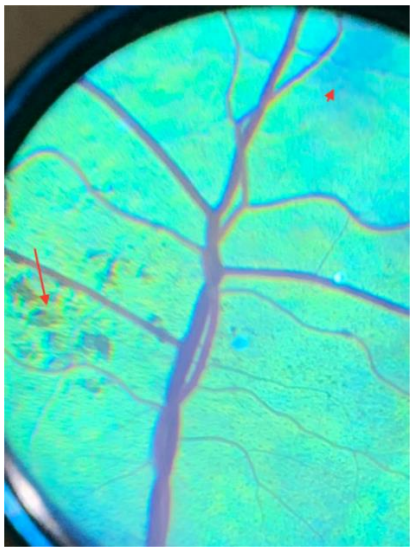

Figure 5.2. Focal area of the tapetal ocular fundus along the dorsal retinal venule and arteriole of blind Hereford cow V10 with moderate retinal vessel attenuation in addition to diffuse altered tapetal hyper-reflectivity (short arrow) and multifocal pigment clumping (long arrow).

Ophthalmic examination found that V3 was nonvisual with absent menace response. Dazzle reflexes and pupillary light reflexes were delayed and incomplete. On ophthalmoscopic examination, diffuse mottling of the tapetum, multifocal areas of altered tapetal reflectivity, and darkened optic nerve heads were noted (Figure 5.3); there was only mild retinal vascular caliber attenuation relative to the clinically normal sibling cow. Both eyes also had multifocal pigment clumping in the tapetal fundus, although this was also seen in her sibling. The remainder of the ophthalmic examination of the sibling was normal. The electroretinogram (ERG) of the clinically affected heifer was extinguished with only regular electrical cycle noise and no discernable or measurable a- or b-wave amplitudes or implicit times (Supplementary Figure 5.1). The ERG of the clinically normal sibling heifer was not able to be comprehensively recorded and measured due to excessive environmental electrical noise. However, the waveforms obtained and seen during attempted acquisition appeared normal and with adequate amplitude. The nonvisual status, diffuse tapetal alterations on fundic examination, and absence of waveforms on the electroretinogram were consistent with a diagnosis of retinal degeneration.

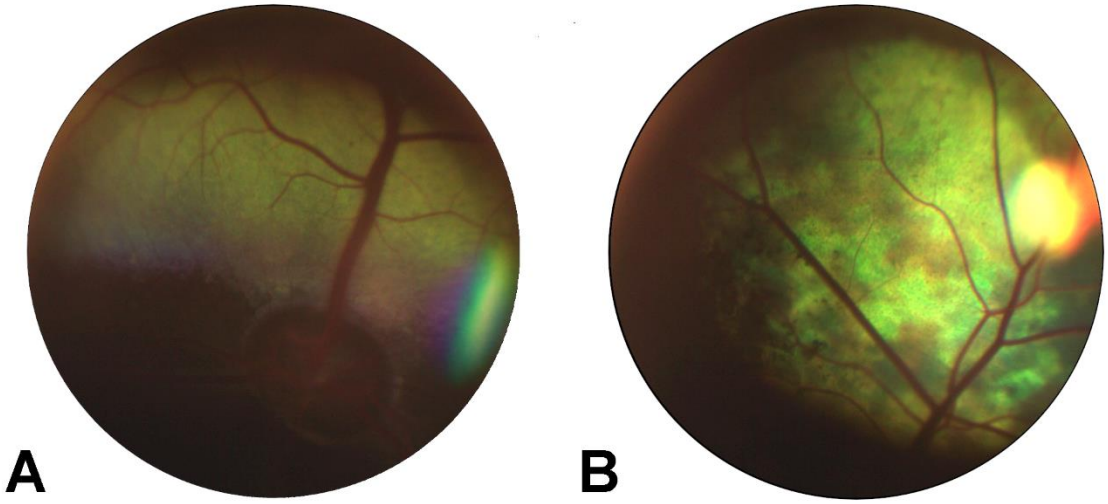

Figure 5.3. Fundus photographs of clinically normal heifer (A) and clinically affected full-sibling heifer (B). A. The clinically normal sibling had a normal (tapetal) fundus bilaterally. B. The clinically affected heifer had diffuse mottling, altered reflectivity of the tapetum, and retinal vessel attenuation. These findings were bilateral and symmetric.

Examination of blind cow VI1 confirmed her blindness and reported similar fundoscopic changes consistent with retinal degeneration.

Pathology report

The retinas and brain tissues of the 6 control cattle were examined and determined to be normal. These animals served as controls for pathology and RNA expression.

Ocular histology confirmed the clinical diagnosis of blind cows V10 and V11. The anterior segment was normal in both cows. The retina easily detached and retained connection only near the optic disc and ora ciliaris retinae through processing. Marked retinal degeneration was present, evidenced by the absence of rod and cone cells in the

outer and inner segments (Figure 5.4). The retinal pigment epithelium (RPE) was intact. The outer nuclear layer was absent, and the outer plexiform layer was diminished. There were rare cellular processes extending from the mildly depleted inner nuclear layer into the outer plexiform layer where a few glial cell nuclei remained. The inner plexiform layer, ganglion cell layer, and nerve fiber layers were intact. No vacuolated lymphocytes were observed in the blood. The histology of the nervous system was also normal. Our histologic diagnosis was severe retinal atrophy with loss of the photoreceptor layer, outer nuclear layer, and outer plexiform layer, with a diminished inner nuclear layer. The two cows were pregnant, and each fetus had normal fetal retinas. In the two cows and their fetuses, other tissues (brain, cardiac muscle, skeletal muscle, liver, kidney, lung, spleen, lymph node) were normal.

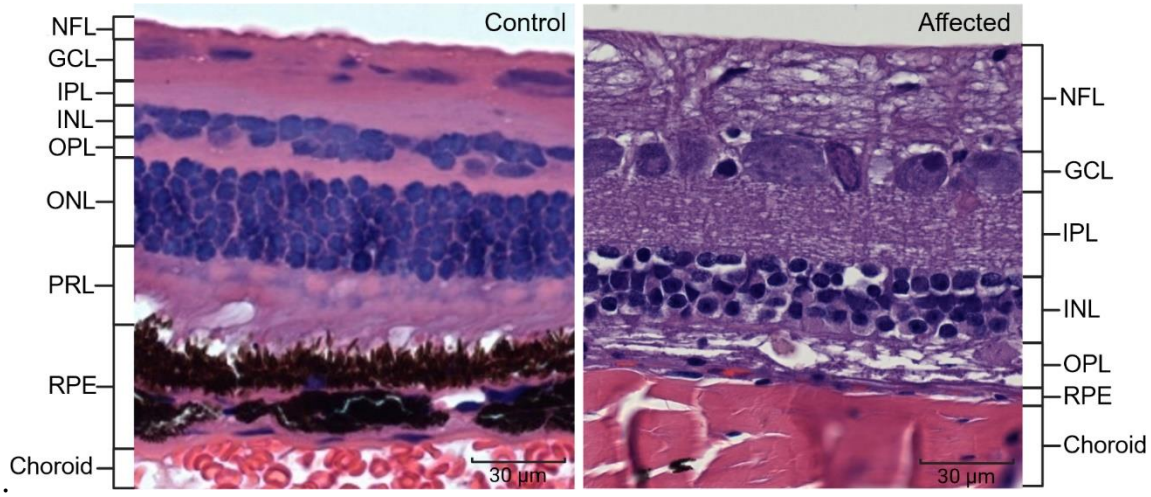

Figure 5.4. Retinal layers of a clinically normal cow (left) and a clinically affected cow (right). The outer nuclear layer (ONL) and photoreceptor layer (PRL, rods and cones) are absent in the affected retina. GCL = ganglion cell layer; INL = inner nuclear layer; IPL = inner plexiform layer; NFL = nerve fiber layer; OPL = outer plexiform layer; RPE = retinal pigment epithelium. Bars = 30 µm

A histologic view of the retina from affected cow V10 showed that the outer nuclear, and inner and outer photoreceptor layers, were missing (Supplementary Figure 5.2).

Sequencing results

After filtering whole-genome sequence data of 9 blind cattle and 7 unaffected relatives for loci that were homozygous for the alternative allele only in the blind cattle, 280 loci (Supplementary Table 5.3), all in chromosome 25, matched the criteria. Of those, all but 37 variants had been previously documented as determined by reference single-nucleotide variation (rs) identifiers. Three loci, one novel, were predicted to impact protein function (Table 5.2).

Table 5.2. Variants fitting filter criteria with a predicted impact (variant effect predictor) on gene function. Variant positions are in relationship to reference genome ARS-UCD1.2.

Gene ID	Location	Ref/Var allele	Type of mutation	Previously reported	Predicted impact
CLN3	Chr25: 26043842	CG/C	Frameshift deletion	No	High
ITGAM	Chr25: 27355870	T/C	Splice region variant	rs797903403	Low
ITGAM	Chr25: 27378703	G/A	Splice region variant	rs208133830	Low

For the 2 candidate loci in Table 2 that were previously documented, the SRA search of 327 samples labeled “Hereford” found 8 heterozygotes for rs797903403 and 20 heterozygotes plus 2 homozygotes for the rs208133830 variant. Whole-genome sequence data from the University of Missouri, which included ~5,500 cattle (Robert Schnabel,

pers. comm., 2023), found the rs797903403 variant present in 14 different breeds (allele frequency = 0.004), and the rs208133830 variant in 153 breeds (allele frequency = 0.335). The rare rs797903403 variant was not homozygous in any animals; the more common rs208133830 variant was homozygous in 1,144 animals. Given the distribution of these variants across several breeds, both *ITGAM* variants were determined to be unlikely as causative of blindness in these Hereford cattle. In searches of both the SRA and University of Missouri databases, the novel frameshift deletion in *CLN3* (chr25 g.26043843del) was only observed in Hereford animals. The 18 Herefords in which it was found were each heterozygous. This variant in *CLN3* thus became the primary candidate due to being restricted to the Hereford breed and only being observed in the homozygous state in cattle reported to be blind. The *CLN3* frameshift deletion (c.1106del) in exon 16 (ENSBTAT00000023952.6) is predicted to result in amino acid changes (p. Pro369Argfs*8) until a premature stop codon truncates the normally 438 amino acid protein at residue 375.

Through either WGS or Sanger sequencing, 462 Hereford cattle were genotyped for the *CLN3* mutation (Table 5.3); 367 were genotyped in our laboratory, and 95 genotypes from WGS were provided by the American Hereford Association. All blind cattle available for genotyping (n = 11 out of 13) were homozygous for the variant. All parents of the blind cattle that were available for genotyping (n = 12 out of 14) were confirmed carriers of the deletion. The common ancestor, I1, was confirmed to be a carrier as was his maternal grandsire; DNA was not available from other ancestors of I1. The full-sibling of V3, 2 full-siblings of V10 and V11 (through embryo transfer), and the fetuses of V10 and V11 were carriers of the variant. The 6 abattoir cattle genotyped as

wild type. A query of the American Hereford Association herd book, which includes ~4.5 million animals, identified 1.2 million descendants (dead and living) of the oldest genotyped carrier of the *CLN3* variant. Genotyping performed for research reduced the number to ~700,000 potential carriers by identifying influential descendants that did not inherit the mutation.

Table 5.3. Genotypes for 462 Hereford cattle genotyped for the *CLN3* mutation (chr25 g.26043843del).

	Phenotype	
Genotype	Blind	Normal
Homozygous (DEL/DEL)	11	0
Carrier (G/DEL)	0	69
Wild type (G/G)	0	382

DEL = deletion. Animals in the "Normal" category were either confirmed normal through examinations or presumed normal if no information was provided to suspect otherwise.

Expression of CLN3

Relative qPCR demonstrated that *CLN3* was expressed in the retina of the blind cattle with no significant difference in the expression of *CLN3* compared to control cattle (Supplementary Table 5.4).

Discussion

We found that delayed-onset retinal degeneration and blindness in Hereford cattle was associated with a homozygous deletion in *CLN3* predicted to truncate the protein.

The deletion was only observed in Hereford cattle and could be traced to a common ancestor. Though the gene was expressed in the retina of affected individuals similarly to normal cattle, the observed retinal degeneration provides evidence that the truncated CLN3 protein is dysfunctional, leading to blindness.

The protein encoded by *CLN3*, battenin, is a membrane transporter expressed in the RPE that plays a role in photoreceptor recycling (Mirza et al., 2019; Collin et al., 2020; Sieck et al., 2020). Targeting studies found that battenin localizes to lysosomes and endosomes (Kida et al., 1999; Kyttälä et al., 2004), but aberrant proteins may instead be retained in the endoplasmic reticulum or may have altered expression (Miller et al., 2013; Mirza et al., 2019). One explanation for altered localization of the variant protein may be the loss of a lysosomal targeting motif in the cytoplasmic C-terminal tail, which normally guides the protein to lysosomes (Kyttälä et al., 2005; Cotman and Staropoli, 2012). However, human studies suggest that the truncated CLN3 protein may possess partial function if the N-terminal is retained (Cotman and Staropoli, 2012). Therefore, despite the predicted truncation of the cytoplasmic tail, the variant Hereford protein may retain some functionality due to the unaltered N-terminus (Kyttälä et al., 2005; Cotman and Staropoli, 2012; Mirza et al., 2019). Although we did not assess protein function and expression, our real-time PCR results demonstrated that expression of *CLN3* in the retinas of the blind cattle was similar to that of the control cattle.

In human medicine, recessive variation in *CLN3* has been identified as causative of juvenile-onset retinal and neuronal neurodegeneration, named juvenile neuronal ceroid lipofuscinosis (JNCL), or Batten disease (Ouseph et al., 2016). JNCL is part of a group of neurodegenerative disorders termed neuronal ceroid lipofuscinoses (NCL) that cause

blindness due to retinal degeneration and may include seizures and death due to neuronal atrophy; the disorders are classified by the age of onset (Johnson et al., 2019). The causative genes of JNCL disorders are members of the CLN family: *CLN1–3*, *CLN5*, *CLN6*, and *CLN8* (Weimer et al., 2002; Johnson et al., 2019). In human JNCL patients, one of the most common disease-causing variants is a 1.02-kb deletion of exons 8 and 9 of *CLN3*, although missense and nonsense mutations, duplications, and other deletions have also been implicated (Miller et al., 2013; Mirza et al., 2019; Wright et al., 2020). Several studies have associated mutations in *CLN3* with lysosomal dysfunction (Kitzmüller et al., 2008; Wright et al., 2020). Normally, the RPE serves to continuously remove waste produced by the outer segments of rods and cones utilizing lysosomes for waste degradation (Young, 1967; Collin et al., 2020). Lysosome dysfunction leads to accumulation of degradative byproducts (lipofuscins), particularly in the eye, causing atrophy of the diffuse RPE of the macula (Bok and Hall, 1971; Wavre-Shapton et al., 2015; Ouseph et al., 2016).

Although we did not observe lipofuscin accumulation in the retina of the blind cattle, the retinal degeneration is very similar to that reported in JNCL patients. The loss of the photoreceptor layer in humans results in undetectable rod and cone responses during ERG recordings (Wright et al., 2020; Smirnov et al., 2021), another result observed in our blind cattle. JNCL patients have sub-retinal dots or sub-foveal deposits, which may translate to the altered tapetal reflectivity observed in blind cattle V3, V10, and V11 (Smirnov et al., 2021). Though overt tapetal hyper-reflectivity was observed in blind heifers V10 and V11, the tapetum of blind heifer V3 was diffusely mottled with altered, but not overt, hyper-reflectivity. Retinal vascular attenuation in blind heifer V3

was also only mild. These minor differences are possibly due to her younger age (15 months) at the time of examination compared to cows V10 and V11 (24 months). Another common fundic finding in JNCL patients is retinal vessel attenuation (Smirnov et al., 2021). There was minor observer variance due to subjectivity of fundic examination findings in the interpretation of the level of retinal vessel attenuation in the blind cattle; the consensus was that all examined blind cattle had some level of retinal vessel attenuation. The blind cattle lacked the signs of neurodegeneration such as seizures and ataxia reported in human patients with JNCL (Johnson et al., 2019). However, there is variation in the JNCL phenotype; patients can have mild-to-severe retinal dystrophy but lack neurologic symptoms (Smirnov et al., 2021).

There is evidence in the literature that the progression and severity of CLN3 disease are influenced by sex, though it is not yet understood why. In humans, female JNCL patients have a later onset but faster progression of the disease than males (Cialone et al., 2012). Most blind cattle in our study were female (n = 12 of 13), which may support the hypothesis that sex influences the severity of CLN3 disease. However, this discrepancy may also be due to differences in the management of male and female cattle in beef systems, as males are more often sent to a feedlot to ultimately be harvested whereas a higher proportion of females are retained for breeding. Additional studies are necessary to elucidate whether sex impacts the expression of disease in these cattle as well as if carriers of the mutation may have a subclinical phenotype. Even so, the similarity of these blind cattle to JNCL patients presents the possibility of cattle serving as a model for human non-syndromic JNCL disease.

Our study provides evidence that a 1-bp deletion in CLN3 caused the observed retinal degeneration and blindness in Hereford cattle. Although the cattle were otherwise healthy, blindness can create challenges in navigating unknown terrain, in interactions with other animals, and can cause issues with animal handling, generally impacting the animals' overall well-being. Given the number of cattle in the herd book that are descendent of carriers, commercial genotyping for the *CLN3* variant is ongoing.

Acknowledgments

We thank the Hereford breeders and American Hereford Association staff/personnel for their cooperation and contribution of information and samples. Daniel Garrick, Theta Solutions, facilitated data transfer. Lianna Walker contributed to the RT-PCR analysis. Harvest was facilitated by the faculty and staff of the University of Nebraska's Loeffel Meat Lab. Portions of this work were completed utilizing the Holland Computing Center of the University of Nebraska, which receives support from the Nebraska Research Initiative. SEM was carried out at the Microscopy Research Core Facility of the Center for Biotechnology, which is partially funded by the Nebraska Center for Integrated Biomolecular Communication COBRE grant P20 GM113126, and the Nebraska Research Initiative.

Funding

This project was funded in part by the American Hereford Association.

Data availability

Whole-genome sequence files are available at the NCBI Sequence Read Archive (accession PRJNA1013498). Variant data for this study have been deposited in the European Variation Archive (EVA) at EMBL-EBI under accession PRJEB71833.

Supplementary Tables and Figures

Supplemental Table 5.1. Genotyping primers for the *CLN3* mutation.

Primer	Sequence
Forward	5′-CGTTTGGGAAGAGGAATGAG-3′
Reverse	5′-GCAAAGGTGAGGCTTCAGTC-3′

Supplemental Table 5.2. qPCR primers used to quantify expression of *CLN3* and *ACTB.*

Gene	Primer	Sequence
CLN3	Forward	5′-CTACTTTACCACCTAGAGGAAGTTT-3′
	Reverse	5′-GGTCTTCTCTCTGACTTCGTTT-3′
ACTB	Forward	5′-AGAAGAGCTACGAGCTTCCTGA-3′
	Reverse	5′-TCCATGCCCAGGAAGGAA-3′

Supplemental Table 5.3. Variants in which only blind cattle were homozygous for the alternative allele (XLSX, 21.9 KB).

Supplemental Table 5.4. Relative expression of *CLN3* in retina tissue between blind cattle and control cattle.

Sample	Mean normalized expression	Log_{10} +1	*p*
Blind cow retina	0.000434	0.000188	0.611
Control cow retina	0.000132	0.000058	

(*ACTB*) was used as the reference gene.

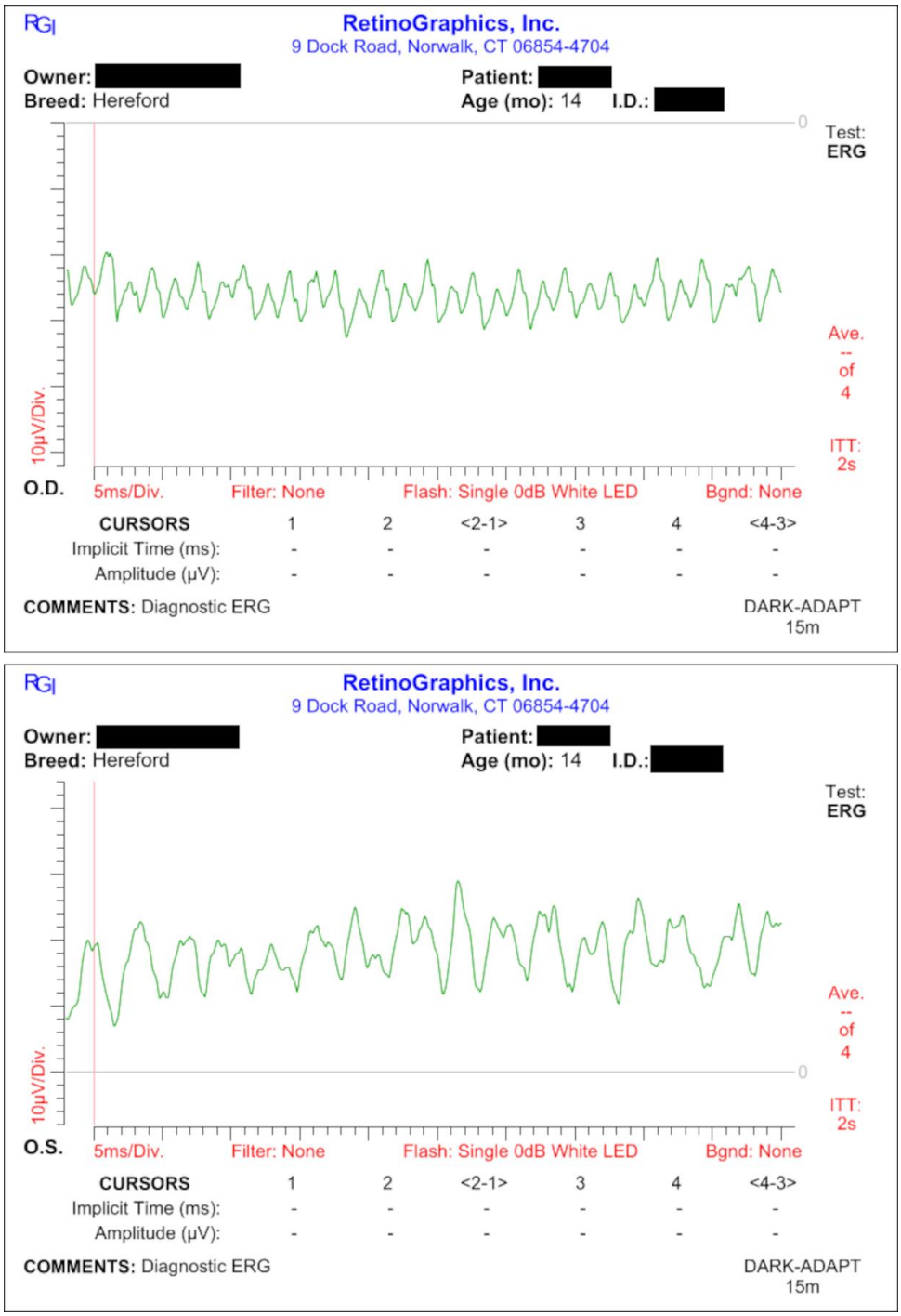

Supplementary Figure 5.1. Electroretinogram tracings for the right (OD) and left (OS) eye of clinically affected heifer (V3). Note the regular electrical cycle noise and no discernible or measurable a- or b-wave amplitudes or implicit times. Tracings were produced on RetinoGraphics BPM-300.

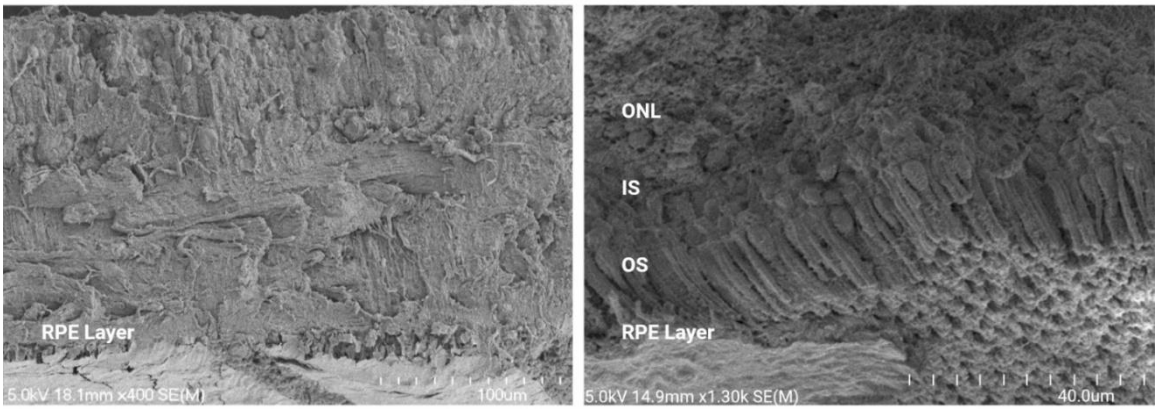

Supplementary Figure 5.2. Side view of retina from blind cow V10 (left) and an example of a normal retina from a pig (right). The blind cow retina is missing the outer nuclear layer (ONL), inner photoreceptor segment (IS), and outer photoreceptor segment (OS) layers above the retinal pigment epithelium (RPE).

CHAPTER 6: A DE NOVO MUTATION IN *CACNA1A* IS ASSOCIATED WITH AUTOSOMAL DOMINANT BOVINE FAMILIAL CONVULSIONS AND ATAXIA IN ANGUS CATTLE

This chapter was published in *Animal Genetics*. Supplementary material can be found online with the article.

Reith, R. R., et al. 2024. A de novo mutation in CACNA1A is associated with autosomal dominant bovine familial convulsions and ataxia in Angus cattle. Anim. Genet. 55:344–351. doi:10.1111/age.13409.

Introduction

Bovine familial convulsions and ataxia (BFCA), also known as cerebellar abiotrophy, was first described in Angus cattle (*Bos taurus*) in 1968 (Barlow et al., 1968). Subsequently, the syndrome was reported to occur in Holstein heifers (White et al., 1975), a Charolais calf (Cho and Leipold, 1978), an Angus calf in the USA (Wallace et al., 1996), and Angus calves in Canada (Fournier et al., 2004). Usually, clinical signs of seizures and ataxia are reported within the first few days of life, although there have been reported cases of onset as late as three months of age (Barlow et al., 1968; White et al., 1975; Fournier et al., 2004). In some reports, calves that survive the first few months may seemingly recover, only to relapse weeks later, while others survive and outgrow the seizures by two years old (Barlow et al., 1968). Each of these cases was suspected to be due to unique autosomal dominant variants with incomplete penetrance resulting in similar presentation of BFCA phenotypes (Barlow et al., 1968; White et al., 1975; Cho and Leipold, 1978; Wallace et al., 1996; Fournier et al., 2004). In humans, multiple autosomal dominant gene variants are associated with familial ataxia (Jen and Wan,

2018). However, no reports identifying the causative genetic variant exists in cattle. No gross lesions are reported in BFCA; microscopic lesions include degeneration and swelling of the Purkinje cells of the lingual and uvula of the cerebellar cortex (Barlow et al., 1968; Barlow, 1981), which is more apparent in calves eight to seventeen months old exhibiting maximal clinical signs compared with affected newborn calves. Lesions detectable by routine histology are limited, easily missed in casual sampling, and not reported in all cases. Clinical disease seems to precede histologic lesion development.

This report describes BFCA in an East Texas cattle operation. In December 2016, fifty-seven (2 to 3-year-old) Brangus-type females were exposed to two recently purchased Angus bulls. The cows had a body condition score of 5-6 on a 1-9 scale. The cattle, grazing a well-managed Coastal Bermuda grass pasture, were current on vaccinations (killed IBR, PI3, BVDV, BRSV, and VL5). The females calved in September through November. The rancher observed neurologic signs, including ataxia and seizures in nine calves (Group A). Six calves were stillborn or died shortly after birth, and thirteen females did not deliver a calf. Routine screening for viruses/bacteria causing stillbirths, pregnancy loss, and neurologic signs did not result in a definitive diagnosis. Parentage testing of affected calves indicated all were the progeny of one bull. Given the relatedness of affected calves and the prior reported dominance of BFCA variants (White et al., 1975; Cho and Leipold, 1978), 36 additional cows were bred to this bull, resulting in an additional 12 affected calves, supporting the hypothesized dominant mode of inheritance. Whole-genome sequencing was subsequently performed to explore genotypic variation associated with BFCA in this family with the goal of elucidating the origin of BFCA in this family of cattle.

Materials and Methods

This study was approved by the Institutional Animal Care and Use Committee at Texas A&M University (TAMU 2017-0395).

Animals

Semen from the sire of the affected calves was collected, processed and frozen for future diagnostic investigation. Tissue and blood samples from one necropsied calf were sent to the Texas A&M Veterinary Medical Diagnostic Laboratory resulting in no definitive diagnosis. Two neurologically affected calves were euthanized and submitted to the Texas A&M School of Veterinary Medicine & Biomedical Sciences necropsy service.

Twenty-five cows at Texas A&M University were impregnated with semen from the sire of the ataxic calves to control for environment and to generate material for sequence analysis. Pregnancies carried to term, resulted in two stillborn, eleven neurologic, and 12 normal calves (Group B). Ten of the neurologic calves exhibited seizures and ataxia within a few days after birth and were submitted to the diagnostic lab between one and two weeks of age. One calf exhibited signs at six months of age and was subsequently euthanized. Eleven cows at the University of Illinois were artificially inseminated using the sire of interest's semen. Eight pregnancies were carried to term and one of the eight calves produced was diagnosed with BFCA and submitted to the lab within days of birth (Group C).

At the time of necropsy, the entire brain of two ataxic calves from Group B were flash-frozen, then stored at -80 °C. Sections of routinely processed cerebellum from other calves were stained with hematoxylin and eosin. Further cerebellum tissues were fixed in 10% formaldehyde and processed routinely for histopathologic examination. Additional

four-micron sections of the cerebellar blocks of three affected calves and one control calf were immune-stained at the University of Nebraska Veterinary Diagnostic Center. CaV2.1 polyclonal antibodies (Invitrogen #PA5-19598 and Invitrogen #PA5-77295) were used as the primary antibody with a hematoxylin counter stain. The primary antibody, 19598, is a Rabbit IgG that targeted peptide residues 1-100 of Rat CACNA1A and was predicted by sequence homology to react with bovine CaV2.1. The second primary antibody, 77295, targeted peptide (C)PSSPERAPGREGPYGRE, corresponding to amino acid residues 865-881 of rat CaV 2.1.

DNA from Groups A (n=7) and C (n=8) as well as DNA from the sire was obtained from whole blood (EDTA). DNA from Group B (6 affected, 7 unaffected) was obtained in the form of ear notches or whole blood. DNA was isolated from the proband sire's semen and from semen of the paternal grandsire. DNA was also obtained from blood cards of the sire's dam, two of the sire's paternal half-siblings, eight offspring from a different paternal half-sibling of the sire, and a distant descendant of the sire's sire.

DNA Isolation

DNA was isolated from ear tissues and blood of the calves, sire's semen, and blood cards using the Gentra Puregene Blood Kit (Qiagen, Venlo, Netherlands) following the protocol described in Sieck et al., (2020). Hole punches from the blood cards were used as samples and DNA isolation followed the same protocol as mentioned. DNA concentration for all samples was obtained using the EPOCH Microplate Reader (BioTek, Winooski, VT, USA).

Whole-genome sequencing (WGS)

Isolated DNA from Group B (6 affected, 7 unaffected), and the sire (semen) was sent to Admera Health (South Plainfield, NJ) for KAPA library preparation and 150-bp paired-end sequencing on an Illumina NovaSeq to a targeted depth of 20X for the sire and 12X for the calves. Raw data were processed by trimming adapters and poor-quality bases using TrimGalore (Krueger et al., 2023). Reads were mapped to the ARS-UCD1.2 reference genome with BWA-MEM (Li and Durbin, 2009), duplicates were marked with Samtools (Danecek et al., 2021). GATK Haplotype Caller was used to realign indels and call variants (Van der Auwera and O'Connor, 2020). A combined variant file was created by merging the variant call format files (VCFs) of the 14 related cattle sequenced for this project with 135 control cattle previously sequenced from other projects in our lab (including Angus, Brangus, Red Angus, Hereford, Charolais, crossbred, and composites (Red Angus, Simmental, Gelbvieh)). A case control analysis (Cingolani et al., 2012) was run with the sire and 5 ataxic calves identified as cases and the 142 other cattle assumed to be unaffected. The phenotype of the calf with late onset ataxia was also labeled as "unknown" in the analysis. Assuming the BFCA came from a dominant genotype for which the sire was heterozygous, the variant file was filtered to identify loci where the *P*-value assuming a dominant model was < 0.00001.

The next set of filtering criteria included the removal of loci where the alternate allele appeared in cattle unrelated to the sire of interest. Then, loci where any calf was homozygous for an alternate allele were removed, as were loci for which the sire had the reference genotype. The final criterion, to allow for some error in phenotyping and/or incomplete penetrance, was to remove loci where fewer than 4 of the 6 affected calves

were heterozygous and more than two unaffected calves were heterozygous for the variant. The consequence of the remaining loci was predicted by Ensembl's Variant Effect Predictor (VEP; McLaren *et al.*, 2016).

DELLY (Rausch et al., 2012) was run on the bam files of Group B and the sire to identify insertions, deletions, duplications, and other structural variants in the genome. Results from DELLY were filtered using the case-control function of SNPSift as described before, keeping variants with a *P*-value < 0.05. Loci were filtered for variants where the sire and at least four affected calves were heterozygous and, at most, two unaffected calves are heterozygous for the variant. Ensembl's VEP was utilized to find predicted impact of variants on gene function.

Sanger sequencing was used to determine genotypes for the candidate variant in *CACNA1A*. Primers were designed using Primer3 (Supplementary Table 6.1; Untergasser *et al.*, 2012). PCR using those primers was performed using a FastStart kit (Sigma-Aldrich, St. Louis, MO, USA) following the PCR protocol described in Sieck et al,. (2020). PCR product cleanup was performed using 0.75 μL ExoSAP-IT (Applied Biosystems, Foster City, CA, USA) per 4 μL PCR product and incubation thermal cycling at 37 °C for 30 min, 80 °C for 15 min, and a 15 °C hold. Samples were sent to ACGT (Wheeling, IL, USA) for Sanger sequencing. Sequencing results were visualized with Sequencher ('Sequencher® version 5.4.6 DNA sequence analysis software'). Poor quality base pairs at the ends of the sequences were trimmed to improve alignment.

ddPCR

Droplet Digital PCR (ddPCR) was utilized to ascertain the proportion of wild type and variant *CACNA1A* alleles in the sire's semen and blood and compare the proportion

with that of his heterozygous calves. Primers were designed using Primer3 (Supplementary Table 6.2; Untergasser *et al.*, 2012) with the *CACNA1A* variant site as the final (3') base of each forward primer; the WT primer had the wild type allele (C) and the MUT primer the variant allele (T). To promote separation by fluorescent amplitude between the allele types, a long tail (39 bp) was added to the 5' end of the WT primer and a short tail (6 bp) was added to the 5' end of the MUT primer. A single reverse primer was designed for use with both forward primers. The ddPCR reactions were performed using the standard protocol on a QX200 ddPCR system (Bio-Rad Laboratories, Hercules, CA, USA). A non-template (negative) control and positive controls, consisting of DNA from two heterozygous ataxic calves (100 ng), a wild type unaffected calf (10 ng), and a gBlock template (1 pg) homozygous for the variant were included. The reaction also included DNA from the sire's semen and from his blood (100 ng). Samples were run in either duplicate or triplicate. The reaction included 2X ddPCR Supermix for Evagreen (Bio-Rad Laboratories, Hercules, CA, USA), 1 ul of template DNA (concentration previously described), 200 nM WT primer, 50 nM MUT primer and 100 nM reverse in a reaction volume of 22 μL. Primer concentrations were varied to allow for distinct separation of the droplet clouds generated by allele type. Reactions were converted into ~20,000 droplets of 1 nL using the QX200 Droplet Generator. Thermocycling included 5 min of enzyme activation at 95 °C and 40 cycles of denaturation (95 °C, 30 s) followed by annealing/extension (62 °C, 1 min). Signal stabilization (4 °C, 5 min then 90 °C, 5 min) concluded the cycle. The plate was read in the QX100 Droplet Reader (Bio-Rad Laboratories, Hercules, CA, USA) and the results were analyzed using QuantaSoft Software (Bio-Rad Laboratories, Hercules, CA, USA). Droplets were clustered by

amplitude as WT, MUT, or negative droplets. The proportion of MUT droplets for each sample type was calculated within each well, then averaged across well replicates. A proportional two-tailed z-test was performed in R using the average proportion of MUT droplets previously described, comparing the sire's blood and sire's semen to the affected, heterozygous calves separately with significance specified at $\alpha=0.05$.

Relative Quantification Real Time PCR

While still frozen, cerebellar vermis was dissected from the brains of two ataxic calves (both male, < 7d old). Flash frozen cerebellar samples were also available from two normal, unrelated calves (1 male, 1 male, both < 1d old). RNA was isolated from each sample following the Homogenized RNeasy Lipid Tissue Mini Handbook (Qiagen, Germantown, MD) with the DNase I option. RNA for each sample was converted into cDNA using Cytiva First-Strand Synthesis Kit (Cat# 27926101) following manufacturer protocol.

The expression of *CACNA1A* was quantified using SYBR Green PCR Master Mix Kit (Cat# 4309155, Applied Biosystems) and CFX384 Real Time PCR (BioRad). The qPCR was performed in 10 µL reactions containing 1x SYBR Green Master Mix, 1 µM forward primer, 1 µM reverse primer, 3 µL of water, and 1 µL of cDNA template. Samples were run in triplicate with negative controls. The qPCR primers (Supplementary Table 6.3) were designed using IDT PrimerQuest Tool software (www.idtdna.com). *CACNA1A* primers crossed exons 31 and 32. Beta-actin was used as the housekeeping gene. Thermal cycling conditions consisted of 95 °C for 10 min, 40 cycles of 98 °C for 15 sec, 58 °C for 30 sec, 72 °C for 30 sec, then a final extension of 72 °C for 60 sec. The mean normalized expression (MNE) was calculated using the cycle crossing thresholds

(CT) of the replicates, incorporating qPCR efficiencies of each gene. The mean normalized expression values were then $\log_{10}$ transformed and used to compare the phenotype groups by t-test.

The synthesized cDNA from the cerebellar vermis of the same two ataxic calves and two unrelated control calves were Sanger sequenced using the qPCR primers. PCR and PCR product cleanup were performed as previously described. Samples were sent to Eurofins Genomics (Louisville, KY, USA) for Sanger sequencing. Sequencing results were visualized with Sequencher (Gene Codes, Ann Arbor, MI USA). Poor-quality base pairs at the ends of the sequences were trimmed to improve alignment.

Results

Pathology

All brains were grossly normal at necropsy. A detailed postmortem examination revealed cerebellar lesions in one of the original (Group A) affected calves indicative of cerebellar abiotrophy associated with BFCA. Lesions included ganglion cell neuron (Purkinje cells) degeneration and axonal swelling in the cerebellar granular layer, most commonly along the interface between the Purkinje cells and granular cell layer, consistent with Purkinje cell axons (Figure 6.1). Rare swollen axons were also seen deeper in the granular cell layer. Minimal axonal degeneration was evident multifocally in the cervical, thoracic, and lumbar spinal cord. Similar but even milder lesions were seen in the cerebellum and spinal cord of the other calf from Group A. The lesions were not apparent in calves that developed neurologic signs and autopsied before two weeks of age (Groups B and C).

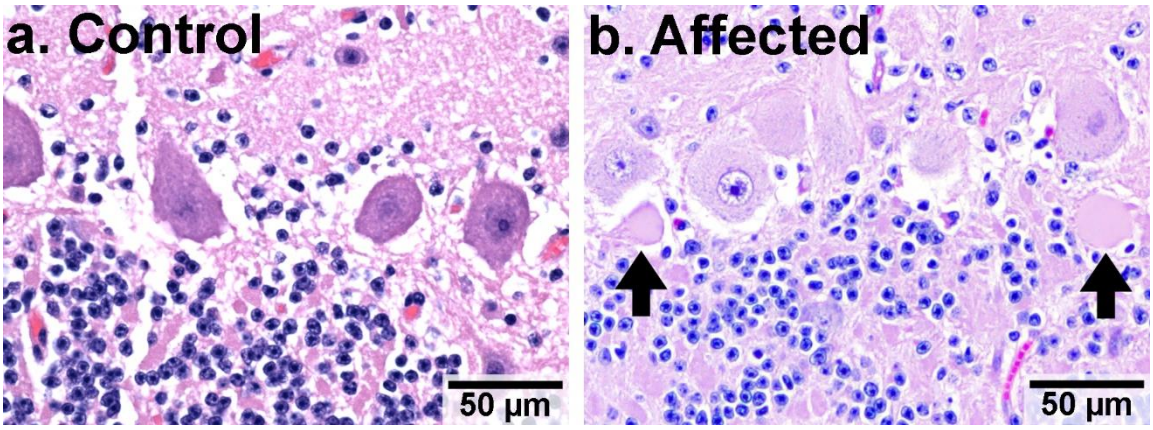

Figure 6.1. Cerebellar tissue at the Purkinje cell layer from an unrelated control calf (a) and an affected calf (b). Arrows point toward swollen Purkinje cell axons.

In the examined Group B calves, one calf had interstitial pneumonia and suppurative meningitis with bacteria in the brain and spinal cord, consistent with neonatal sepsis. Immunohistochemistry of three affected calves and one control calf with the CaV2.1 primary antibody was negative and failed to demonstrate aggregation of the calcium channel protein within the cytoplasm and dendrites of Purkinje cells reported in human cases of spinocerebellar ataxia type 6 (Ishiguro et al., 2010). All Group B calves lacked the histologic brain lesions seen in the two Group A calves. The affected calf from Group C was not necropsied.

WGS to Identify Candidate Variants

Variant calling in GATK identified 66.5 million variants among the 149 cattle (6 affected calves, 7 unaffected calves, their sire, and 135 control cattle). After filtering, 252 loci fit the previously mentioned criteria for a hypothesized dominant condition (Supplementary Table 6.4). VEP predicted five variants to have either a moderate or a high impact on gene function (Table 6.1).

Table 6.1. Variants fitting a hypothesized dominant mode of inheritance with a predicted impact on gene function. Variant positions are in relationship to reference genome ARS-UCD1.2. The ratio of affected to unaffected calves reports the number of calves of each classification heterozygous for the variant (of 6 affected and 7 unaffected).

Location (chr:bp)	Ref/var Allele	Gene ID	Variant type	SNP identifier	Predicted Impact	Affected calves: unaffected calves
1:94757019	G/A	*ECT2*	Missense	rs799486535	Moderate	4:1
7:12367906	C/T	*CACNA1A*	Stop gained	No	High	5:0
7:72240819	A/G	*ATP10B*	Missense	No	Moderate	5:2
12:72826501	C/G	*ABCC4*	Splice acceptor variant	rs383647407	High	4:0
26:31375612	G/A	*RBM20*	Missense	rs432716670	Moderate	4:1

Variants in *ECT2*, *ABCC4*, and *RBM20* were deemed unlikely to be causative given their prior identification in cattle without clinical signs of BFCA and due to their incomplete segregation with the phenotype (each variant was present in only 4 of 6 cases, and the *ECT2* and *RBM20* variants were each present in one control calf). The variant in *ATP10B* was present in two unaffected calves, thus was not considered a primary candidate. The remaining variant with a predicted effect on gene function in the calcium voltage-gated channel subunit alpha1 gene (*CACNA1A*, NM_001075129.1; chr7 g.12367906C>T) predicted to cause a premature stop codon in exon 32 of 47 (NP_001068597.1, c.5073C>T, p.Arg1681*) and which had not been previously reported in cattle. This predicted premature stop codon is expected to truncate the protein by 817 amino acids. The Ensembl Genomic Evolutionary Rate Profiling (GERP) score for

chr7:12367897-12367926 of the bovine genome, which includes the variant site, is 345.7 (p-value ~ 0.0); this site is therefore highly conserved across the 63 eutherian mammals used to calculate the score. Because of its expected impact on gene function, uniqueness to the cattle in the proband family, presence in all but one of the affected calves and absence in the controls, the *CACNA1A* variant was prioritized as a candidate for producing BFCA in this family.

There were 164 variants identified by DELLY after filtering (Supplementary Table 6.5). None of those variants segregated perfectly between cases and controls, with four of the six cases, at most, sharing any one variant that also was not in an unaffected calf. When the WGS of the sire and calves were compared to the WGS of three unrelated Angus cattle in Integrative Genomics Viewer, 225 of the 245 variants were found in other, unrelated Angus cattle. The remaining variants overlap with structural variants reported in ENSEMBL, making them less likely to be the cause of BFCA. As none of the variants identified with DELLY segregated by phenotype and thus were removed from consideration.

Genotyping of the Candidate Variant

As determined by Sanger sequencing, all eight ataxic calves among Group A and C were heterozygous for the *CACNA1A* variant while the unaffected calves did not have the variant (Table 6.2). The variant was absent in all additional relatives including both the sire and dam of the bull that sired the affected calves. One ataxic calf from Group B was wild type; both WGS and Sanger sequencing confirmed that calf's genotype. The BCFA affected calf with meningitis (Group B) was heterozygous for the variant.

Table 6.2. Distribution of *CACNA1A* genotype and BFCA phenotype among the sire of interest, his sampled calves, and WGS control cattle.

Phenotype	Data Source	Group	C/C	C/T
Unaffected	WGS	Sire	0	1
	Sanger	Group A	0	0
	WGS	Group B	7	0
	Sanger	Group C	7	0
	WGS	Angus-based	21	0
		Brangus	9	0
		Charolais	7	0
		Hereford-based	56	0
		Red Angus-based	41	0
		Total	148	1
Affected	Sanger	Group A	0	7
	WGS	Group B	1	5
	Sanger	Group C	0	1
		Total	1	13

Whole-genome sequence data from the University of Missouri, which included about 5,500 cattle (Dr. Robert Schnabel, personal communication), did not identify any instances of the *CACNA1A* variant. Additionally, the variant was not found in WGS data queried from USDA Meat Animal Research Center database (Snelling et al., 2020).

CACNA1A Expression

The ddPCR results showed that the proportion of variant alleles in the DNA from both the blood and semen of the sire was not significantly different from the proportion observed in two affected, heterozygous calves, nor was there a difference in the proportion when comparing the sire's blood to semen (Supplementary Table 6.6).

Relative quantification real time PCR demonstrated that *CACNA1A* was expressed in the cerebellar vermis of the two ataxic calves and had similar expression compared to the controls ($P = 0.09$). Sanger sequencing of the cDNA revealed that both

the wildtype and variant alleles are expressed in the cerebellar vermis of the ataxic calves (Supplementary Figure 6.1).

Discussion

Sequence analysis of the sire and his half-sibling calves born to three different herds and genotype data of additional related and unrelated animals strongly support the chr7 g.12367906C>T variant of *CACNA1A* as both de novo in the sire and causative of the observed BFCA. The CACNA1A protein is involved in calcium-dependent processes including neurotransmitter release and muscle contractions (Sintas et al., 2017). In humans and mice, the gene is expressed in a variety of types of nervous tissue, especially in the cerebellum and cerebral cortex (Fagerberg et al., 2014; Yue et al., 2014). As further support of this variant being causative in these calves, several variants in *CACNA1A* are associated with dominant episodic ataxia in humans (Mantuano et al., 2010). Similar to the variant identified in this family, the *CACNA1A* variant rs1555738369 in humans also results in a premature stop codon in exon 32. The nonsense variant in humans, Arg1665*, is located the fourth transmembrane protein of the fourth domain (IVS4); based on similarity of the cattle sequence to that of humans and mice, the variant identified in this family of cattle (Arg1681*) is predicted to be in IVS4 or in the cytoplasm between IVS4 and IVS5 (Starr et al., 1991; Mantuano et al., 2010; Paysan-Lafosse et al., 2023). The fourth segment (S4) of each domain is important for voltage sensor activation (Catterall, 2000). Substitution of arginine residues such as Arg1673Pro and Arg1680Cys in S4 segments have been implicated in severe cases of ataxia (Starr et al., 1991; Luo et al., 2017; Indelicato and Boesch, 2021), thus nonsense variants are likely to have a similar impact. Based on human data from the gnomAD database (Karczewski et al., 2020),

CACNA1A has a probability of loss-of-function intolerance score of 1, further supporting the proposed role of the truncating variant identified in this study having a severe and possible haploinsufficient effect on protein function.

Haploinsufficiency of the locus is also supported in the literature, which indicates that the presence of a mutant channel, even with co-expression of a wild type channel, is likely sufficient to cause ataxia (Jeng et al., 2006; Mezghrani et al., 2008). In a functional study of a *CACNA1A* variant (Arg1669*) in a human patient with early onset ataxia (Choi et al., 2017), the injection of Arg1669* cRNA into frog oocytes decreased the voltage currents in the resulting protein, causing a loss of function (Jeng et al., 2006). When wild type and mutant channels were co-expressed at a 1:1 ratio, the wild type channels had decreased amplitude currents compared to that of the wild type control, supporting the importance of this region of the protein to calcium channel signaling. Mutant CACNA1A channels can also inhibit trafficking and downregulate expression of the wild type channel (Mezghrani et al., 2008), supporting the hypothesized dominant mode of action in BFCA. The qPCR and cDNA sequencing results show that the *CACNA1A* variant is expressed alongside the wild type allele in the ataxic calves. This provides evidence that the BFCA is due to dysfunction at the protein level, likely haploinsufficiency as previously described literature suggests. Mutant, calcium-channel, protein migration from the endoplasmic reticulum to the plasma membrane is disrupted in some human cases of episodic ataxia; the abnormal proteins have been reported to aggregate along the endoplasmic reticulum (Jeng et al., 2008). However, IHC failed to identify aggregates in these BFCA samples, suggesting that the morphologic lesions reported are secondary to dysfunction and thus not required for histological signs.

Both BFCA and episodic ataxia in humans have reported cases of incomplete penetrance. The Arg1665* variant in humans was detected in a patient with ataxic episodes beginning at age 17 (Mantuano et al., 2010). The mother of this patient was identified as an unaffected heterozygote, indicating possible incomplete penetrance of the variant similar to prior reports in cattle (Wallace et al., 1996). Notably, the clinically normal sire in this study carried the mutation in his germ line and blood. Incomplete penetrance as observed in BFCA previous cases may have lessened the severity of the predicted haploinsufficiency in the sire. It is possible the sire had subtle or unnoticed clinical signs of BFCA as a calf that were unreported; the owners of the bull did not raise him as a calf. Based on published reports, clinical signs of BFCA are varied, can diminish after 18 months, and may even disappear after two years (Barlow, 1981; Fournier et al., 2004). Other than incomplete penetrance, there is the possibility that he was mosaic in some of his somatic cells, including his brain. Unfortunately, additional samples from the sire were not available to investigate the mosaic hypothesis after variant identification.

The fact that one calf, classified as ataxic, lacked the candidate variant, confirmed by multiple DNA isolations and sequence analyses, is unexplained. The calf probably had a different cause of ataxia and represented a phenocopy in our study owing to a lack of pathologic examination of each case. This calf did not receive a full necropsy. Although its brain was examined histologically, no cause of ataxia was identified.

Histologic lesions were observed only in Group A calves, and they consisted of mild axonal swelling in the cerebellar cortex and very mild axonal degeneration in the spinal cord. These lesions are similar to those described previously in BFCA (White et al., 1975; Cho and Leipold, 1978; Barlow, 1981; Wallace et al., 1996). Findings

described in previous reports that were not convincingly observed in this study include Purkinje cell degeneration and loss and vacuolation within the cerebellar nuclei. The two calves necropsied that were found to have lesions were approximately 2-3 months of age (Group A), while the necropsied Group B calves ranged in age from 1-4 days, suggesting that the lesions require time to develop and thus are preceded by clinical signs. Previous reports of BFCA that describe more severe lesions, including Purkinje cell loss, have been in animals that are generally older than 3 months (Barlow, 1981; Fournier et al., 2004).

This research supports that the *CACNA1A* nonsense variant has an autosomal dominant effect resulting in BFCA clinical signs. Overall, identification of causative *CACNA1A* variants in humans with similar conditions, and its effect on protein function, give credence to the bovine *CACNA1A* variant causing BFCA in this family of cattle. Given the dominant mode of inheritance of this pathogenic variant, culling of the bull has eliminated this genetic form of ataxia from the population. Limitations of this investigation include uncertainty of how the sire was seemingly unaffected and the assumed phenocopy as one calf classified as ataxic was not heterozygous for the *CACNA1A* variant. This investigation, however, provides evidence of the role *CACNA1A* plays in this phenotype and sequencing the gene in future familial cases may be enlightening.

Data Availability

Whole-genome sequence files of the 14 cattle whole-genome sequenced for this study are available at the NCBI Sequence Read Archive (SRA accession no.

PRJNA994471). WGS data from 96 cattle utilized as healthy controls are available under SRA accession nos PRJNA1042814, PRJNA1042650, PRJNA1013498, PRJNA936134, PRJNA663547 and PRJNA513064. Sequence data from 22 control cattle are being evaluated for other projects; those data will become available after those projects are published and are available via a Data Use Agreement with the authors.

Acknowledgements

The American Angus Association partially funded the investigation. Portions of this work were completed utilizing the Holland Computing Center of the University of Nebraska, which receives support from the Nebraska Research Initiative.

Supplementary Tables and Figures

Supplementary Table 6.1. PCR primers for Sanger sequencing of the *CACNA1A* variant.

Genotyping method	Variant Location	Forward Primer 5'-3'	Reverse Primer 5'-3'	Fragment Length (bp)	Annealing Temp (°C)
Sanger	7:12367906	CCCCATCCCC TACTTCATTT	TGGAGCCCTCAA GACATACC	522	58

Supplementary Table 6.2. ddPCR Primers for assaying the *CACNA1A* variant. Lowercase letters indicate the added tail.

Primer set	Forward Primer 5'-3'	Reverse Primer 5'-3'	Length (bp)	Annealing Temp (°C)
CACNA1A-WT	Aaataaataaataaataaataaataa ataaataaataaaCCGTCAGG GTTACACCATCC	TGGGGCTCACC TTGAAGGAC	104	62
CACNA1A-MUT	gggggCCGTCAGGGTTA CACCATCT	TGGGGCTCACCT TGAAGGAC	71	62

Supplementary Table 6.3. qPCR primers for relative semi-quantification of *CACNA1A* expression.

Primer set	Forward Primer 5'-3'	Reverse Primer 5'-3'	Length (bp)	Annealing Temp (°C)
CACNA1A ex 31-32	GTGACCGAGTTTG GGAATAAC	ACTGCACAAAGG TCCAGAGA	124	58
ACTB	AGAAGAGCTACGA GCTTCCTGA	TCCATGCCCAGGA AGGAA	100	58

Supplementary Table 6.4. WGS loci after filtering with predicted impact on gene function (XLSX, 22.7 KB).

Supplementary Table 6.5. Structural variants shared among the sire, at least four affected Group B calves, and at most two unaffected Group B calves (XLSX, 29.4 KB).

Supplementary Table 6.6. ddPCR results for proportion of *CACNA1A* variant in DNA samples.

Samples	Average percent of mutant droplets (standard deviation)	P-value vs affected calves	P-value vs semen DNA
Sire's Blood	0.447 (±0.035)	0.905	0.966
Sire's Semen	0.477 (±0.009)	0.904	
Heterozygous calves	0.364 (±0.035)		

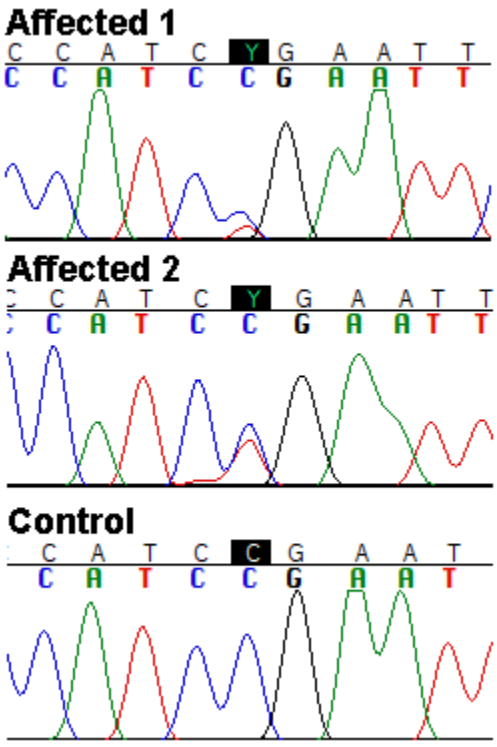

Supplementary Figure 6.1. Sanger sequencing of *CACNA1A* cDNA from cerebellar vermis of two ataxic calves and a control.

REFERENCES

Abravaya, K., M. P. Myers, S. P. Murphy, and R. I. Morimoto. 1992. The human heat shock protein hsp70 interacts with HSF, the transcription factor that regulates heat shock gene expression. Genes Dev. 6:1153–1164. doi:10.1101/gad.6.7.1153.

Ahmad, S. S., K. Ahmad, E. J. Lee, Y.-H. Lee, and I. Choi. 2020. Implications of Insulin-Like Growth Factor-1 in Skeletal Muscle and Various Diseases. Cells. 9:1773. doi:10.3390/cells9081773.

Akalin, A., M. Kormaksson, S. Li, F. E. Garrett-Bakelman, M. E. Figueroa, A. Melnick, and C. E. Mason. 2012. methylKit: a comprehensive R package for the analysis of genome-wide DNA methylation profiles. Genome Biol. 13:R87. doi:10.1186/gb-2012-13-10-r87.

Akdis, M., A. Aab, C. Altunbulakli, K. Azkur, R. A. Costa, R. Crameri, S. Duan, T. Eiwegger, A. Eljaszewicz, R. Ferstl, R. Frei, M. Garbani, A. Globinska, L. Hess, C. Huitema, T. Kubo, Z. Komlosi, P. Konieczna, N. Kovacs, U. C. Kucuksezer, N. Meyer, H. Morita, J. Olzhausen, L. O'Mahony, M. Pezer, M. Prati, A. Rebane, C. Rhyner, A. Rinaldi, M. Sokolowska, B. Stanic, K. Sugita, A. Treis, W. van de Veen, K. Wanke, M. Wawrzyniak, P. Wawrzyniak, O. F. Wirz, J. S. Zakzuk, and C. A. Akdis. 2016. Interleukins (from IL-1 to IL-38), interferons, transforming growth factor β, and TNF-α: Receptors, functions, and roles in diseases. J. Allergy Clin. Immunol. 138:984–1010. doi:10.1016/j.jaci.2016.06.033.

Anastasiadi, D., A. Esteve-Codina, and F. Piferrer. 2018. Consistent inverse correlation between DNA methylation of the first intron and gene expression across tissues and species. Epigenetics Chromatin. 11:37. doi:10.1186/s13072-018-0205-1.

Andrews, S. 2010. FASTQC. A quality control tool for high throughput sequence data.

Angelos, J. A. 2022. Infectious Keratoconjunctivitis in Animals - Eye Diseases and Disorders. Merck Vet. Man.

Anjali, G. Vk, L. Sarma, M. Tripathi, M. R. Verma, V. Verma, M. C. Pathak, H. A. Samad, V. P. Maurya, V. S. Chouhan, and G. Singh. 2023. Thyroid hormone dynamics of Tharparkar and Sahiwal cattle during induced heat stress. Trop. Anim. Health Prod. 55:57. doi:10.1007/s11250-023-03477-8.

Arp, T. S., S. T. Howard, D. R. Woerner, J. A. Scanga, DAY. R. McKenna, W. H. Kolath, P. L. Chapman, J. D. Tatum, and K. E. Belk. 2014. Effects of dietary ractopamine hydrochloride and zilpaterol hydrochloride supplementation on performance, carcass traits, and carcass cutability in beef steers1. J. Anim. Sci. 92:836–843. doi:10.2527/jas.2013-7122.

Asea, A. 2008. Heat Shock Proteins and Toll-Like Receptors. In: S. Bauer and G. Hartmann, editors. Toll-Like Receptors (TLRs) and Innate Immunity. Vol. 183. Springer Berlin Heidelberg, Berlin, Heidelberg. p. 111–127.

Asea, A., S.-K. Kraeft, E. A. Kurt-Jones, M. A. Stevenson, L. B. Chen, R. W. Finberg, G. C. Koo, and S. K. Calderwood. 2000. HSP70 stimulates cytokine production through a CD14-

dependant pathway, demonstrating its dual role as a chaperone and cytokine. Nat. Med. 6:435–442. doi:10.1038/74697.

Auclair, G., S. Guibert, A. Bender, and M. Weber. 2014. Ontogeny of CpG island methylation and specificity of DNMT3 methyltransferases during embryonic development in the mouse. Genome Biol. 15:545. doi:10.1186/s13059-014-0545-5.

Babraham Bioinformatics - Trim Galore!
https://www.bioinformatics.babraham.ac.uk/projects/trim_galore/

Bagath, M., G. Krishnan, C. Devaraj, V. P. Rashamol, P. Pragna, A. M. Lees, and V. Sejian. 2019. The impact of heat stress on the immune system in dairy cattle: A review. Res. Vet. Sci. 126:94–102. doi:10.1016/j.rvsc.2019.08.011.

Barlow, D. P., and M. S. Bartolomei. 2014. Genomic Imprinting in Mammals. Cold Spring Harb. Perspect. Biol. 6:a018382–a018382. doi:10.1101/cshperspect.a018382.

Barlow, R. L., K. A. Linklater, and G. E. Young. 1968. Familial Convulsions and Ataxia in Angus Calves. Vet. Rec. 83:60–65.

Barlow, R. M. 1981. Morphogenesis of Cerebellar Lesions in Bovine Familial Convulsions and Ataxia. Vet. Pathol. 18:151–162. doi:10.1177/030098588101800202.

Barnes, T. L., C. N. Cadaret, K. A. Beede, T. B. Schmidt, J. L. Petersen, and D. T. Yates. 2019. Hypertrophic muscle growth and metabolic efficiency were impaired by chronic heat stress, improved by zilpaterol supplementation, and not affected by ractopamine supplementation in feedlot lambs1. J. Anim. Sci. 97:4101–4113. doi:10.1093/jas/skz271.

Baumgard, L. H., and R. P. Rhoads. 2013. Effects of heat stress on postabsorptive metabolism and energetics. Annu. Rev. Anim. Biosci. 1:311–337. doi:10.1146/annurev-animal-031412-103644.

Belhadj Slimen, I., T. Najar, A. Ghram, H. Dabbebi, M. Ben Mrad, and M. Abdrabbah. 2014. Reactive oxygen species, heat stress and oxidative-induced mitochondrial damage. A review. International Journal of Hyperthermia. 30:513–523. doi:10.3109/02656736.2014.971446.

Bharati, J., S. S. Dangi, S. R. Mishra, V. S. Chouhan, V. Verma, O. Shankar, M. K. Bharti, A. Paul, D. K. Mahato, G. Rajesh, G. Singh, V. P. Maurya, S. Bag, P. Kumar, and M. Sarkar. 2017. Expression analysis of Toll like receptors and interleukins in Tharparkar cattle during acclimation to heat stress exposure. J. Therm. Biol. 65:48–56. doi:10.1016/j.jtherbio.2017.02.002.

Bodine, S. C., T. N. Stitt, M. Gonzalez, W. O. Kline, G. L. Stover, R. Bauerlein, E. Zlotchenko, A. Scrimgeour, J. C. Lawrence, D. J. Glass, and G. D. Yancopoulos. 2001. Akt/mTOR pathway is a crucial regulator of skeletal muscle hypertrophy and can prevent muscle atrophy in vivo. Nat. Cell Biol. 3:1014–1019. doi:10.1038/ncb1101-1014.

Bogoyevitch, M. A., K. R. W. Ngoei, T. T. Zhao, Y. Y. C. Yeap, and D. C. H. Ng. 2010. c-Jun N-terminal kinase (JNK) signaling: Recent advances and challenges. Biochim. Biophys. Acta BBA - Proteins Proteomics. 1804:463–475. doi:10.1016/j.bbapap.2009.11.002.

Bok, D., and M. O. Hall. 1971. The role of the pigment epithelium in the etiology of inherited retinal dystrophy in the rat. J. Cell Biol. 49:664–682. doi:10.1083/jcb.49.3.664.

Booth, M. W., M. F. Breed, G. A. Kendrick, P. E. Bayer, A. A. Severn-Ellis, and E. A. Sinclair. 2022. Tissue-specific transcriptome profiles identify functional differences key to understanding whole plant response to life in variable salinity. Biol. Open. 11:bio059147. doi:10.1242/bio.059147.

Boyd, B. M., S. D. Shackelford, K. E. Hales, T. M. Brown-Brandl, B. Bremer, M. L. Spangler, T. L. Wheeler, DAY. A. King, and G. E. Erickson. 2015. Effects of shade and feeding zilpaterol hydrochloride to finishing steers on performance, carcass quality, heat stress, mobility, and body temperature. J. Anim. Sci. 93:5801–5811. doi:10.2527/jas.2015-9613.

Brandt, C., and B. K. Pedersen. 2010. The Role of Exercise-Induced Myokines in Muscle Homeostasis and the Defense against Chronic Diseases. J Biomed Biotechnol. 2010:520258. doi:10.1155/2010/520258.

Brasier, A. R. 2006. The NF-κB Regulatory Network. Cardiovasc. Toxicol. 6:111–130. doi:10.1385/CT:6:2:111.

Braun, M., A.-K. Struck, S. Reinartz, M. Heppelmann, J. Rehage, J. C. Eule, M. Ciurkiewicz, A. Beineke, J. Metzger, and O. Distl. 2019. Study of congenital Morgagnian cataracts in Holstein calves. PLoS ONE. 14. doi:10.1371/journal.pone.0226823.

Brown-Brandl, T. M. 2018. Understanding heat stress in beef cattle. Rev. Bras. Zootec. 47. doi:10.1590/rbz4720160414.

Cargnello, M., and P. P. Roux. 2011. Activation and Function of the MAPKs and Their Substrates, the MAPK-Activated Protein Kinases. Microbiol. Mol. Biol. Rev. MMBR. 75:50–83. doi:10.1128/MMBR.00031-10.

Catterall, W. A. 2000. Structure and Regulation of Voltage-Gated Ca2+ Channels. Annu. Rev. Cell Dev. Biol. 16:521–555. doi:10.1146/annurev.cellbio.16.1.521.

Chatterjee, A., E. J. Rodger, I. M. Morison, M. R. Eccles, and P. A. Stockwell. 2017. Tools and Strategies for Analysis of Genome-Wide and Gene-Specific DNA Methylation Patterns. In: G. J. Seymour, M. P. Cullinan, and N. C. K. Heng, editors. Oral Biology: Molecular Techniques and Applications. Springer, New York, NY. p. 249–277.

Chen, L., H. Deng, H. Cui, J. Fang, Z. Zuo, J. Deng, Y. Li, X. Wang, and L. Zhao. 2017. Inflammatory responses and inflammation-associated diseases in organs. Oncotarget. 9:7204–7218. doi:10.18632/oncotarget.23208.

Chen, X., B. Zhang, T. Wang, A. Bonni, and G. Zhao. 2020. Robust principal component analysis for accurate outlier sample detection in RNA-Seq data. BMC Bioinformatics. 21:269. doi:10.1186/s12859-020-03608-0.

Cho, D. Y., and H. W. Leipold. 1978. Cerebellar cortical atrophy in a Charolais calf. Vet. Pathol. 15:264–266. doi:10.1177/030098587801500212.

Choi, K.-D., J.-S. Kim, H.-J. Kim, I. Jung, S.-H. Jeong, S.-H. Lee, D. U. Kim, S.-H. Kim, S. Y. Choi, J.-H. Shin, D.-S. Kim, K.-P. Park, H.-S. Kim, and J.-H. Choi. 2017. Genetic Variants Associated with Episodic Ataxia in Korea. Sci. Rep. 7:13855. doi:10.1038/s41598-017-14254-7.

Cialone, J., H. Adams, E. F. Augustine, F. J. Marshall, J. M. Kwon, N. Newhouse, A. Vierhile, E. Levy, L. S. Dure, K. R. Rose, D. Ramirez-Montealegre, E. A. de Blieck, and J. W. Mink. 2012. Females experience a more severe disease course in batten disease. J. Inherit. Metab. Dis. 35:549–555. doi:10.1007/s10545-011-9421-6.

Cingolani, P., D. Ruden, V. Patel, M. Coon, T. Nguyen, S. Land, and X. Lu. 2012. Using Drosophila melanogaster as a Model for Genotoxic Chemical Mutational Studies with a New Program, SnpSift. Front. Genet. 3.

Collin, G. B., N. Gogna, B. Chang, N. Damkham, J. Pinkney, L. F. Hyde, L. Stone, J. K. Naggert, P. M. Nishina, and M. P. Krebs. 2020. Mouse Models of Inherited Retinal Degeneration with Photoreceptor Cell Loss. Cells. 9:931. doi:10.3390/cells9040931.

Corcoran, S. E., and L. A. J. O'Neill. 2016. HIF1α and metabolic reprogramming in inflammation. J. Clin. Invest. 126:3699–3707. doi:10.1172/JCI84431.

Cotman, S. L., and J. F. Staropoli. 2012. The juvenile Batten disease protein, CLN3, and its role in regulating anterograde and retrograde post-Golgi trafficking. Clin. Lipidol. 7:79–91. doi:10.2217/clp.11.70.

Cramer, P. 2019. Organization and regulation of gene transcription. Nature. 573:45–54. doi:10.1038/s41586-019-1517-4.

Cuadrado, A., and A. R. Nebreda. 2010. Mechanisms and functions of p38 MAPK signalling. Biochem. J. 429:403–417. doi:10.1042/BJ20100323.

Danecek, P., J. K. Bonfield, J. Liddle, J. Marshall, V. Ohan, M. O. Pollard, A. Whitwham, T. Keane, S. A. McCarthy, R. M. Davies, and H. Li. 2021. Twelve years of SAMtools and BCFtools. GigaScience. 10:giab008. doi:10.1093/gigascience/giab008.

Deaton, A. M., and A. Bird. 2011. CpG islands and the regulation of transcription. Genes Dev. 25:1010–1022. doi:10.1101/gad.2037511.

Del Corvo, M., B. Lazzari, E. Capra, L. Zavarez, M. Milanesi, Y. T. Utsunomiya, A. T. H. Utsunomiya, A. Stella, G. de Paula Nogueira, J. F. Garcia, and P. Ajmone-Marsan. 2021. Methylome Patterns of Cattle Adaptation to Heat Stress. Front. Genet. 12.

Diaz, F. A., E. J. Gutierrez-Castillo, B. A. Foster, P. T. Hardin, K. R. Bondioli, and Z. Jiang. 2021. Evaluation of Seasonal Heat Stress on Transcriptomic Profiles and Global DNA Methylation of Bovine Oocytes. Front. Genet. 12:699920. doi:10.3389/fgene.2021.699920.

Dobin, A., C. A. Davis, F. Schlesinger, J. Drenkow, C. Zaleski, S. Jha, P. Batut, M. Chaisson, and T. R. Gingeras. 2013. STAR: ultrafast universal RNA-seq aligner. Bioinformatics. 29:15–21. doi:10.1093/bioinformatics/bts635.

Domené, S., and H. M. Domené. 2020. The role of acid-labile subunit (ALS) in the modulation of GH-IGF-I action. Mol. Cell. Endocrinol. 518:111006. doi:10.1016/j.mce.2020.111006.

Doyle, S. L., and L. A. J. O'Neill. 2006. Toll-like receptors: From the discovery of NFκB to new insights into transcriptional regulations in innate immunity. Biochem. Pharmacol. 72:1102–1113. doi:10.1016/j.bcp.2006.07.010.

Elam, N. A., J. T. Vasconcelos, G. Hilton, DAY. L. VanOverbeke, T. E. Lawrence, T. H. Montgomery, W. T. Nichols, M. N. Streeter, J. P. Hutcheson, D. A. Yates, and M. L. Galyean. 2009. Effect of zilpaterol hydrochloride duration of feeding on performance and carcass characteristics of feedlot cattle1. J. Anim. Sci. 87:2133–2141. doi:10.2527/jas.2008-1563.

Ely, B. R., A. T. Lovering, M. Horowitz, and C. T. Minson. 2014. Heat acclimation and cross tolerance to hypoxia: Bridging the gap between cellular and systemic responses. Temperature. 1:107–114. doi:10.4161/temp.29800.

Elzo, M. A., D. D. Johnson, J. G. Wasdin, and J. DAY. Driver. 2012. Carcass and meat palatability breed differences and heterosis effects in an Angus–Brahman multibreed population. Meat Science. 90:87–92. doi:10.1016/j.meatsci.2011.06.010.

Emami, N. K., U. Jung, B. Voy, and S. Dridi. 2021. Radical Response: Effects of Heat Stress-Induced Oxidative Stress on Lipid Metabolism in the Avian Liver. Antioxidants. 10:35. doi:10.3390/antiox10010035.

Fagerberg, L., B. M. Hallström, P. Oksvold, C. Kampf, DAY. Djureinovic, J. Odeberg, M. Habuka, S. Tahmasebpoor, A. Danielsson, K. Edlund, A. Asplund, E. Sjöstedt, E. Lundberg, C. A.-K. Szigyarto, M. Skogs, J. O. Takanen, H. Berling, H. Tegel, J. Mulder, P. Nilsson, J. M. Schwenk, C. Lindskog, F. Danielsson, A. Mardinoglu, Å. Sivertsson, K. von Feilitzen, M. Forsberg, M. Zwahlen, I. Olsson, S. Navani, M. Huss, J. Nielsen, F. Ponten, and M. Uhlén. 2014. Analysis of the Human Tissue-specific Expression by Genome-wide Integration of Transcriptomics and Antibody-based Proteomics *. Mol. Cell. Proteomics. 13:397–406. doi:10.1074/mcp.M113.035600.

Ferlay, A., and Y. Chilliard. 2018. Responses of body fat mobilization to isoproterenol or epinephrine challenge in adult cows: influence of energy level, breed, and body fatness. J. Anim. Sci. 96:331–342. doi:10.1093/jas/skx020.

Ferlay, A., and Y. Chilliard. 2018. Responses of body fat mobilization to isoproterenol or epinephrine challenge in adult cows: influence of energy level, breed, and body fatness. J. Anim. Sci. 96:331–342. doi:10.1093/jas/skx020.

Fournier, DAY., N. Keppie, and E. Simko. 2004. Bovine familial convulsions and ataxia in Saskatchewan and Alberta. Can. Vet. J. 45:845–848.

Fuda, N. J., M. B. Ardehali, and J. T. Lis. 2009. Defining mechanisms that regulate RNA polymerase II transcription in vivo. Nature. 461:186–192. doi:10.1038/nature08449.

Ganesan, S., C. M. Summers, S. C. Pearce, N. K. Gabler, R. J. Valentine, L. H. Baumgard, R. P. Rhoads, and J. T. Selsby. 2017. Short-term heat stress causes altered intracellular signaling in oxidative skeletal muscle. J. Anim. Sci. 95:2438–2451. doi:10.2527/jas2016.1233.

Ganesan, S., C. M. Summers, S. C. Pearce, N. K. Gabler, R. J. Valentine, L. H. Baumgard, R. P. Rhoads, and J. T. Selsby. 2018. Short-term heat stress altered metabolism and insulin signaling in skeletal muscle. J. Anim. Sci. 96:154–167. doi:10.1093/jas/skx083.

Ganesan, S., C. Reynolds, K. Hollinger, S. C. Pearce, N. K. Gabler, L. H. Baumgard, R. P. Rhoads, and J. T. Selsby. 2016. Twelve hours of heat stress induces inflammatory signaling in porcine skeletal muscle. Am. J. Physiol.-Regul. Integr. Comp. Physiol. 310:R1288–R1296. doi:10.1152/ajpregu.00494.2015.

Garner, J. B., A. J. Chamberlain, C. V. Jagt, T. T. T. Nguyen, B. A. Mason, L. C. Marett, B. J. Leury, W. J. Wales, and B. J. Hayes. 2020. Gene expression of the heat stress response in bovine peripheral white blood cells and milk somatic cells in vivo. Sci. Rep. 10. doi:10.1038/s41598-020-75438-2.

Gaughan, J. B., S. Bonner, I. Loxton, T. L. Mader, A. Lisle, and R. Lawrence. 2010. Effect of shade on body temperature and performance of feedlot steers1. J. Anim. Sci. 88:4056–4067. doi:10.2527/jas.2010-2987.

Gill, J. K., J. S. Arora, B. V. Sunil Kumar, C. S. Mukhopadhyay, S. Kaur, and N. Kashyap. 2017. Cellular thermotolerance is independent of HSF 1 expression in zebu and crossbred non-lactating cattle. Int. J. Biometeorol. 61:1687–1693. doi:10.1007/s00484-017-1350-0.

Gimeno, R. E., A. M. Ortegon, S. Patel, S. Punreddy, P. Ge, Y. Sun, H. F. Lodish, and A. Stahl. 2003. Characterization of a heart-specific fatty acid transport protein. J Biol Chem. 278:16039–16044. doi:10.1074/jbc.M211412200.

Gonzalez-Rivas, P. A., S. S. Chauhan, M. Ha, N. Fegan, F. R. Dunshea, and R. D. Warner. 2020. Effects of heat stress on animal physiology, metabolism, and meat quality: A review. Meat Sci. 162:108025. doi:10.1016/j.meatsci.2019.108025.

Greer, S. N., J. L. Metcalf, Y. Wang, and M. Ohh. 2012. The updated biology of hypoxia-inducible factor: The updated biology of HIF. The EMBO Journal. 31:2448–2460. doi:10.1038/emboj.2012.125.

Grijalva, P. C., R. Reith, R. L. Sieck, R. Swanson, T. B. Schmidt, J. L. Petersen, D. T. Yates, S. Garcia, and DAY. Diaz. 2020. PSI-14 Feeding β-agonists under heat stress conditions in feedlot cattle. J. Anim. Sci. 98:266–266. doi:10.1093/jas/skaa278.479.

Gruber, S. L., J. DAY. Tatum, T. E. Engle, M. A. Mitchell, S. B. Laudert, A. L. Schroeder, and W. J. Platter. 2007. Effects of ractopamine supplementation on growth performance and carcass characteristics of feedlot steers differing in biological type. J Anim Sci. 85:1809–1815. doi:10.2527/jas.2006-634.

Gruys, E., M. J. M. Toussaint, T. A. Niewold, and S. J. Koopmans. 2005. Acute phase reaction and acute phase proteins. J Zhejiang Univ Sci B. 6:1045–1056. doi:10.1631/jzus.2005.B1045.

Guibert, S., T. Forné, and M. Weber. 2012. Global profiling of DNA methylation erasure in mouse primordial germ cells. Genome Res. 22:633–641. doi:10.1101/gr.130997.111.

Haberle, V., and A. Stark. 2018. Eukaryotic core promoters and the functional basis of transcription initiation. Nat. Rev. Mol. Cell Biol. 19:621–637. doi:10.1038/s41580-018-0028-8.

Häfliger, I. M., E. Marchionatti, M. Stengård, S. Wolf-Hofstetter, J. M. Paris, J. G. P. Jacinto, C. Watté, K. Voelter, L. M. Occelli, A. M. Komáromy, A. Oevermann, C. Goepfert, A. Borgo, R. Roduit, M. Spengeler, F. R. Seefried, and C. Drögemüller. 2021. CNGB3 Missense Variant Causes Recessive Achromatopsia in Original Braunvieh Cattle. Int. J. Mol. Sci. 22:12440. doi:10.3390/ijms222212440.

Hammond, A. C., T. H. Elsasser, and T. A. Olson. 1991. Endocrine Characteristics of a Miniature Condition in Brahman Cattle: Circulating Concentrations of Some Growth-Related Hormones. Proceedings of the Society for Experimental Biology and Medicine. 197:450–457. doi:10.3181/00379727-197-43281.

Han, X., X. Wang, B. Zhao, G. Chen, Y. Sheng, W. Wang, and M. Teng. 2017. MicroRNA-187 inhibits tumor growth and metastasis via targeting of IGF-1R in hepatocellular carcinoma. Mol. Med. Rep. 16:2241–2246. doi:10.3892/mmr.2017.6788.

Hay, N., and N. Sonenberg. 2004. Upstream and downstream of mTOR. Genes Dev. 18:1926–1945. doi:10.1101/gad.1212704.

Hill, B., R. Holroyd, and M. Sullivan. 2009. Clinical and pathological findings associated with congenital hypovitaminosis A in extensively grazed beef cattle. Aust. Vet. J. 87:94–98. doi:10.1111/j.1751-0813.2009.00398.x.

Hill, M., A. Wernig, and G. Goldspink. 2003. Muscle satellite (stem) cell activation during local tissue injury and repair. J. Anat. 203:89–99. doi:10.1046/j.1469-7580.2003.00195.x.

Hinkelbein, J., L. Böhm, O. Spelten, D. Sander, S. Soltész, and S. Braunecker. 2015. Hyperoxia-Induced Protein Alterations in Renal Rat Tissue: A Quantitative Proteomic Approach to Identify Hyperoxia-Induced Effects in Cellular Signaling Pathways. Dis. Markers. 2015:964263. doi:10.1155/2015/964263.

Houweling, P. J., J. A. L. Cavanagh, D. N. Palmer, T. Frugier, N. L. Mitchell, P. A. Windsor, H. W. Raadsma, and I. Tammen. 2006. Neuronal ceroid lipofuscinosis in Devon cattle is caused by a single base duplication (c.662dupG) in the bovine CLN5 gene. Biochim. Biophys. Acta BBA - Mol. Basis Dis. 1762:890–897. doi:10.1016/j.bbadis.2006.07.008.

HTStream. https://s4hts.github.io/HTStream/

Hu, C.-J., L.-Y. Wang, L. A. Chodosh, B. Keith, and M. C. Simon. 2003. Differential Roles of Hypoxia-Inducible Factor 1α (HIF-1α) and HIF-2α in Hypoxic Gene Regulation. Mol. Cell. Biol. 23:9361–9374. doi:10.1128/MCB.23.24.9361-9374.2003.

Hu, R., Y. He, M. A. Arowolo, S. Wu, and J. He. 2019. Polyphenols as Potential Attenuators of Heat Stress in Poultry Production. Antioxidants. 8:67. doi:10.3390/antiox8030067.

Hu, Z., and W.-W. Tee. 2017. Enhancers and chromatin structures: regulatory hubs in gene expression and diseases. Biosci. Rep. 37:BSR20160183. doi:10.1042/BSR20160183.

Huang, D. W., B. T. Sherman, and R. A. Lempicki. 2009. Bioinformatics enrichment tools: paths toward the comprehensive functional analysis of large gene lists. Nucleic Acids Res. 37:1–13. doi:10.1093/nar/gkn923.

Huynh, H. 2000. Post-transcriptional and post-translational regulation of insulin-like growth factor binding protein-3 and -4 by insulin-like growth factor-I in uterine myometrial cells. Growth Horm. IGF Res. 10:20–27. doi:10.1054/ghir.2000.0137.

Hwang, J. H., M. E. Spurlock, J. C. Kube, X. Z. Li, and S. B. Smith. 2021. Characterization of β-adrenergic receptors in bovine intramuscular and subcutaneous adipose tissue: comparison of lubabegron fumarate with β-adrenergic receptor agonists and antagonists. J Anim Sci. 99:skab116. doi:10.1093/jas/skab116.

Indelicato, E., and S. Boesch. 2021. From Genotype to Phenotype: Expanding the Clinical Spectrum of CACNA1A Variants in the Era of Next Generation Sequencing. Front. Neurol. 12.

Ishiguro, T., K. Ishikawa, M. Takahashi, M. Obayashi, T. Amino, N. Sato, M. Sakamoto, H. Fujigasaki, F. Tsuruta, R. Dolmetsch, T. Arai, H. Sasaki, K. Nagashima, T. Kato, M. Yamada, H. Takahashi, Y. Hashizume, and H. Mizusawa. 2010. The carboxy-terminal fragment of alpha(1A) calcium channel preferentially aggregates in the cytoplasm of human spinocerebellar ataxia type 6 Purkinje cells. Acta Neuropathol. (Berl.). 119:447–464. doi:10.1007/s00401-009-0630-0.

Jen, J. C., and J. Wan. 2018. Chapter 33 - Episodic ataxias. In: D. H. Geschwind, H. L. Paulson, and C. Klein, editors. Handbook of Clinical Neurology. Vol. 148. Elsevier, Amsterdam, Netherlands. p. 521–529.

Jeng, C.-J., M.-C. Sun, Y.-W. Chen, and C.-Y. Tang. 2008. Dominant-negative effects of episodic ataxia type 2 mutations involve disruption of membrane trafficking of human P/Q-type Ca2+ channels. J. Cell. Physiol. 214:422–433. doi:10.1002/jcp.21216.

Jeng, C.-J., Y.-T. Chen, Y.-W. Chen, and C.-Y. Tang. 2006. Dominant-negative effects of human P/Q-type Ca2+ channel mutations associated with episodic ataxia type 2. Am. J. Physiol.-Cell Physiol. 290:C1209–C1220. doi:10.1152/ajpcell.00247.2005.

Jiang, H., and X. Ge. 2014. MEAT SCIENCE AND MUSCLE BIOLOGY SYMPOSIUM—Mechanism of growth hormone stimulation of skeletal muscle growth in cattle1. J. Anim. Sci. 92:21–29. doi:10.2527/jas.2013-7095.

Johnson, B. J., S. B. Smith, and K. Y. Chung. 2014. Historical Overview of the Effect of β-Adrenergic Agonists on Beef Cattle Production. Asian-Australas J Anim Sci. 27:757–766. doi:10.5713/ajas.2012.12524.

Johnson, T. B., J. T. Cain, K. A. White, DAY. Ramirez-Montealegre, DAY. A. Pearce, and J. M. Weimer. 2019. Therapeutic landscape for Batten disease: current treatments and future prospects. Nat. Rev. Neurol. 15:161–178. doi:10.1038/s41582-019-0138-8.

Ju, X.-H., H.-J. Xu, Y.-H. Yong, L.-L. An, P.-R. Jiao, and M. Liao. 2014. Heat stress upregulation of Toll-like receptors 2/4 and acute inflammatory cytokines in peripheral blood mononuclear cell (PBMC) of Bama miniature pigs: an in vivo and in vitro study. Anim. Int. J. Anim. Biosci. 8:1462–1468. doi:10.1017/S1751731114001268.

Jubb, T., and N. Perkins. 2022. The Veterinary Handbook for the Livestock Export Industry. Aust. Livest. Export Corp. Ltd.

Kabe, Y., K. Ando, S. Hirao, M. Yoshida, and H. Handa. 2005. Redox Regulation of NF-κB Activation: Distinct Redox Regulation Between the Cytoplasm and the Nucleus. Antioxid. Redox Signal. 7:395–403. doi:10.1089/ars.2005.7.395.

Kang, S., C. Park, and K. Seo. 2017. Ocular abnormalities associated with hypovitaminosis A in Hanwoo calves: a report of two cases. J. Vet. Med. Sci. 79:1753–1756. doi:10.1292/jvms.17-0166.

Karczewski, K. J., L. C. Francioli, G. Tiao, B. B. Cummings, J. Alföldi, Q. Wang, R. L. Collins, K. M. Laricchia, A. Ganna, DAY. P. Birnbaum, L. D. Gauthier, H. Brand, M. Solomonson, N. A. Watts, DAY. Rhodes, M. Singer-Berk, E. M. England, E. G. Seaby, J. A. Kosmicki, R. K. Walters, K. Tashman, Y. Farjoun, E. Banks, T. Poterba, A. Wang, C. Seed, N. Whiffin, J. X. Chong, K. E. Samocha, E. Pierce-Hoffman, Z. Zappala, A. H. O'Donnell-Luria, E. V. Minikel, B. Weisburd, M. Lek, J. S. Ware, C. Vittal, I. M. Armean, L. Bergelson, K. Cibulskis, K. M. Connolly, M. Covarrubias, S. Donnelly, S. Ferriera, S. Gabriel, J. Gentry, N. Gupta, T. Jeandet, D. Kaplan, C. Llanwarne, R. Munshi, S. Novod, N. Petrillo, DAY. Roazen, V. Ruano-Rubio, A. Saltzman, M. Schleicher, J. Soto, K. Tibbetts, C. Tolonen, G. Wade, M. E. Talkowski, B. M. Neale, M. J. Daly, and D. G. MacArthur. 2020. The mutational constraint spectrum quantified from variation in 141,456 humans. Nature. 581:434–443. doi:10.1038/s41586-020-2308-7.

Kida, E., W. Kaczmarski, A. A. Golabek, A. Kaczmarski, M. Michalewski, and K. E. Wisniewski. 1999. Analysis of intracellular distribution and trafficking of the CLN3 protein in fusion with the green fluorescent protein in vitro. Mol. Genet. Metab. 66:265–271. doi:10.1006/mgme.1999.2837.

Kim, W. S., J. R. Daddam, B. H. Keng, Jaehwan Kim, and Jongkyoo Kim. 2023. Heat shock protein 27 regulates myogenic and self-renewal potential of bovine satellite cells under heat stress. J. Anim. Sci. 101:skad303. doi:10.1093/jas/skad303.

Kim, W.-S., D.-Q. Peng, Y.-H. Jo, J. G. Nejad, and H.-G. Lee. 2021. Responses of beef calves to long-term heat stress exposure by evaluating growth performance, physiological, blood and behavioral parameters. J. Therm. Biol. 100:103033. doi:10.1016/j.jtherbio.2021.103033.

Kitzmüller, C., R. L. Haines, S. Codlin, D. F. Cutler, and S. E. Mole. 2008. A function retained by the common mutant CLN3 protein is responsible for the late onset of juvenile neuronal ceroid lipofuscinosis. Hum. Mol. Genet. 17:303–312. doi:10.1093/hmg/ddm306.

Kobayashi, H., T. Sakurai, M. Imai, N. Takahashi, A. Fukuda, O. Yayoi, S. Sato, K. Nakabayashi, K. Hata, Y. Sotomaru, Y. Suzuki, and T. Kono. 2012. Contribution of Intragenic

DNA Methylation in Mouse Gametic DNA Methylomes to Establish Oocyte-Specific Heritable Marks. PLOS Genet. 8:e1002440. doi:10.1371/journal.pgen.1002440.

Kolde, R. 2019. pheatmap: Pretty Heatmaps. https://CRAN.R-project.org/package=pheatmap

Krueger, F., and S. R. Andrews. 2011. Bismark: a flexible aligner and methylation caller for Bisulfite-Seq applications. Bioinforma. Oxf. Engl. 27:1571–1572. doi:10.1093/bioinformatics/btr167.

Krueger, F., F. James, P. Ewels, E. Afyounian, M. Weinstein, B. Schuster-Boeckler, G. Hulselmans, and sclamons. 2023. FelixKrueger/TrimGalore: v0.6.10 - add default decompression path. doi:10.5281/zenodo.7598955. https://zenodo.org/record/7598955

Kubik, R. M., S. M. Tietze, T. B. Schmidt, D. T. Yates, and J. L. Petersen. 2018. Investigation of the skeletal muscle transcriptome in lambs fed β adrenergic agonists and subjected to heat stress for 21 d1. Transl. Anim. Sci. 2:S53–S56. doi:10.1093/tas/txy053.

Kyttälä, A., G. Ihrke, J. Vesa, M. J. Schell, and J. P. Luzio. 2004. Two motifs target Batten disease protein CLN3 to lysosomes in transfected nonneuronal and neuronal cells. Mol. Biol. Cell. 15:1313–1323. doi:10.1091/mbc.e03-02-0120.

Kyttälä, A., K. Yliannala, P. Schu, A. Jalanko, and J. P. Luzio. 2005. AP-1 and AP-3 Facilitate Lysosomal Targeting of Batten Disease Protein CLN3 via Its Dileucine Motif*. J. Biol. Chem. 280:10277–10283. doi:10.1074/jbc.M411862200.

Lean, I. J., J. M. Thompson, and F. R. Dunshea. 2014. A meta-analysis of zilpaterol and ractopamine effects on feedlot performance, carcass traits and shear strength of meat in cattle. PLoS One. 9:e115904. doi:10.1371/journal.pone.0115904.

Li, H., and R. Durbin. 2009. Fast and accurate short read alignment with Burrows-Wheeler transform. Bioinforma. Oxf. Engl. 25:1754–1760. doi:10.1093/bioinformatics/btp324.

Li, H.-S., Y.-N. Zhou, L. Li, S.-F. Li, DAY. Long, X.-L. Chen, J.-B. Zhang, L. Feng, and Y.-P. Li. 2019. HIF-1α protects against oxidative stress by directly targeting mitochondria. Redox Biol. 25:101109. doi:10.1016/j.redox.2019.101109.

Li, S., J. Zhang, S. Huang, and X. He. 2018. Genome-wide analysis reveals that exon methylation facilitates its selective usage in the human transcriptome. Brief. Bioinform. 19:754–764. doi:10.1093/bib/bbx019.

Li, Y., G. L. Wright, and J. M. Peterson. 2017. C1q/TNF-Related Protein 3 (CTRP3) Function and Regulation. Compr. Physiol. 7:863–878. doi:10.1002/cphy.c160044.

Li, Y., L. Kong, M. Deng, Z. Lian, Y. Han, B. Sun, Y. Guo, G. Liu, and DAY. Liu. 2019. Heat Stress-Responsive Transcriptome Analysis in the Liver Tissue of Hu Sheep. Genes. 10:395. doi:10.3390/genes10050395.

Liu, T., L. Zhang, DAY. Joo, and S.-C. Sun. 2017. NF-κB signaling in inflammation. Signal Transduct. Target. Ther. 2:1–9. doi:10.1038/sigtrans.2017.23.

Liu, Y., H. Cai, X. Guo, A. Aierken, J. Hua, B. Ma, and S. Peng. 2022. Melatonin alleviates heat stress-induced testicular damage in dairy goats by inhibiting the PI3K/AKT signaling pathway. Stress Biol. 2:47. doi:10.1007/s44154-022-00068-9.

Livernois, A. M., B. A. Mallard, S. L. Cartwright, and A. Cánovas. 2021. Heat stress and immune response phenotype affect DNA methylation in blood mononuclear cells from Holstein dairy cows. Sci. Rep. 11:11371. doi:10.1038/s41598-021-89951-5.

Lo, Y. Y. C., J. M. S. Wong, and T. F. Cruz. 1996. Reactive Oxygen Species Mediate Cytokine Activation of c-Jun NH2-terminal Kinases *. J. Biol. Chem. 271:15703–15707. doi:10.1074/jbc.271.26.15703.

Lokk, K., V. Modhukur, B. Rajashekar, K. Märtens, R. Mägi, R. Kolde, M. Koltšina, T. K. Nilsson, J. Vilo, A. Salumets, and N. Tõnisson. 2014. DNA methylome profiling of human tissues identifies global and tissue-specific methylation patterns. Genome Biol. 15:3248. doi:10.1186/gb-2014-15-4-r54.

Love, M. I., W. Huber, and S. Anders. 2014. Moderated estimation of fold change and dispersion for RNA-seq data with DESeq2. Genome Biology. 15:550. doi:10.1186/s13059-014-0550-8.

Lu, Z., M. Chu, Q. Li, M. Jin, X. Fei, L. Ma, L. Zhang, and C. Wei. 2019. Transcriptomic Analysis Provides Novel Insights into Heat Stress Responses in Sheep. Animals. 9:387. doi:10.3390/ani9060387.

Luna-Ramirez, R. I., S. W. Limesand, R. Goyal, A. L. Pendleton, G. Rincón, X. Zeng, G. Luna-Nevárez, J. R. Reyna-Granados, and P. Luna-Nevárez. 2023. Blood Transcriptomic Analyses Reveal Functional Pathways Associated with Thermotolerance in Pregnant Ewes Exposed to Environmental Heat Stress. Genes. 14:1590. doi:10.3390/genes14081590.

Luo, X., J. A. Rosenfeld, S. Yamamoto, T. Harel, Z. Zuo, M. Hall, K. J. Wierenga, M. T. Pastore, D. Bartholomew, M. R. Delgado, J. Rotenberg, R. A. Lewis, L. Emrick, C. A. Bacino, M. K. Eldomery, Z. C. Akdemir, F. Xia, Y. Yang, S. R. Lalani, T. Lotze, J. R. Lupski, B. Lee, H. J. Bellen, M. F. Wangler, and M. of the Udn. 2017. Clinically severe CACNA1A alleles affect synaptic function and neurodegeneration differentially. PLOS Genet. 13:e1006905. doi:10.1371/journal.pgen.1006905.

Lynam-Lennon, N., B. A. S. Bibby, A. M. Mongan, L. Marignol, C. N. Paxton, K. Geiersbach, M. P. Bronner, J. O'Sullivan, J. V. Reynolds, and S. G. Maher. 2016. Low MiR-187 Expression Promotes Resistance to Chemoradiation Therapy In Vitro and Correlates with Treatment Failure in Patients with Esophageal Adenocarcinoma. Mol. Med. 22:388–397. doi:10.2119/molmed.2016.00020.

Majmundar, A. J., W. J. Wong, and M. C. Simon. 2010. Hypoxia-Inducible Factors and the Response to Hypoxic Stress. Mol. Cell. 40:294–309. doi:10.1016/j.molcel.2010.09.022.

Maloyan, A., L. Eli-Berchoer, G. L. Semenza, G. Gerstenblith, M. DAY. Stern, and M. Horowitz. 2005. HIF-1α-targeted pathways are activated by heat acclimation and contribute to acclimation-

ischemic cross-tolerance in the heart. Physiol Genomics. 23:79–88. doi:10.1152/physiolgenomics.00279.2004.

Mantuano, E., S. Romano, L. Veneziano, C. Gellera, B. Castellotti, S. Caimi, DAY. Testa, M. Estienne, G. Zorzi, M. Bugiani, Y. A. Rajabally, M. J. G. Barcina, S. Servidei, A. Panico, M. Frontali, and C. Mariotti. 2010. Identification of novel and recurrent CACNA1A gene mutations in fifteen patients with episodic ataxia type 2. J. Neurol. Sci. 291:30–36. doi:10.1016/j.jns.2010.01.010.

Martín, A. I., T. Priego, and A. López-Calderón. 2018. Hormones and Muscle Atrophy. In: J. Xiao, editor. Muscle Atrophy. Springer, Singapore. p. 207–233.

Mateescu, R. G., K. M. Sarlo Davila, A. S. Hernandez, A. N. Andrade, G. A. Zayas, E. E. Rodriguez, S. Dikmen, and P. A. Oltenacu. 2023. Impact of Brahman genetics on skin histology characteristics with implications for heat tolerance in cattle. Front Genet. 14:1107468. doi:10.3389/fgene.2023.1107468.

Mateescu, R. G., K. M. Sarlo-Davila, S. Dikmen, E. Rodriguez, and P. A. Oltenacu. 2020. The effect of Brahman genes on body temperature plasticity of heifers on pasture under heat stress. J Anim Sci. 98:skaa126. doi:10.1093/jas/skaa126.

McLaren, W., L. Gil, S. E. Hunt, H. S. Riat, G. R. S. Ritchie, A. Thormann, P. Flicek, and F. Cunningham. 2016. The Ensembl Variant Effect Predictor. Genome Biol. 17:122. doi:10.1186/s13059-016-0974-4.

Mezghrani, A., A. Monteil, K. Watschinger, M. J. Sinnegger-Brauns, C. Barrère, E. Bourinet, J. Nargeot, J. Striessnig, and P. Lory. 2008. A Destructive Interaction Mechanism Accounts for Dominant-Negative Effects of Misfolded Mutants of Voltage-Gated Calcium Channels. J. Neurosci. 28:4501–4511. doi:10.1523/JNEUROSCI.2844-07.2008.

Michot, P., S. Chahory, A. Marete, C. Grohs, D. Dagios, E. Donzel, A. Aboukadiri, M.-C. Deloche, A. Allais-Bonnet, M. Chambrial, S. Barbey, L. Genestout, M. Boussaha, C. Danchin-Burge, S. Fritz, D. Boichard, and A. Capitan. 2016. A reverse genetic approach identifies an ancestral frameshift mutation in RP1 causing recessive progressive retinal degeneration in European cattle breeds. Genet. Sel. Evol. GSE. 48:56. doi:10.1186/s12711-016-0232-y.

Miller, J. N., C.-H. Chan, and D. A. Pearce. 2013. The role of nonsense-mediated decay in neuronal ceroid lipofuscinosis. Hum. Mol. Genet. 22:2723–2734. doi:10.1093/hmg/ddt120.

Min, L., N. Zheng, S. Zhao, J. Cheng, Y. Yang, Y. Zhang, H. Yang, and J. Wang. 2016. Long-term heat stress induces the inflammatory response in dairy cows revealed by plasma proteome analysis. Biochem. Biophys. Res. Commun. 471:296–302. doi:10.1016/j.bbrc.2016.01.185.

Mirza, M., A. Vainshtein, A. DiRonza, U. Chandrachud, L. J. Haslett, M. Palmieri, S. Storch, J. Groh, N. Dobzinski, G. Napolitano, C. Schmidtke, and DAY. M. Kerkovich. 2019. The CLN3 gene and protein: What we know. Mol. Genet. Genomic Med. 7:e859. doi:10.1002/mgg3.859.

Mishra, S. R. 2022. Significance of molecular chaperones and micro RNAs in acquisition of thermo-tolerance in dairy cattle. Anim. Biotechnol. 33:765–775. doi:10.1080/10495398.2020.1830788.

Mitlöhner, F. M., J. L. Morrow, J. W. Dailey, S. C. Wilson, M. L. Galyean, M. F. Miller, and J. J. McGlone. 2001. Shade and water misting effects on behavior, physiology, performance, and carcass traits of heat-stressed feedlot cattle. J Anim Sci. 79:2327–2335. doi:10.2527/2001.7992327x.

Molgora, M., D. Supino, A. Mantovani, and C. Garlanda. 2018. Tuning inflammation and immunity by the negative regulators IL-1R2 and IL-1R8. Immunol. Rev. 281:233–247. doi:10.1111/imr.12609.

Moore, L. D., T. Le, and G. Fan. 2013. DNA Methylation and Its Basic Function. Neuropsychopharmacol. 38:23–38. doi:10.1038/npp.2012.112.

Motiejunaite, J., L. Amar, and E. Vidal-Petiot. 2021. Adrenergic receptors and cardiovascular effects of catecholamines. Annales day'Endocrinologie. 82:193–197. doi:10.1016/j.ando.2020.03.012.

Murphy, M. P. 2009. How mitochondria produce reactive oxygen species. Biochem J. 417:1–13. doi:10.1042/BJ20081386.

Nan, J., H. Yang, L. Rong, Z. Jia, S. Yang, and S. Li. 2023. Transcriptome analysis of multiple tissues reveals the potential mechanism of death under acute heat stress in chicken. BMC Genomics. 24:459. doi:10.1186/s12864-023-09564-2.

Nolfi-Donegan, D., A. Braganza, and S. Shiva. 2020. Mitochondrial electron transport chain: Oxidative phosphorylation, oxidant production, and methods of measurement. Redox Biol. 37:101674. doi:10.1016/j.redox.2020.101674.

Oeckinghaus, A., and S. Ghosh. 2009. The NF-κB Family of Transcription Factors and Its Regulation. Cold Spring Harb. Perspect. Biol. 1:a000034. doi:10.1101/cshperspect.a000034.

Okada, K., D. Mori, Y. Makii, H. Nakamoto, Y. Murahashi, F. Yano, S. H. Chang, Y. Taniguchi, H. Kobayashi, H. Semba, N. Takeda, W. Piao, K. Hanaoka, T. Nagano, S. Tanaka, and T. Saito. 2020. Hypoxia-inducible factor-1 alpha maintains mouse articular cartilage through suppression of NF-κB signaling. Sci. Rep. 10:5425. doi:10.1038/s41598-020-62463-4.

Ouseph, M. M., M. E. Kleinman, and Q. J. Wang. 2016. Vision loss in juvenile neuronal ceroid lipofuscinosis (CLN3 disease). Ann. N. Y. Acad. Sci. 1371:55–67. doi:10.1111/nyas.12990.

Paysan-Lafosse, T., M. Blum, S. Chuguransky, T. Grego, B. L. Pinto, G. A. Salazar, M. L. Bileschi, P. Bork, A. Bridge, L. Colwell, J. Gough, D. H. Haft, I. Letunić, A. Marchler-Bauer, H. Mi, D. A. Natale, C. A. Orengo, A. P. Pandurangan, C. Rivoire, C. J. A. Sigrist, I. Sillitoe, N. Thanki, P. D. Thomas, S. C. E. Tosatto, C. H. Wu, and A. Bateman. 2023. InterPro in 2022. Nucleic Acids Res. 51:D418–D427. doi:10.1093/nar/gkac993.

Petersen, J. L., T. S. Kalbfleisch, M. Parris, S. M. Tietze, and J. Cruickshank. 2020. MC1R and KIT Haplotypes Associate With Pigmentation Phenotypes of North American Yak (Bos grunniens). J. Hered. 111:182–193. doi:10.1093/jhered/esz070.

Qi, Y., Y. Zhang, J. Zhang, J. Wang, and Q. Li. 2022. The alteration of N6-methyladenosine (m6A) modification at the transcriptome-wide level in response of heat stress in bovine mammary epithelial cells. BMC Genomics. 23:829. doi:10.1186/s12864-022-09067-6.

Qian, L., X. Song, H. Ren, J. Gong, and S. Cheng. 2004. Mitochondrial mechanism of heat stress-induced injury in rat cardiomyocyte. Cell Stress Chaperon. 9:281–293. doi:10.1379/csc-20r.1.

Ranjan, N., V. Pandey, M. K. Panigrahi, L. Klumpp, U. Naumann, and P. P. Babu. 2021. The Tumor Suppressor MTUS1/ATIP1 Modulates Tumor Promotion in Glioma: Association with Epigenetics and DNA Repair. Cancers. 13:1245. doi:10.3390/cancers13061245.

Rausch, T., T. Zichner, A. Schlattl, A. M. Stütz, V. Benes, and J. O. Korbel. 2012. DELLY: structural variant discovery by integrated paired-end and split-read analysis. Bioinformatics. 28:i333–i339. doi:10.1093/bioinformatics/bts378.

Reith, R. R., R. L. Sieck, P. C. Grijalva, E. M. Duffy, R. M. Swanson, A. M. Fuller, K. A. Beede, J. K. Beard, D. E. Diaz, T. B. Schmidt, D. T. Yates, and J. L. Petersen. 2020. Heat stress and β-adrenergic agonists alter the adipose transcriptome and fatty acid mobilization in ruminant livestock. Transl. Anim. Sci. 4:S141–S144. doi:10.1093/tas/txaa122.

Reith, R. R., R. L. Sieck, P. C. Grijalva, R. M. Swanson, A. M. Fuller, D. E. Diaz, T. B. Schmidt, D. T. Yates, and J. L. Petersen. 2022. Transcriptome analyses indicate that heat stress-induced inflammation in white adipose tissue and oxidative stress in skeletal muscle is partially moderated by zilpaterol supplementation in beef cattle. J Anim Sci. 100:skac019. doi:10.1093/jas/skac019.

Rhoads, M. L., R. P. Rhoads, M. J. VanBaale, R. J. Collier, S. R. Sanders, W. J. Weber, B. A. Crooker, and L. H. Baumgard. 2009. Effects of heat stress and plane of nutrition on lactating Holstein cows: I. Production, metabolism, and aspects of circulating somatotropin1. J. Dairy Sci. 92:1986–1997. doi:10.3168/jds.2008-1641.

Rios, A. P., P. C. C. Grijalva, R. R. Reith, S. R. Garcia, C. Webster, J. K. Beard, J. L. L. Peterson, D. T. Yates, T. B. B. Schmidt, and D. E. E. Diaz. 2023. PSVIII-A-8 Growth and Physiological Responses to Heat Stress and Zilpaterol Hydrochloride in Angus and Brahman Steers. J. Anim. Sci. 101:473–474. doi:10.1093/jas/skad281.561.

Saxonov, S., P. Berg, and D. L. Brutlag. 2006. A genome-wide analysis of CpG dinucleotides in the human genome distinguishes two distinct classes of promoters. Proc. Natl. Acad. Sci. U. S. A. 103:1412–1417. doi:10.1073/pnas.0510310103.

Schakman, O., S. Kalista, C. Barbé, A. Loumaye, and J. P. Thissen. 2013. Glucocorticoid-induced skeletal muscle atrophy. Int. J. Biochem. Cell Biol. 45:2163–2172. doi:10.1016/j.biocel.2013.05.036.

Sherman, B. T., M. Hao, J. Qiu, X. Jiao, M. W. Baseler, H. C. Lane, T. Imamichi, and W. Chang. 2022. DAVID: a web server for functional enrichment analysis and functional annotation of gene lists (2021 update). Nucleic Acids Res. 50:W216-221. doi:10.1093/nar/gkac194.

Sieck, R. L., A. M. Fuller, P. S. Bedwell, J. A. Ward, S. K. Sanders, S.-H. Xiang, S. Peng, J. L. Petersen, and D. J. Steffen. 2020. Mandibulofacial Dysostosis Attributed to a Recessive Mutation of CYP26C1 in Hereford Cattle. Genes. 11:1246. doi:10.3390/genes11111246.

Sieck, R. L., L. K. Treffer, A. M. Fuller, M. Ponte Viana, O. Khalimonchuk, T. B. Schmidt, D. T. Yates, and J. L. Petersen. 2022. Short Communication: Beta-adrenergic agonists alter oxidative phosphorylation in primary myoblasts. J. Anim. Sci. 100:skac208. doi:10.1093/jas/skac208.

Sintas, C., O. Carreño, N. Fernàndez-Castillo, R. Corominas, M. Vila-Pueyo, C. Toma, E. Cuenca-León, I. Barroeta, C. Roig, V. Volpini, A. Macaya, and B. Cormand. 2017. Mutation Spectrum in the CACNA1A Gene in 49 Patients with Episodic Ataxia. Sci. Rep. 7:2514. doi:10.1038/s41598-017-02554-x.

Smirnov, V. M., M. Nassisi, C. Solis Hernandez, C. Méjécase, S. El Shamieh, C. Condroyer, A. Antonio, I. Meunier, C. Andrieu, S. Defoort-Dhellemmes, S. Mohand-Said, J.-A. Sahel, I. Audo, and C. Zeitz. 2021. Retinal Phenotype of Patients With Isolated Retinal Degeneration Due to CLN3 Pathogenic Variants in a French Retinitis Pigmentosa Cohort. JAMA Ophthalmol. 139:278–291. doi:10.1001/jamaophthalmol.2020.6089.

Snelling, W. M., J. L. Hoff, J. H. Li, L. A. Kuehn, B. N. Keel, A. K. Lindholm-Perry, and J. K. Pickrell. 2020. Assessment of Imputation from Low-Pass Sequencing to Predict Merit of Beef Steers. Genes. 11:1312. doi:10.3390/genes11111312.

Söllner, J. F., G. Leparc, T. Hildebrandt, H. Klein, L. Thomas, E. Stupka, and E. Simon. 2017. An RNA-Seq atlas of gene expression in mouse and rat normal tissues. Sci. Data. 4:170185. doi:10.1038/sdata.2017.185.

Song, Y., X. Zhao, A. Aihemaiti, A. Haire, Y. Gao, C. Niu, P. Yang, G. Liu, G. Jia, and A. Wusiman. 2022. The Mechanism of Heat Stress Resistance During Spermatogenesis in Turpan Black Sheep. Front. Vet. Sci. 9:846981. doi:10.3389/fvets.2022.846981.

Song, Y.-H., J. L. Song, P. Delafontaine, and M. P. Godard. 2013. The therapeutic potential of IGF-I in skeletal muscle repair. Trends Endocrinol. Metab. TEM. 24:310–319. doi:10.1016/j.tem.2013.03.004.

Starr, T. V., W. Prystay, and T. P. Snutch. 1991. Primary structure of a calcium channel that is highly expressed in the rat cerebellum. Proc. Natl. Acad. Sci. U. S. A. 88:5621–5625.

St-Pierre, N. R., B. Cobanov, and G. Schnitkey. 2003. Economic Losses from Heat Stress by US Livestock Industries1. J. Dairy Sci. 86:E52–E77. doi:10.3168/jds.S0022-0302(03)74040-5.

Su, Y., S. He, Q. Chen, H. Zhang, C. Huang, Qian Zhao, Y. Pu, X. He, L. Jiang, Y. Ma, and Qianjun Zhao. 2024. Integrative ATAC-seq and RNA-seq analysis of myogenic differentiation of ovine skeletal muscle satellite cell. Genomics. 116:110851. doi:10.1016/j.ygeno.2024.110851.

Sugimoto, N., O. Shido, K. Matsuzaki, M. Katakura, Y. Hitomi, M. Tanaka, T. Sawaki, Y. Fujita, T. Kawanami, Y. Masaki, T. Okazaki, H. Nakamura, S. Koizumi, A. Yachie, and H. Umehara. 2014. Long-term Heat Exposure Prevents Hypoxia-Induced Apoptosis in Mouse Fibroblast Cells. Cell Biochem Biophys. 70:301–307. doi:10.1007/s12013-014-9912-9.

Swanson, R. M., R. G. Tait, B. M. Galles, E. M. Duffy, T. B. Schmidt, J. L. Petersen, and D. T. Yates. 2020. Heat stress-induced deficits in growth, metabolic efficiency, and cardiovascular function coincided with chronic systemic inflammation and hypercatecholaminemia in ractopamine-supplemented feedlot lambs. J. Anim. Sci. 98:skaa168. doi:10.1093/jas/skaa168.

Tedesco, B., R. Cristofani, V. Ferrari, M. Cozzi, P. Rusmini, E. Casarotto, M. Chierichetti, F. Mina, M. Galbiati, M. Piccolella, V. Crippa, and A. Poletti. 2022. Insights on Human Small Heat Shock Proteins and Their Alterations in Diseases. Front. Mol. Biosci. 9. doi:10.3389/fmolb.2022.842149.

Thornton, P., G. Nelson, D. Mayberry, and M. Herrero. 2022. Impacts of heat stress on global cattle production during the 21st century: a modelling study. Lancet Planet. Health. 6:e192–e201. doi:10.1016/S2542-5196(22)00002-X.

Todorov, V., and P. Filzmoser. 2009. An Object-Oriented Framework for Robust Multivariate Analysis. J Stat Softw. 32:1–47. doi:10.18637/jss.v032.i03.

Treinin, M., J. Shliar, H. Jiang, J. A. Powell-Coffman, Z. Bromberg, and M. Horowitz. 2003. HIF-1 is required for heat acclimation in the nematode Caenorhabditis elegans. Physiol Genomics. 14:17–24. doi:10.1152/physiolgenomics.00179.2002.

Tucci, V., A. R. Isles, G. Kelsey, A. C. Ferguson-Smith, V. Tucci, M. S. Bartolomei, N. Benvenisty, D. Bourc'his, M. Charalambous, C. Dulac, R. Feil, J. Glaser, L. Huelsmann, R. M. John, G. I. McNamara, K. Moorwood, F. Muscatelli, H. Sasaki, B. I. Strassmann, C. Vincenz, J. Wilkins, A. R. Isles, G. Kelsey, and A. C. Ferguson-Smith. 2019. Genomic Imprinting and Physiological Processes in Mammals. Cell. 176:952–965. doi:10.1016/j.cell.2019.01.043.

Untergasser, A., I. Cutcutache, T. Koressaar, J. Ye, B. C. Faircloth, M. Remm, and S. G. Rozen. 2012. Primer3—new capabilities and interfaces. Nucleic Acids Res. 40:e115. doi:10.1093/nar/gks596.

Uslu, C., E. Kapan, and A. Lyakhovich. 2024. Cancer resistance and metastasis are maintained through oxidative phosphorylation. Cancer Lett. 587:216705. doi:10.1016/j.canlet.2024.216705.

Van der Auwera, G. A., and B. D. O'Connor. 2020. Genomics in the Cloud: Using Docker, GATK, and WDL in Terra. O'Reilly Media, Inc., Sebastopol, CA.

Van Donkersgoed, J., and E. G. Clark. 1988. Blindness caused by hypovitaminosis A in feedlot cattle. Can. Vet. J. 29:925–927.

Wallace, M. A., W. K. Scarratt, M. V. Crisman, D. A. Prater, and B. S. Jortner. 1996. Familial convulsions and ataxia in an Aberdeen Angus calf. Prog. Vet. Neurol. USA. 7:154–148.

Wang, Y., R. Ye, L. Fan, X. Zhao, L. Li, H. Zheng, Y. Qiu, X. He, and Y. Lu. 2023. A TNF-α blocking peptide that reduces NF-κB and MAPK activity for attenuating inflammation. Bioorg. Med. Chem. 92:117420. doi:10.1016/j.bmc.2023.117420.

Wang, Y., X. Jia, J. C. F. Hsieh, M. S. Monson, J. Zhang, DAY. Shu, Q. Nie, M. E. Persia, M. F. Rothschild, and S. J. Lamont. 2021. Transcriptome Response of Liver and Muscle in Heat-Stressed Laying Hens. Genes. 12:255. doi:10.3390/genes12020255.

Wavre-Shapton, S. T., A. A. Calvi, M. Turmaine, M. C. Seabra, D. F. Cutler, C. E. Futter, and H. M. Mitchison. 2015. Photoreceptor phagosome processing defects and disturbed autophagy in retinal pigment epithelium of Cln3Δex1-6 mice modelling juvenile neuronal ceroid lipofuscinosis (Batten disease). Hum. Mol. Genet. 24:7060–7074. doi:10.1093/hmg/ddv406.

Weber, K., and D. A. Pearce. 2013. Large Animal Models for Batten Disease: A Review. J. Child Neurol. 28:1123–1127. doi:10.1177/0883073813493666.

Weimer, J. M., E. Kriscenski-Perry, Y. Elshatory, and D. A. Pearce. 2002. The neuronal ceroid lipofuscinoses. NeuroMolecular Med. 1:111–124. doi:10.1385/NMM:1:2:111.

Wheelock, J. B., R. P. Rhoads, M. J. VanBaale, S. R. Sanders, and L. H. Baumgard. 2010. Effects of heat stress on energetic metabolism in lactating Holstein cows. J. Dairy Sci. 93:644–655. doi:10.3168/jds.2009-2295.

White, M. E., R. H. Whitlock, and A. de Lahunta. 1975. A cerebellar abiotrophy of calves. Cornell Vet. 65:476–491.

White, M. G., O. Saleh, D. Nonner, E. F. Barrett, C. T. Moraes, and J. N. Barrett. 2012. Mitochondrial dysfunction induced by heat stress in cultured rat CNS neurons. J. Neurophysiol. 108:2203–2214. doi:10.1152/jn.00638.2011.

Williams, DAY. L. 2010. Welfare Issues in Farm Animal Ophthalmology. Vet. Clin. North Am. Food Anim. Pract. 26:427–435. doi:10.1016/j.cvfa.2010.08.005.

Wright, G. A., M. Georgiou, A. G. Robson, N. Ali, A. Kalhoro, S. K. Holthaus, N. Pontikos, N. Oluonye, E. R. de Carvalho, M. M. Neveu, R. G. Weleber, and M. Michaelides. 2020. Juvenile Batten Disease (CLN3): Detailed Ocular Phenotype, Novel Observations, Delayed Diagnosis, Masquerades, and Prospects for Therapy. Ophthalmol. Retina. 4:433–445. doi:10.1016/j.oret.2019.11.005.

Wright, S. A., P. Ramos, DAY. DAY. Johnson, J. M. Scheffler, M. A. Elzo, R. G. Mateescu, A. L. Bass, C. C. Carr, and T. L. Scheffler. 2018. Brahman genetics influence muscle fiber properties, protein degradation, and tenderness in an Angus-Brahman multibreed herd. Meat Sci. 135:84–93. doi:10.1016/j.meatsci.2017.09.006.

Xie, Y., X. Shi, K. Sheng, G. Han, W. Li, Q. Zhao, B. Jiang, J. Feng, J. Li, and Y. Gu. 2019. PI3K/Akt signaling transduction pathway, erythropoiesis and glycolysis in hypoxia (Review). Mol. Med. Rep. 19:783–791. doi:10.3892/mmr.2018.9713.

Xin, H., X. Zhang, D. Sun, C. Zhang, Y. Hao, and X. Gu. 2018. Chronic heat stress increases insulin-like growth factor-1(IGF-1) but does not affect IGF-binding proteins in growing pigs. J. Therm. Biol. 77:122–130. doi:10.1016/j.jtherbio.2018.08.008.

Xun, W., L. Shi, T. Cao, C. Zhao, P. Yu, DAY. Wang, G. Hou, and H. Zhou. 2015. Dual Functions in Response to Heat Stress and Spermatogenesis: Characterization of Expression Profile of Small Heat Shock Proteins 9 and 10 in Goat Testis. BioMed Res. Int. 2015:686239. doi:10.1155/2015/686239.

Yang, L., G.-Y. Tan, Y.-Q. Fu, J.-H. Feng, and M.-H. Zhang. 2010. Effects of acute heat stress and subsequent stress removal on function of hepatic mitochondrial respiration, ROS production and lipid peroxidation in broiler chickens. Comp. Biochem. Physiol. Part C Toxicol. Pharmacol. 151:204–208. doi:10.1016/j.cbpc.2009.10.010.

Young, R. W. 1967. The renewal of photoreceptor cell outer segments. J. Cell Biol. 33:61–72. doi:10.1083/jcb.33.1.61.

Yue, F., Y. Cheng, A. Breschi, J. Vierstra, W. Wu, T. Ryba, R. Sandstrom, Z. Ma, C. Davis, B. DAY. Pope, Y. Shen, D. D. Pervouchine, S. Djebali, R. E. Thurman, R. Kaul, E. Rynes, A. Kirilusha, G. K. Marinov, B. A. Williams, D. Trout, H. Amrhein, K. Fisher-Aylor, I. Antoshechkin, G. DeSalvo, L.-H. See, M. Fastuca, J. Drenkow, C. Zaleski, A. Dobin, P. Prieto, J. Lagarde, G. Bussotti, A. Tanzer, O. Denas, K. Li, M. A. Bender, M. Zhang, R. Byron, M. T. Groudine, D. McCleary, L. Pham, Z. Ye, S. Kuan, L. Edsall, Y.-C. Wu, M. D. Rasmussen, M. S. Bansal, M. Kellis, C. A. Keller, C. S. Morrissey, T. Mishra, DAY. Jain, N. Dogan, R. S. Harris, P. Cayting, T. Kawli, A. P. Boyle, G. Euskirchen, A. Kundaje, S. Lin, Y. Lin, C. Jansen, V. S. Malladi, M. S. Cline, D. T. Erickson, V. M. Kirkup, K. Learned, C. A. Sloan, K. R. Rosenbloom, B. Lacerda de Sousa, K. Beal, M. Pignatelli, P. Flicek, J. Lian, T. Kahveci, D. Lee, W. J. Kent, M. Ramalho Santos, J. Herrero, C. Notredame, A. Johnson, S. Vong, K. Lee, D. Bates, F. Neri, M. Diegel, T. Canfield, P. J. Sabo, M. S. Wilken, T. A. Reh, E. Giste, A. Shafer, T. Kutyavin, E. Haugen, D. Dunn, A. P. Reynolds, S. Neph, R. Humbert, et al. 2014. A comparative encyclopedia of DNA elements in the mouse genome. Nature. 515:355–364. doi:10.1038/nature13992.

Zabidi, M. A., and A. Stark. 2016. Regulatory enhancer–core-promoter communication via transcription factors and cofactors. Trends Genet. TIG. 32:801–814. doi:10.1016/j.tig.2016.10.003.

Zeng, J., J. Cai, D. Wang, H. Liu, H. Sun, and J. Liu. 2023. Heat stress affects dairy cow health status through blood oxygen availability. J. Anim. Sci. Biotechnol. 14:112. doi:10.1186/s40104-023-00915-3.

Zeng, Y., and T. Chen. 2019. DNA Methylation Reprogramming during Mammalian Development. Genes. 10:257. doi:10.3390/genes10040257.

Zhang, J., H. Sheng, C. Hu, F. Li, B. Cai, Yanfen Ma, Y. Wang, and Yun Ma. 2023. Effects of DNA Methylation on Gene Expression and Phenotypic Traits in Cattle: A Review. Int. J. Mol. Sci. 24. doi:10.3390/ijms241511882.

Zhang, X., D. Wang, and J. Liu. 2023. Hypoxia-inducible factor-1α is involved in the response to heat stress in lactating dairy cows. J. Therm. Biol. 112:103460. doi:10.1016/j.jtherbio.2023.103460.

Zheng, H.-T., Z.-X. Zhuang, C.-J. Chen, H.-Y. Liao, H.-L. Chen, H.-C. Hsueh, C.-F. Chen, S.-E. Chen, and S.-Y. Huang. 2021. Effects of acute heat stress on protein expression and histone modification in the adrenal gland of male layer-type country chickens. Sci. Rep. 11:6499. doi:10.1038/s41598-021-85868-1.

Zhou, Y., S. Liu, Y. Hu, L. Fang, Y. Gao, H. Xia, S. G. Schroeder, B. D. Rosen, E. E. Connor, C. Li, R. L. Baldwin, J. B. Cole, C. P. Van Tassell, L. Yang, L. Ma, and G. E. Liu. 2020. Comparative whole genome DNA methylation profiling across cattle tissues reveals global and tissue-specific methylation patterns. BMC Biol. 18:85. doi:10.1186/s12915-020-00793-5.

Ziller, M. J., H. Gu, F. Müller, J. Donaghey, L. T.-Y. Tsai, O. Kohlbacher, P. L. De Jager, E. D. Rosen, D. A. Bennett, B. E. Bernstein, A. Gnirke, and A. Meissner. 2013. Charting a dynamic DNA methylation landscape of the human genome. Nature. 500:477–481. doi:10.1038/nature12433.